Experimental, numerical and multivariate regression analysis of dolerite–Xorex fibre shotcrete for underground excavation support

By

Vhuhwavho Pertunia Mudau

Submitted in accordance with the requirements for the degree of

DOCTOR OF PHILOSOPHY

in the subject

ENGINEERING

at the

UNIVERSITY OF SOUTH AFRICA

Supervisor: Prof Francois Mulenga

Co-Supervisor: Prof Bolanle Ikotun

December 2025

Declaration

Name: Vhuhwavho pertunia Mudau

Student number: 11446781

Degree: PhD (Engineering)

*I declare that: (*Exact wording of the title of the thesis as appearing on the electronic copy submitted for examination)

Experimental, numerical and multivariate regression analysis of dolerite-Xorex fibre shotcretes for underground excavation support

I declare that the thesis is my own work and that all the sources that I have used or quoted have been indicated and acknowledged by means of complete references, and that any use of Artificial Intelligence (AI) has been fully disclosed.

I further declare that I submitted the thesis to the appropriate originality detection system which is endorsed by Unisa and that it falls within the accepted requirements for originality.

I further declare that I have not previously submitted this work, or part of it, for examination at Unisa for another qualification or at any other higher education institution.

I further declare that where Artificial Intelligence (AI) tools have been used in the preparation of this thesis/dissertation, their use has been limited to ethical permissible support, has been fully disclosed, and does not replace my own original research, my independent critical thinking and analysis, or authorship responsibilities.

I understand that failure to disclose AI use, plagiarism and/or lack of academic integrity may constitute academic misconduct under Unisa's policies.

(The thesis will not be examined unless this statement has been included.)

VP Mudau

12/11/2025

SIGNATURE

DATE

Acknowledgements

This PhD journey has been one of the most challenging yet rewarding chapters of my life, and it would not have been possible without the invaluable support, guidance, and encouragement of many individuals and organisations who walked alongside me in countless ways.

I am profoundly grateful to my supervisors, Prof Francois Mulenga and Prof Bolanle Ikotun, whose wisdom, patience, and unwavering encouragement lit the path when it felt unclear. Their insightful feedback not only sharpened the direction of this research but also inspired me to pursue excellence with determination and resilience. Their mentorship has left an indelible mark on both my academic and personal growth.

This work would not have been possible without the generous support of organisations who believed in the vision of this study. My heartfelt appreciation goes to the AfriSam team and special gratitude to Portia Manavhela whose provision of dolerite aggregates formed the very foundation of this research. I am deeply thankful to Mr. Donald Khoza from Chryso who sponsored the superplasticizer and whose faith in this project was a constant reminder of its potential impact. I am also sincerely grateful to Fibsol South Africa for providing their innovative Xorex fibres and for their continuous encouragement, which became a source of motivation throughout this journey.

To Prof Fhatuwani Sengani, I owe you a special gratitude for pushing me towards furthering my studies and for believing in my research capability when it mattered most. Your early support planted the seed that grew into this PhD.

I also wish to acknowledge the financial support received from the engineering departmental Bursary and the National Research Foundation (NRF). Their assistance not only eased the financial burden but also made it possible for me to devote my energy fully to this research.

Lastly, and most importantly, I extend my deepest love and gratitude to my family, friends, and peers. Their unwavering support, endless patience, and words of encouragement carried me through the difficult moments and celebrated with me in the moments of triumph. This achievement is as much theirs as it is mine a reflection of shared belief, sacrifice, and collaboration.

Dedications

Above all, I dedicate this work to God, the unwavering source of my strength, clarity, and perseverance. Through moments of doubt, exhaustion, and triumph, His grace has been my constant companion. Without His divine guidance and steadfast presence, this achievement would not have been possible.

To my husband, Matimba Maringa, thank you for being my rock, my laughter during tension, and my safe space when the world felt heavy. Your unwavering love and support steadied me when I felt unsteady, and for that, I am endlessly grateful.

To my precious daughters, Dakalo Rokunda Maringa and Asakundwi Hulisani Maringa, you have been my greatest source of inspiration. At only five and one years old, you may not yet understand the long nights, the sacrifices, or the weight of this journey, but every page of this work has carried pieces of you. Through this PhD, I want you to witness that dreams are valid, voices matter, and paths can be carved with courage and determination. If this journey teaches you anything, let it be that resilience and purpose will always make the impossible possible.

To my parents, Rosina Tshililo Mudau and Makondelele Elijah Mudau, your prayers, quiet strength, and unconditional love carried me through the darkest valleys. Even when the language of academia felt foreign, you listened with genuine interest and offered encouragement that nourished my spirit. This degree is as much yours as it is mine you are my anchor and my foundation.

To my siblings, Shudufhadzo Malelelo, Mpho Mudau, and Mukhethwa Nephawe, your steady support has been a pillar for me, making this accomplishment one we share together.

I also cherish the memory of my late grandmothers, Mrs Mafunisa Felicia Mudau and Mrs Tshinakaho Martha Tshidavhu, and my dearest cousin Mrs Annah Ligudu who were blessed to witness my early years and whose

presence shaped the foundation of who I am. Though they are no longer with me in person, I continue to feel their resilient spirit guiding and sustaining me. Their prayers, strength, and love remain an enduring source of comfort and inspiration. This achievement stands as a tribute to their lives, a continuation of their dreams, and a legacy I am deeply honoured to carry forward.

Being the first in my family to earn a PhD is not only a personal milestone but also a declaration that cycles can be broken, ceilings can be lifted, and stories can be rewritten. This journey has always been about more than an academic pursuit; it has been about expanding the horizon of what is possible for my family and for generations to come.

To my friends Vhuhwavhohau Nengovhela, Dipako Jessica Phalane, Mankwana Ramadi, Muneiwa Marindi, Oratile Mokoto, Siviwe Vilakazi, Themedi Matloga, Mpho Shongwane, Tshepang Madire, Basani Mnisi, Rinae Netshithuthuni and Tshenolo Mashaba, thank you for being my cheerleaders, for lifting my spirits in moments of doubt, and for reminding me that I was never walking this path alone.

Ultimately, this work is dedicated to every young Black woman who has ever felt invisible or uncertain in spaces where her presence was doubted. To every girl who chooses to dream boldly in male-dominated fields, may this serve as living proof that you belong, that you are capable, and that you can rise. Let it stand as a quiet yet unwavering reminder that your dreams hold value, your voice carries power, and your path is yours to shape with confidence and purpose.

Abstract

Shotcrete has gained significant popularity as an effective support material for underground excavations owing to its fast application, early gain of strength and suitability for complicated excavations. There are, however, very few studies that have developed mathematical models for assessing the effectiveness of shotcrete support system including sustainable materials. In this study, an attempt has been made to develop a sustainable dolerite-Xorex fibre reinforced shotcrete system based on experimental, numerical and multivariate approach.

The rationale behind this research comes from the depletion of natural sand sources and the increase in mining wastes, mainly dolerite rocks. Fibre reinforced shotcretes improve the properties of shotcrete system; but ordinary steel fibres are not durable owing to their corrosive nature. The Xorex fibre system, which is a non-corrosive one, needs more investigation.

A total of 48 specimens were prepared using dolerite aggregate, Xorex fibres (0.02 wt%) and water reducing superplasticizer. The samples were then tested after 4 days, 7 days, 28 days and 56 days of curing using uniaxial compressive strength, triaxial compressive strength, tensile strength and shrinkage test. Numerical evaluation was done using Rocscience software such as Unwedge, RocSupport, RS2, and Ground Reaction Curve analysis. The Pearson correlation and multiple regression analyses were used to determine the main factors affecting the performance of shotcrete.

It was evident that there was progressive mechanical improvement due to increased curing time. The compressive strength increased from 10.85 MPa to 22.07 MPa, elastic modulus from 12.44 GPa to 20.34 GPa and tensile strength from 1.67 MPa to 4.21 MPa after 4 and 56 days. In the triaxial test, it was evident that there was improved confined behaviour where cohesion increased from 3.5 MPa to 5.3 MPa and friction angle from 46.6° to 51.6°. From the numerical modelling, it was clear that with increase in depth of excavation, there would be deformation and with increase in curing time,

there would less displacement. The regression models have excellent prediction capability (R= 0.99937-0.99967; R^2>0.998). Limitations of the study include lack of a control mixture, lower fibre content and using laboratory and numerical modelling. Future studies need to look at optimising the dosage of fibres, their durability and performance through field tests conducted underground.

Keywords: Shotcrete, dolerite aggregates, Xorex fibres, mechanical properties numerical modelling, multivariate regression modelling

List of publications

Mudau, V.P., Mulenga, F., Ikotun, B.D. *Mechanical performance of shotcrete incorporating coal waste-derived dolerite aggregates and Xorex fibres* (in preparation).

Mudau, V.P., Mulenga, F., Ikotun, B.D. *The impact of aggregates' angularity on the bond strength between shotcrete and substrate: An experimental study* (in preparation).

Mudau, V.P., Mulenga, F., Ikotun, B.D. *Performance of the newly developed shotcrete–fibres in static and dynamic conditions: Using surface and underground mines as case studies* (in preparation).

Mudau, V.P., Mulenga, F., Ikotun, B.D. *Development of a multivariate predictive model on factors contributing to the performance of shotcrete* (in preparation).

Mudau, V.P., Mulenga, F., Ikotun, B.D. *Regression-based analysis of curing time on strength evolution in dolerite–Xorex fibre shotcrete* (in preparation).

Table of contents

List of figures xiii
List of tables xvi
List of abbreviations xvii
List of Symbols xx
Chapter 1: Introduction 1
1.1 Context of the study 1
1.2 Statement of the research problem 3
1.3 Aims and objectives of the research 4
1.4 Research questions 4
1.5 Envisaged contribution of the research 5
1.6 Structure of the thesis 5
Chapter 2: Literature review 7
2.1 Introduction 7
2.1.1 Overview of shotcrete composition 8
2.2 Mechanical properties of shotcrete 15
2.2.1 Compressive behaviour of shotcrete 16
2.2.2 Tensile behaviour of shotcrete 17
2.2.3 Shear strength of shotcrete 18
2.2.4 Elastic response of shotcrete 19
2.2.5 Typical shotcrete deformation 20
2.3 Causes of shotcrete degradation 22
2.3.1 Mechanical attack 22
2.3.2 Steel corrosion 25
2.4 Failure modes of shotcrete 27
2.4.1 Compressive failure 27
2.4.2 Tensile failure 29
2.5 Factor of safety in shotcrete lining 29
2.5.1 Ground reaction curve of shotcrete 31
2.6 Implications of shotcrete failure in underground mines 32
2.7 Constitutive modelling 34
2.7.1 Meschke model 35
2.7.2 Schädlich and Schweiger model 39
2.7.3 Shotcrete damage plasticity model 41

2.7.4 Need for multivariate regression modelling 44
2.8 Research gaps and motivations 45
2.9 Concluding remarks 46
Chapter 3: Collection of experimental data and research methodology 48
3.1 Introduction 48
3.2 Mix ingredients 49
3.2.1 On-site collection of bulk aggregates 50
3.2.2 Selection of cement 52
3.2.3 Xorex fibre reinforcement 53
3.2.4 Mixing water used in the preparation of shotcrete 54
3.2.5 Characteristics of the superplasticizer used 55
3.3 Experimental design 55
3.4 Mechanical tests 59
3.4.1 Triaxial compressive strength and shear strength test 60
3.4.2 Tensile strength tests 62
3.4.3 Shrinkage tests 64
3.4.4 Uniaxial Compressive strength tests 65
3.5 Development of multivariate regression models 66
3.6 Numerical simulations under static and dynamic loads 68
3.6.1 Simulations using Unwedge Deterministic analysis tool 68
3.6.2 Simulation of Ground Reaction Curve 71
3.6.3 Simulations of the selected tunnel in RS2 software 76
3.7 Limitation of the work and challenges encountered 78
Chapter 4: Effect of dolerite aggregates and Xorex fibres on shotcrete properties 80
4.1 Introduction 80
4.2 Evolution of the Uniaxial Compressive Strength with time 80
4.2.1 Uniaxial Compressive strength of the fibre-reinforced shotcrete 80
4.2.2 Stress-strain relationship under Uniaxial Compressive Strength testing conditions 83
4.2.3 Role of fibre type and dosage in the development of the Uniaxial Compressive Strength 87
4.2.4 Triaxial Compressive Strength of dolerite-Xorex fibre-reinforced shotcrete 92
4.3 Mohr-Coulomb parameters 94

4.3.1 Determination of cohesion and friction angle of reinforced shotcrete 94
4.3.2 Strengthening parameter relative to the reinforced shotcrete 95
4.4 Tensile strength development 96
4.4.1 Effect of fibre dosage and fibre type on tensile strength 97
4.5 Time-dependent shrinkage behaviour 98
4.6 Shear strength of shotcrete 100
4.7 Comparison of experimental results with existing constitutive models 100
4.8 Significant findings from the study 103
Chapter 5: Static and dynamic mechanical performance of dolerite-Xorex fibre-reinforced shotcrete 106
5.1 Introduction 106
5.2 Findings from the numerical simulations with Unwedge 107
5.2.1 Unsupported tunnel case 107
5.2.2 Supported tunnel with dolerite-Xorex fibre-reinforced shotcrete 109
5.2.3 Comparison between supported and unsupported tunnels 113
5.3 Ground Reaction Curves (GRC) of shotcrete support 115
5.4 Shotcrete performance in RS2 tunnel analysis 119
5.5 Summary of the findings 129
Chapter 6: Multivariate regression modelling of dolerite-Xorex fibre-reinforced shotcrete 132
6.1 Introduction to multivariate and regression models 132
6.1.1 Correlation analysis of predictor variables 132
6.1.2 Modelling shotcrete behaviour using multiple linear regression techniques 137
6.2 Regression-based analysis of strength evolution in dolerite-Xorex fibre shotcrete 140
6.3 Discussions of regression models 143
6.4 Summary of the main findings 144
Chapter 7: Conclusions and recommendations 146
7.1. Introduction 146
7.2 Summary of key research findings 146
7.2.1 Effect of dolerite aggregates and Xorex fibres on shotcrete properties 146
7.2.2 Development of numerical simulations 147

7.2.3 Development of a multivariate predictive model for shotcrete behaviour 148
7.3 Research contributions to the body of knowledge 149
7.4 Limitations of the study 150
7.5 Recommendations for future research 150
References 152
Appendices 169
Appendix A: Shrinkage data 170
Appendix B: Triaxial compressive strength data 171
Appendix C: Tensile strength data 172
Appendix D: Uniaxial compressive strength data 173
Appendix E: Information of tunnel Deformation 174
Appendix F: Output parameters from Ground Reaction Curve (GRC) 175
Appendix G: MATLAB code for the correlation multivariate modelling 176
Appendix H: Short-term statistical modelling of 4 days 181
Appendix I: Short term statistical modelling of 7 days 182
Appendix J: Long-term statistical modelling of 28 days 183
Appendix K: Long-term statistical modelling of 56 days 184
Appendix L: Input parameters for conventional shotcrete 185

List of figures

Figure 2-1: Components of a typical sprayed concrete mix, in (%), established based on mass values (Mahoney, 2014) 8

Figure 2-2: Types of shotcrete deformation experienced upon application in underground excavations 21

Figure 2-3: Failure form of sand-based shotcrete specimen 25

Figure 2-4: Example of steel fibre corrosion that eventually affects the durability of shotcrete lining 26

Figure 2-5: Compressive strength failure at three common areas 28

Figure 2-6: The creep constitutive model associated the viscoplastic multisurface theory after Meschke (1996) 37

Figure 2-7: Predictive ability of the Meschke Model against experimental data and similar models (after Meshcke, 1996; Schädlich and Schweiger,2014; Neuner et al., 2017) 39

Figure 2-8: Predictive ability of the Schädlich and Schweiger model against experimental data and similar models (after Meshcke, 1996; Schädlich and Schweiger, 2014; Neuner et al., 2017) 40

Figure 2-9: Predictive ability of the SCDP Model against experimental data and similar models (after Meshcke, 1998; Schädlich and Schweiger, 2014; Neuner et al., 2017) 43

Figure 2-10: Evolution of elastic modulus depicted from various models. 44

Figure 3-1: Geographical location of the Rooikraal quarry sampling site (Coordinates: 6°00'0.0"N, 12°00'0.0"E) 50

Figure 3-2: (A) Stockpile of coarse dolerite aggregates (10 mm); (B) Collected 10 mm dolerite aggregates; (C) Stockpile of fine dolerite aggregates (5 mm) and; (D) Collected 5 mm dolerite aggregates 51

Figure 3-3: Xorex fibres 54

Figure 3-4: The mix design ingredients – (A) Cement; (B) Coarse dolerite aggregates; (C) Fine dolerite aggregates; (D) Water; (E) Xorex fibres; and (F) Chryso® superplasticizer 57

Figure 3-5: Casting of specimens – (A) Cylinder and (B) thick Perspex 58

Figure 3-6: Air curing of specimen in a sealed vacuum desiccator 59

Figure 3-7:Triaxial compressive strength sample testing setup. (A) Mold assembly with ports and sleeve for sample preparation. (B) Compressive strength testing machine 62

Figure 3-8: Tensile strength testing 63

Figure 3-9: Shotcrete cores with strain gauges 64

Figure 3-10: Shotcrete specimen instrumented with both axial and lateral strain 65

Figure 3-11:Cross-section dimensions used in this study 69

Figure 3-12: Stereonet of the simulated underground situation using Unwedge. 71

Figure 3-13: Tunnel entry for the first and second tunnel 72

Figure 3-14: Estimation of rock mass properties – (a) intact uniaxial compressive strength of sandstone and (b) disturbance factor of the tunnel..... 73

Figure 3-15: Estimation of rock mass properties – (a) Geological Strength Index of sandstone and (b) Maximum peak strength of the rock..... 74

Figure 3-16: Estimated stresses of the rock mass – (a) Plot showing major and minor stress and (b) Shear stress and Normal stress of the rock unit 75

Figure 3-17: Input material parameters for the Mohr–Coulomb model of dolerite–Xorex fibre-reinforced shotcrete..... 78

Figure 4-1: Stress-strain relationships for axial and radial deformation under uniaxial compression at varying curing durations (4, 7, 28, and 56 days)..... 84

Figure 4-2: UCS values of shotcrete at 28 days for this study and published literature with error bars representing 95% confidence range 87

Figure 4-3: Variation of Mohr-Coulomb shear strength parameters of fibre-reinforced shotcrete over different curing ages 92

Figure 4-4: Development of the tensile strength of the reinforced shotcrete over various curing days with error bars representing 95% confidence range..... 96

Figure 4-5: Comparison of 28-day tensile strength of shotcrete in this study and published literature with error bars representing 95% confidence range 98

Figure 4-6: Shrinkage development of the reinforced shotcrete over various curing days 99

Figure 4-7: Shrinkage comparison with constitutive models..... 101

Figure 4-8: Compressive strength comparison with constitutive models 102

Figure 4-9:Elastic Modulus comparison with constitutive models..... 102

Figure 5-1: 3D visualisation of rock wedge geometry under unsupported excavation conditions 108

Figure 5-2: Simulated tunnel response using 50 mm of shotcrete at 4 days 111

Figure 5-3: Simulated tunnel response using 50 mm of shotcrete at 7 days 111

Figure 5-4: Simulated tunnel response using 50 mm of shotcrete at 28 days .. 112

Figure 5-5: Simulated tunnel response using 50 mm of shotcrete at 56 days .. 112

Figure 5-6: 3D visualisation of rock wedge geometry supported with conventional shotcrete..... 113

Figure 5-7: Ground Reaction Curves of an unsupported tunnel 116

Figure 5-8: Ground Reaction Curve with the application of shotcrete cured for 4 days..... 117

Figure 5-9:Ground Reaction Curve with the application of shotcrete cured for 7 days 118

Figure 5-10: Ground Reaction Curve with the application of shotcrete cured for 28 days 118

Figure 5-11:Ground Reaction Curve with the application of shotcrete cured for 56 days 119

Figure 5-12: Key geomechanical properties of conventional shotcrete at 28 days – (A) Maximum shear strain, (B) Strength factor, (C) Total displacement, and (D) Volumetric strain 122

Figure 5-13: Key geomechanical properties of Dolerite–Xorex shotcrete at 4 days – (A) Maximum shear strain, (B) Strength factor, (C) Total displacement, and (D) Volumetric strain 123

Figure 5-14: Key geomechanical properties of Dolerite–Xorex shotcrete at 7 days – (A) Maximum shear strain, (B) Strength factor, (C) Total displacement, and (D) Volumetric strain 124

Figure 5-15: Key geomechanical properties of Dolerite-Xorex shotcrete at 28 days – (A) Maximum shear strain, (B) Strength factor, (C) Total displacement, and (D) Volumetric strain 125

Figure 5-16: Key geomechanical properties of dolerite-Xorex shotcrete at 56 days – (A) Maximum shear strain, (B) Strength factor, (C) Total displacement, and (D) Volumetric strain 126

Figure 6-1: Pearson correlation heatmap of short-term performance of shotcrete with predictor variables at 4 days 133

Figure 6-2: Pearson correlation heatmap of short-term performance of shotcrete with predictor variables at 7 days 134

Figure 6-3: Pearson correlation heatmap of long-term performance of shotcrete with predictor variables at 28 days 135

Figure 6-4:Pearson correlation heatmap of long-term performance of shotcrete with predictor variables at 56 days 136

Figure 6-5: Logarithmic relationship between curing time and the Uniaxial Compressive Strength 141

Figure 6-6: Logarithmic relationship between curing time and elastic modulus (E) 142

Figure 6-7: Logarithmic relationship between curing time and maximum stress143

List of tables

Table 3-1: Engineering properties of dolerite aggregates 52

Table 3-2: Shotcrete mix design ingredients 56

Table 3-3: Input parameters used for Unwedge simulations 70

Table 3-4: Input parameters for the simulation of Ground Reaction Curve 75

Table 3-5: Material properties of shotcrete applied for the tunnel 76

Table 4-1: Mean and standard deviation of UCS, Young's modulus, and Poisson's ratio at various curing ages 81

Table 4-2: Comparison of Poisson's ratio (ν) ranges between EFNARC (2019) and Xorex-dolerite reinforced shotcrete 89

Table 4-3: Comparative table of Young's modulus for shotcrete with sand and steel fibres 91

Table 4-4: Development of cohesion (C), internal friction angle (ϕ) and strengthening parameter (β) with curing duration for the shotcrete specimens .. 94

Table 4-5: Average shrinkage (%) of fibre-reinforced shotcrete over different curing ages 99

Table 4-6: Shear strength of shotcrete specimens with dolerite aggregates at different curing ages 100

Table 5-1: Factor of safety and weights of unsupported tunnel 107

Table 5-2: FoS values for floor, lower right, upper left, and roof wedges at curing ages of 4, 7, 28, and 56 days 109

Table 5-3: Wedge Stability (FoS) across wedges – Unsupported conventional shotcrete and dolerite–Xorex fibre shotcrete 114

Table 5-4:Output parameters for dolerite-Xorex fibre-reinforced shotcrete at varying depths and curing periods 121

Table 6-1. Description of parameters used in the regression models 139

Table 6-2: Summary of Regression Coefficients for Models 140

List of abbreviations

Abbreviation / Symbol	Full Form / Description
ACI	American Concrete Institute
ASTM	American Society for Testing and Materials
BFSC	Blast Furnace Slag Cement
BS	British Standard
C–S–H	Calcium Silicate Hydrate (hydration product)
COV	Coefficient of Variation
CT	Computed Tomography
DA	Dolerite Aggregate
DAQ	Data Acquisition System
EDC	Early-age Development of Cohesion
EFNARC	European Federation of National Associations Representing Concrete
FEA	Finite Element Analysis
FEM	Finite Element Method
FOG	Fall of Ground
FoS	Factor of Safety
FOS	Factor of Safety
FRS	Fibre-Reinforced Shotcrete
FRSC	Fibre-Reinforced Shotcrete
GGBS	Ground Granulated Blast-Furnace Slag
GGBFS	Ground Granulated Blast-Furnace Slag
GPa	Giga-Pascal

GRC	Ground Reaction Curve
IS	International Standard
ITS	Indirect Tensile Strength
ITZ	Interfacial Transition Zone
kg/m³	Kilogrammes per cubic metre
LA	Los Angeles Abrasion
LVDT	Linear Variable Differential Transformer
MC	Mohr–Coulomb
MINCOSA	Mine Health and Safety Council of South Africa
MLR	Multiple Linear Regression
mm	Millimetre
MPa	Megapascal
N	Newton
NTM	Numerical Testing Method
OPC	Ordinary Portland Cement
p	Probability Value
PCA	Principal Component Analysis
RH	Relative Humidity
RS2	Rock and Soil 2-Dimensional Analysis Program
SCDP	Shotcrete Damage Plasticity Model
SD	Standard Deviation
SEE	Standard Error of Estimate
SEM	Scanning Electron Microscopy
SFRC	Steel Fibre-Reinforced Shotcrete

TCS	Triaxial Compressive Strength
TSL	Thin Spray-on Liner
UCS	Uniaxial Compressive Strength
UCT	Unconfined Compression Test
USD	Underground Support Design
UTM	Universal Testing Machine
VIF	Variance Inflation Factor
Xorex	Trade Name for Corrosion-Resistant Steel Fibres
ZAR	Zuid-Afrikaanse Rand, which is Dutch for South African Rand, the South African currency

List of Symbols

Symbol	Description	Unit / Type
A	Cross-sectional area of specimen	mm² / m²
a_E	Smooth time transition parameter	Dimensionless
b_E	Smooth time transition parameter	Dimensionless
C	Cohesion	MPa
c_E	Smooth time transition parameter	Dimensionless
C_t	Time / Curing age	Days or Hours
d_E	Smooth time transition parameter	Dimensionless
E	Young's modulus / Elastic modulus	GPa or MPa
E_m	Elastic modulus	GPa
$E(t)$	Young's modulus at time t	GPa
$E^{(1)}$	Young's modulus after 1 day	GPa
$E^{(28)}$	Young's modulus at 28 days	GPa
$\bar{E}$	Mean Young's modulus	GPa
E_σ	Standard deviation of Young's modulus	GPa
F	Maximum load / Tensile load	N
FoS	Factor of Safety	Dimensionless
FOS	Factor of Safety	Dimensionless
f_c	Compressive strength under triaxial loading	MPa
F_c	Compressive strength under triaxial loading	MPa
f_t	Tensile strength	MPa
GSI	Geological Strength Index	Dimensionless

Symbol	Description	Unit / Type
L	Specimen length	mm
L_0	Original length of shotcrete specimen	mm
M	Mass of specimen	g
P	Applied load at failure	kN
P	Spearman Correlation Coefficient	Dimensionless
q_1	Material compliance	GPa
q_2	Short-term creep evolution parameters [units depend on calibration]	Dimensionless / GPa
q_3	Short-term creep evolution parameters [units depend on calibration]	Dimensionless / GPa
r	Pearson Correlation Coefficient	Dimensionless
R^2	Coefficient of Determination	Dimensionless
SD	Standard deviation	
S_s	Shear Strength	MPa
S_{stiff}	Stiffness parameter of shotcrete [units depend on calibration]	Dimensionless / GPa
t	Time / Curing age	Days or Hours
T_s	Tensile strength	MPa
VIF_i	Variance Inflation Factor	Dimensionless
w/c	Water-to-cement ratio	Dimensionless
x	Original observation	
z	Standardised z-score normalisation variable	
β	Strengthening parameter	Dimensionless

Symbol	Description	Unit / Type
β_E^{II}	Flow constant controlling stiffness evolution	Dimensionless
Δ	Change in stiffness (ratio of moduli, $E(t)/E_0$)	Dimensionless
$\Delta\varepsilon_a$	Change in axial strain	Dimensionless
$\Delta\sigma$	Change in axial stress	MPa
ΔL	Change in length (shrinkage)	mm
ε	Strain	Dimensionless
ε_a	Axial strain	Dimensionless
ε_l	Lateral strain	Dimensionless
ε_s	Shear strain or Axial shrinkage strain	Dimensionless
ε_v	Volumetric strain	Dimensionless
ε^{cr}	Creep strain	Dimensionless
ε^{el}	Elastic strain	Dimensionless
ε^{shr}	Shrinkage strain	Dimensionless
ε^{total}	Total strain	Dimensionless
ε^{vp}	Viscoplastic strain	Dimensionless
ϕ	Internal friction angle	Degrees (°)
σ	Normal stress	MPa
σ_c	Uniaxial compressive strength (UCS)	MPa
σ_{min}	Minimum principal stress	MPa
σ_{max}	Maximum principal stress	MPa
σ_t	Tensile Strength	MPa

Symbol	Description	Unit / Type
σ_1	Major principal stress	MPa
σ_2	Intermediate principal stress	MPa
σ_3	Minor principal stress or Confining pressure	MPa
μ	Mean value of a variable	
ν	Poisson's ratio	Dimensionless
$\bar{\upsilon}$	Mean Poisson's ratio	Dimensionless
υ_σ	Standard deviation of Poisson's ratio	Dimensionless
ρ_s	Spearman correlation coefficient	Dimensionless
τ	Shear stress	MPa

Chapter 1: Introduction

1.1 Context of the study

Shotcrete has emerged as a favoured ground support system because of its rapid application, rapid strength gain, and ability to adhere to irregular surfaces. These features allow prompt stabilisation of newly formed ground and minimise the risk of rock falls during excavation. Therefore, shotcrete is widely used in mining and tunnels because early support is critical for such underground civil engineering works (Yun et al., 2020a). The excellent adhesion of shotcrete to uneven geological surfaces allows it to form a continuous support layer that increases the strength of surrounding rocks and the tunnel (Liu et al., 2024).

Although conventional shotcrete has achieved considerable success, it still faces performance challenges under harsh underground conditions. Repeated loading causes rapid wear. Stress redistribution leads to structural instability. Moisture ingress, temperature changes, and chemical reactions further reduce its resistance and ability to provide proper support (Sjölander et al., 2023b). The problem is more serious in underground mining conditions. High stresses, continuous rock movement, and high mechanical demands place great stress on the ground support system. Thus, durable and reliable shotcrete is crucial for excavation stability (Toderaş and Danciu, 2020).

Most shotcrete innovations have resulted from laboratory research. This research has enhanced knowledge of hydration kinetics, early-age strength gain, fibre-matrix interactions, and the short- and long-term mechanical behaviour of shotcrete (Neville, 2012). While this research has been beneficial, the current knowledge base on shotcrete remains largely experimental. Very little effort has been made to translate laboratory findings into accurate prediction models (Liu et al., 2021; Sjölander et al., 2023b).

Recent developments in numerical modelling and multivariate regression have improved the ability to predict shotcrete performance and make mix design optimisation more efficient before field use. Nevertheless, incorporating experimental data into effective predictive models remains one of the most difficult tasks (Yun et al., 2020b). Current predictive models cannot account for all the interactions that determine the behaviour of shotcrete in underground conditions. Therefore, new modelling techniques and statistical methods are needed to predict shotcrete performance before application (Zhou et al., 2022).

This research addresses two key aspects of shotcrete development: aggregate optimisation and the use of fibres as a reinforcing material. Traditional shotcrete compositions are characterised by extensive use of natural sand as the fine aggregate. However, because of resource depletion, rising extraction costs, and growing environmental issues, there has been an ongoing quest for sustainable alternatives (Pilegis et al., 2016). Dolerite can serve as such an alternative because of its high strength, durability, and angular particle shape (Mwangi et al., 2022; Nkosi et al., 2022).

Dolerite aggregates are plentiful in South Africa, especially at the coal mines of Mpumalanga. The production process generates large volumes of dolerite waste, creating numerous environmental management challenges (Nkosi et al., 2022; Dlamini and Smith, 2024). Using dolerite waste in shotcrete can be seen as an eco-friendly method. Fibres are as important to the success of shotcrete construction as the aggregates are. Although conventional steel fibres provide tensile strength, they can corrode easily in such harsh environments (Neville, 2012). Xorex fibre, a cold-drawn and deformed low-carbon steel fibre, could serve as a good substitute. They have better fibre-matrix bonding, ductility, energy absorption, and shear resistance (Liu et al., 2021).

The novelty of the present study includes the combination of experimental materials characterisation, numerical analysis, and multivariate regression

to create a predictive model for dolerite-Xorex fibre-reinforced shotcrete. This predictive model assesses the short- and long-term behaviour of shotcrete in underground conditions. This predictive model is specifically tailored to engineering design in mining conditions characterised by low stress and dynamic loading.

1.2 Statement of the research problem

Current constitutive shotcrete models such as the Meschke Model (1996), the Schädlich and Schweiger Model (2014), and the Simplified Concrete Damage Plasticity (SCDP) Model (2017) have been developed and tested using one conventional shotcrete mix design. However, their predictive capacity is limited. For example, the Meschke Model predicts higher values for the rate of development of elastic modulus than what occurs. On the other hand, although the Schädlich and Schweiger Model provides good estimates of late-age compressive strength of shotcrete, it cannot predict creep in shotcrete well. Such prediction inaccuracies can lead to erroneous conclusions about the long-term performance of shotcrete in underground openings. The same applies to the predictions made by the SCDP model.

Although SCDP considers the effects of shrinkage, it still overestimates strain, resulting in conservative stress estimates and increasing the perceived risk of cracking. The supply of natural sands is becoming increasingly limited. At the same time, mining companies in Mpumalanga produce huge amounts of dolerite waste, creating both financial and environmental problems (Nkosi et al., 2022; Mokoena and Nkadimeng, 2023; Ubi et al., 2020). Reinforcing shotcrete with fibres has enhanced its strength and crack resistance. However, ordinary steel fibres can corrode in harsh underground environments. Xorex fibres could be a good alternative because of their high corrosion resistance (Liu et al., 2021).

No research studies have examined shotcrete containing dolerite aggregate and Xorex fibres. The behaviour of such a composite material therefore remains unknown from a mechanical point of view, including its time-

dependent behaviour and its performance in underground excavations. Furthermore, because experimental data are lacking, it is not possible to apply numerical modelling techniques or multivariate regression.

1.3 Aims and objectives of the research

The objective of this study is mainly to develop a dolerite- and Xorex fibre-reinforced shotcrete support system for underground excavation. To achieve this aim, the following objectives have been established:

- To investigate the influence of dolerite aggregates and Xorex fibres on the mechanical performance and strength development of shotcrete at curing ages of 4, 7, 28, and 56 days;
- To evaluate the stability and support performance of underground excavations reinforced with dolerite-Xorex fibre shotcrete using numerical simulation techniques; and
- To develop multivariate regression models for predicting the short-term and long-term behaviour of dolerite-Xorex fibre shotcrete based on key material and performance parameters.

1.4 Research questions

- What role do dolerite and Xorex fibres contribute to the strength performance of the shotcrete mixture after various curing periods?
- What impact does the inclusion of dolerite aggregates and Xorex fibres have on the structural stability of underground caverns when analysed using a numerical simulation?
- Are multivariate regression models capable of predicting the short- and long-term performance of dolerite-Xorex fibre reinforced shotcretes from experimental results?

1.5 Envisaged contribution of the research

This research aims to support sustainable mining and the development of sustainable shotcrete by utilising dolerite mine waste. Effective use of dolerite aggregates would reduce waste disposal needs.

Research on the low-dose use of Xorex steel fibres could serve as a stepping stone toward making fibre-reinforced shotcrete mixes more economical. If experimental tests are successful, it may be possible to create mixes with less fibre without affecting structural properties, making them economically feasible.

Creating multivariate regression models may improve predictions of shotcrete mix performance by identifying relationships between mix characteristics and curing age. Moreover, confirming experimental data using computational methods opens possibilities for investigating the suitability of available constitutive models for describing fibre-reinforced dolerite shotcrete. This experimental-numerical approach may help improve modelling techniques and support the development of future design procedures for underground support systems.

In summary, the outcomes of this study can support sustainable material use, economical shotcrete design, and more accurate prediction in mining underground tunnels.

1.6 Structure of the thesis

The thesis is structured into six chapters.

Chapter 1 introduces the study by providing background information on the research project. It identifies gaps in current knowledge and outlines the main objectives. It also highlights the significance of the research.

Chapter 2 reviews the literature on shotcrete, fibre reinforcement, modelling approaches, and performance evaluation methods.

Chapter 3 details the methodology, covering laboratory experiments, numerical modelling, multivariate regression analysis and the approach to predicting results.

Chapter 4 details the development and mechanical properties of dolerite-Xorex fibrous shotcrete. This chapter studies the effect of dolerite aggregates and Xorex fibres on the mechanical properties of the shotcrete.

Chapter 5 presents the numerical models developed for dolerite-Xorex fibre-reinforced shotcrete.

Chapter 6 presents the multivariate regression models created from the dolerite-Xorex fibre-reinforced shotcrete.

Chapter 7 highlights the principal outcomes of the study. It outlines recommendations for engineering practice. It proposes future research to advance shotcrete technology.

Chapter 2: Literature review

2.1 Introduction

The main objective of this research is to design and analyse a dolerite-Xorex fibre-reinforced shotcrete support system for underground mine workings. This research uses experimental and computational analyses, as well as multivariate regression models, to assess the feasibility of including dolerite and Xorex fibres. Optimising the performance characteristics of the support system is one of the objectives of this research. At the same time, development of prediction models is another important objective of this research.

To meet this objective, this chapter critically reviews the literature on shotcrete mix formulation design. It also looks at the significance of shotcrete support in underground excavations. It critically analyses the influence of waste aggregate and fibres on the mechanical behaviour, deformation behaviour, durability, and performance of shotcrete support systems. The emphasis will be on the potential use of dolerite aggregates and Xorex fibres.

Furthermore, the chapter presents a thorough investigation of the failure mechanisms of traditional shotcrete mixes. It reviews their weaknesses and flaws in terms of structural integrity and material characteristics. This still affects the efficiency of conventional shotcrete support systems when applied in underground environments. Moreover, this literature review focuses on the development of multivariate regression and numerical models used to forecast shotcrete performance. This contributes to the process of design and engineering of shotcrete in underground excavations. Based on this literature review, the chapter outlines several key drawbacks of the current state of the art.

2.1.1 Overview of shotcrete composition

Shotcrete composition is an important factor affecting its mechanical properties. Shotcrete composition also affects the development of numerical and multivariate regression models to predict its behaviour under various loadings and environmental conditions, especially in underground mining. According to Holmgren (1998), aggregates, water, and cement are the major components of shotcrete. Figure 2-1 shows an example shotcrete mixture (Mahoney, 2014).

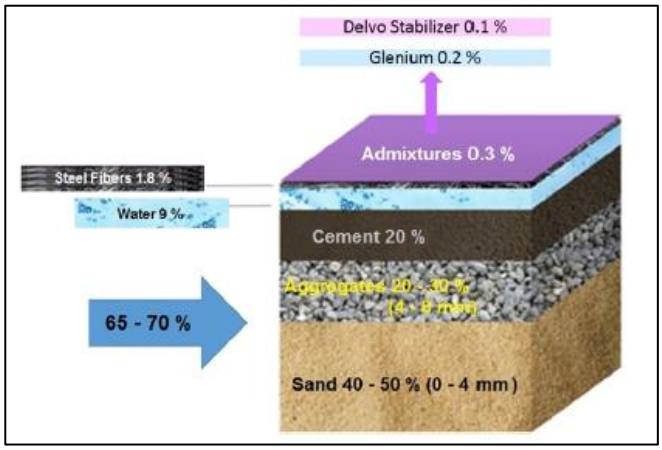


Figure 0-1: Components of a typical sprayed concrete mix, in (%), established based on mass values (Mahoney, 2014)

The following sections provide a detailed examination of the main components of shotcrete.

2.1.1.1 Cementitious material

Cement is an essential element in shotcrete; it acts as a binder that binds the mixture and facilitates the hydration reaction, which provides strength to the shotcrete (Neville, 2012). Cement hydration determines the strength, adhesion, and durability of shotcrete (Neville, 2012). These characteristics make shotcrete useful as a ground support mechanism in underground excavation (Yun et al., 2020).

Ordinary Portland Cement (OPC) remains the standard cement in shotcrete because of its rapid setting and strong early strength development. These

properties make it ideal for the immediate support required in tunnelling and mining (Sjölander et al., 2023b). However, relying solely on OPC is no longer sufficient. Today, demand for durability and sustainability has driven the adoption of blended systems. Additives such as silica fume, fly ash, and ground granulated blast-furnace slag (GGBS) have become essential in enhancing the mechanical properties of shotcrete. These additives refine the cement matrix by reducing porosity and increasing the resistance of shotcrete to exposure to aggressive chemicals (Moyo et al., 2022; Neville, 2012). While cement materials act as the glue that provides strength and cohesion to shotcrete, aggregates form the solid framework that supports and enhances the overall mix. The next section explores aggregates in more detail.

2.1.1.2 Aggregates characteristics

Aggregates account for about 60 to 80 % of the shotcrete mix design (Neville, 2012). They form a solid framework because they make up a large portion of the shotcrete composition (Kalra and Mehmood, 2018). Aggregate characteristics influence shotcrete behaviour (Fathi, 2014). These characteristics include strength, flexibility, durability, and load-carrying capability. Sand, gravel, and crushed aggregate are the most used aggregates (Rameshwar and Shrikant, 2017). The physical and chemical properties of aggregates affect workability, packability, load-carrying capacity, and mixing efficiency (Ubi et al., 2020; Ponzi et al., 2021). Fine aggregates create a smoother mix and improve the finish, while coarse aggregates increase compressive strength, reduce shrinkage, and enhance the resistance to deformation of the shotcrete (Seńczuk et al., 2022; Qu et al., 2024). Selecting the right aggregate is vital in tunnelling and underground applications as it determines whether the shotcrete will perform reliably or fail (Kalra and Mehmood, 2018; Fathi, 2014).

Although various aggregates can be used, crushed stone has gained significant attention because of its superior mechanical contribution to shotcrete.

Xie (2024) highlights a noticeable change in shotcrete technology, with more projects opting for crushed rock aggregates over natural sand. This is more than just a technical improvement. Crushed rock improves shotcrete's toughness and durability while also benefiting the environment by reducing demand for natural sand (Serati et al., 2022). Building on this, the current review focuses on crushed coarse dolerite, specifically recycled dolerite sourced from Mpumalanga coal mine fields. Mining operations typically regard this material as waste (Van Niekerk and Vermeulen, 2004). Repurposing waste dolerite in shotcrete is not only practical but also a smart, sustainable option. Dense, angular, crystalline structure of dolerite offers significant mechanical and durability advantages (Dobiszewska and Beycioğlu, 2020).

Researchers such as Jajbhay (2020), Oden et al. (2018) and Khan et al. (2023) have investigated how concrete performs when dolerite replaces traditional sand aggregates. For instance, Oden et al. (2018) reported compressive strengths ranging from 34 MPa to 56 MPa at 14 and 28 days, respectively. Additionally, concrete mixes with dolerite aggregates exhibited very low water absorption (0.14–1.59%) and demonstrated remarkable durability. These are the qualities desirable in a structural aggregate. Jajbhay (2020) found that concrete beams made with dolerite coarse aggregate withstood shear forces better than those made with sand. Khan et al. (2023) reported that concrete containing up to 75% dolerite aggregate reached about 57.6 MPa compressive strength after 28 days. Dolerite aggregate concrete performed better at higher temperatures than limestone aggregate concrete. This shows that dolerite is very strong and can withstand higher temperatures, making it ideal for use as an aggregate in tough underground conditions. Aggregate choice plays a vital role in determining shotcrete compressive strength and elastic modulus (Kalra and Mehmood, 2018).

The dense, crystalline nature and angular particles of dolerite enable better packing and bonding within the cement matrix. This results in higher compressive and tensile strength (Fathi, 2014; Singh et al., 2016). Ubi et al. (2020) reported a compressive strength of 36.4 MPa after 28 days for concrete with fine dolerite aggregate. This compares with the 28-day compressive strength of concrete with natural sand, which was 32.2 MPa.

Other research supports these findings (Rameshwar and Shrikant, 2017; Reddy and Reddy, 2007). Dolerite clearly showcases advantageous characteristics as a fine aggregate. Additionally, dolerite aggregates display pozzolanic activity, reacting with calcium hydroxide in the cement to form additional calcium silicate hydrate (C-S-H). This process densifies the matrix and enhances long-term durability (Abazi and Suloodja, 2025).

The angular character of dolerite aggregates increases tensile and flexural strength and strengthens the aggregate-cement interface transition zone. It prevents crack formation and reduces porosity (Singh et al., 2016; Dobiszewska and Beycioğlu, 2020). According to Khan et al. (2023), coarse dolerite aggregates enhanced the thermal stability of high-density concrete when subjected to temperatures ranging from 200°C to 1200°C. Ouda (2015) reported similar results for compressive strength, thermal stability, and radiation shielding within the specified temperature range. Eze and Orie (2013) established the compressive strength, low porosity, and durability of dolerite. These properties make it an ideal aggregate for construction. Nonetheless, dolerite is angular.

Additionally, Đokić et al. (2020) established that dolerite aggregates were suitable for pavement material because of their ability to resist fragmentation and wear. Despite these positive mechanical and durability features, the studies covered only traditional concrete and pavement, without considering dolerite-aggregate fibre-reinforced shotcrete in underground excavations. This clearly indicates a major research gap regarding dolerite aggregates in shotcrete applications.

Coal mining produces large quantities of gangue waste, with studies suggesting that gangue waste constitutes about 15% to 20% of coal production (Ulyeva and Yemelyanova, 2024). Rouhani et al. (2023) noted that the current practice of stockpiling mining waste on the surface is linked to many environmental and geotechnical issues. Such issues include land overutilization, air pollution, water pollution, landslides, and self-ignition fires. To address this problem, Serati et al. (2022) showed that waste materials, such as crushed glass, can be used in shotcrete as an alternative to fine sand aggregates.

Research by Alcayaga et al. (2024) showed that coal gangue can be used in shotcrete as a fine-aggregate substitute. Mixes made with these materials show equivalent or better mechanical properties than traditional mixes at early ages and at 28 days of curing. As noted by Fan et al. (2021), graded tailings yield the highest strength among other materials in wet-mix shotcrete. Moreover, Xiao et al. (2020) found that crushed inactive coal gangue is an efficient material for producing shotcrete mixes. In addition, using such materials helps reduce the ecological footprint associated with raw material acquisition and waste disposal. According to Polat and Ozel (2024), ferrochrome slag aggregates improve shotcrete efficiency and provide radiation protection. Past research has shown that different types of mining waste materials can enhance shotcrete performance. However, little work has examined the performance of dolerite mine waste in shotcrete.

Mine waste aggregate can improve the performance and sustainability of shotcrete; however, it has limitations in brittleness and post-cracking performance. Fibre reinforcement is needed to mitigate these problems by increasing ductility, toughness, and energy absorption. The next chapter discusses fibre reinforcement in shotcrete.

2.1.1.3 Fibre reinforcement

For years, steel fibres have been the main fibre used for shotcrete reinforcement, offering higher tensile strength, controlling cracks, and maintaining shotcrete integrity after cracking (Alsaif et al., 2019). Their stiffness and ductility make them well-suited for tunnelling in shallow underground mining (Li et al., 2025). However, steel fibres have shortcomings: they are prone to corrosion, which can cause shotcrete to deteriorate rapidly (Thomas, 2018; Alsaif et al., 2019). This problem becomes more pronounced in underground conditions in South Africa. Exposure to moisture, heat, and corrosive chemicals accelerates shotcrete degradation. It results in higher maintenance needs and decreased efficiency (Ghorbani et al., 2023).

These limitations have prompted a search for fibres that can withstand heat, resist fatigue, and avoid corrosion. Xorex is a hooked-end steel fibre and has emerged as a contender because of its toughness, chemical resistance, reduced carbon footprint, and strong crack-bridging ability (Fibsol, 2023). The configuration and bonding of these fibres play a critical role; hooked ends improve grip and enhance mechanical performance (Alsaif et al., 2019). While Xorex fibres have performed well in conventional concrete applications, their effectiveness in shotcrete remains largely underexplored. Investigating their use could address a significant knowledge gap and offer South African mining and tunnelling sectors durable, environmentally friendly reinforcement options.

With improved bonding and inherent corrosion resistance, Xorex fibres present a promising alternative for long-lasting shotcrete (Fibsol, 2023). Introducing this fibre is not just about creating stronger concrete; it marks a move toward more efficient and sustainable practices throughout civil and mining engineering. While fibres are crucial for enhancing the mechanical performance of shotcrete, water in the mix is equally important. The next section discusses water use and its influence on shotcrete properties.

2.1.1.4 Water-to-cement ratio

Water is central to shotcrete production; it drives hydration, which influences strength and determines shotcrete workability and durability. Hydration is a chemical reaction that occurs between water and cement (Neville, 2012). This reaction begins when water molecules interact with cement compounds to produce calcium silicate hydrate (C–S–H) and other hydration products (Neville, 2012). These hydration products bind the aggregates and fibres, giving shotcrete strength and cohesion (Kosmatka, 2011).

The water-to-cement ratio of shotcrete typically ranges from 0.35 to 0.50 (Neville, 2012). This range ensures complete hydration, sufficient strength development, and low permeability (American Concrete Institute, 2016; Jolin and Beaupré, 2005).

Water quality is just as crucial as the water-to-cement ratio. The water used should be clean to ensure proper hydration. This water should be free of salts, oils, and organic contaminants to ensure proper strength gain in shotcrete (Liu et al., 2024). The water-to-cement ratio determines shotcrete workability and strength. But this ratio alone cannot guarantee proper workability. Superplasticisers are thus added to improve workability. This is done without adding water or losing strength.

2.1.1.5 Superplasticizer

Superplasticisers are essential in high-performance shotcrete. They improve workability while maintaining a low water-to-cement ratio, resulting in easier pumping, smoother spraying, and reduced rebound (Bazli and Abolfazli, 2020; Yurdakul and Rieder, 2015). Improved fluidity makes shotcrete denser and stronger and provides better adhesion, especially in confined or complex areas (Aïtcin and Flatt, 2016).

Schutz (2010) emphasised that superplasticisers act as catalysts by intensifying the hydration reaction during the first 12 h of shotcrete

application. Adding superplasticiser to shotcrete accelerates early strength development and improves adhesion to the application surface. Additionally, chemical admixtures ensure that shotcrete can quickly fulfil its support role, which is critical in reducing re-entry times while providing prompt stabilisation of underground structures. This, in turn, enhances the safety, operational efficiency, and machinery protection of workers (Schutz, 2010). Rapid setting and early strength gain benefit underground excavations where immediate structural reinforcement is essential.

2.2 Mechanical properties of shotcrete

The mechanical strength of shotcrete is a descriptive property of its performance (Zhao et al., 2021). Shotcrete is used in underground tunnels as a primary or secondary lining to support the surrounding rock mass. This minimises ground movement and ensures the safety of underground excavations and their occupants (Uomoto and Sugiyama, 2006). In slope stabilisation, shotcrete acts as a protective layer that controls rock erosion and sustains slope stability under diverse environmental and loading conditions (Khan et al., 2023). Mechanical properties can be assessed through compressive, tensile, and shear strengths as well as elastic modulus. These properties are essential for preparing shotcrete for real-world applications. The following sections present these properties in detail. The mechanical strength of shotcrete is a descriptive property of its performance (Zhao et al., 2021).

Shotcrete is used in underground tunnels as either a primary or secondary lining to support the surrounding rock mass. This minimises ground movement and ensures the safety of underground excavations and their occupants (Uomoto and Sugiyama, 2006). In slope stabilisation, shotcrete acts as a protective layer that controls rock erosion and sustains slope stability under diverse environmental and loading conditions (Khan et al., 2023). Mechanical properties can be assessed through compressive, tensile, and shear strengths, as well as elastic modulus. These properties

are essential for preparing shotcrete for real-world applications. The following sections present these properties in detail.

2.2.1 Compressive behaviour of shotcrete

The compressive strength of shotcrete is its ability to resist compression failure. The American Concrete Institute (2016) reported that, at 28 days of curing, unreinforced shotcrete is expected to reach a compressive strength of about 30–40 MPa for underground excavations. When shotcrete is intended for use as a permanent lining, it must exceed 40 MPa. To estimate compressive strength, the American Concrete Institute (2016) provides the formula presented below:

$$F_c = \frac{P}{A} \tag{2.1}$$

Where F_c is the compressive strength in MPa

P is the load applied to the shotcrete at failure (N)

A is the cross-sectional area of the shotcrete specimen in mm^2.

Compressive strength is fundamental to developing numerical models and multivariate regression models for shotcrete. It defines the entire stress–strain response, influencing both the elastic and plastic behaviour of shotcrete. From the onset of loading, compressive strength dictates the material's response, beginning with linear elasticity and transitioning to plastic deformation once the threshold is surpassed (Mindess and Young, 2003; Mehta and Monteiro, 2014). This property also forms the basis for modelling structural failures such as cracking, strain hardening, or post-peak softening (Kotsovos and Pavlovic, 2013).

The Uniaxial Compressive Strength (UCS) and Triaxial Compressive Strength (TCS) tests determine the mechanical parameters needed to assess shotcrete performance and calibrate elasto-plastic numerical models in support design for underground excavation. The basic compressive strength is determined by UCS testing, which also allows the determination of Young's modulus (E) and Poisson's ratio (ν). These two

parameters can be obtained from the elastic part of the stress–strain curve that describes stiffness and lateral deformability (Clark et al., 2008). UCS provides another parameter, the strengthening parameter (β), which indicates how quickly strength increases with curing time. Since it is an unconfined test. UCS shows naturally evolving strength resulting from hydration; hence, it is widely used in time-dependent numerical models, such as those proposed by Meschke (1996) and Schädlich and Schweiger (2014).

Conversely, TCS testing assesses shear behaviour under confinement conditions. Triaxial results allow Mohr-Coulomb analysis, a geotechnical approach used to forecast the failure characteristics of rock, soil, and shotcrete under stress based on the relationship between shear strength, cohesion, normal stress, and internal friction angle (Das and Sobhan, 2014). This technique is commonly used in underground engineering projects to assess excavation stability. Mohr–Coulomb analysis determines cohesion (C) and internal friction angle (ϕ), parameters controlled by cement bonding, fibre anchorage, and aggregate interlock. Shotcrete with fibre inclusion usually has higher cohesion because cracking is better bridged (Bryne et al., 2014). These parameters from the UCS and TCS tests, which include $E, \nu, C, \phi,$ and β, are crucial for numerically defining shotcrete performance (Neuner et al., 2017). This study used these tests to accurately capture the early-age strength development, shear resistance, and long-term stability of the proposed mix. They provide a reliable basis for performance prediction in underground support applications.

2.2.2 Tensile behaviour of shotcrete

Tensile strength in shotcrete refers to its ability to withstand tensile forces and prevent cracking under bending or tensile stresses. According to the American Concrete Institute (2013), the tensile strength of plain concrete commonly used in underground applications typically ranges between 2 MPa and 5 MPa at 28 days of curing (American Concrete Institute, 2016).

The ultimate tensile strength of shotcrete can be estimated as follows (Neville, 2012):

$$\sigma_t = \frac{F}{A} \tag{2.2}$$

Where σ_t = tensile strength (in Pascals, MPa, or N/mm²)

F = maximum load applied before failure (in newtons, N)

A = original cross-sectional area of the specimen (in mm²)

Tensile strength is essential in underground excavations because it indicates how effectively shotcrete can endure harsh conditions such as seismic events, blasting vibrations, or changing rock stresses (Bernardo, 2015; Thomas, 2018). When shotcrete possesses high tensile strength, it can withstand tension, reduce cracking, and maintain the stability of underground structures (Jolin and Beaupré, 2005; American Concrete Institute, 2016). This property is important in shallow underground tunnels and mines, where ground movement and fluctuating stress patterns are common. Shotcrete should provide tensile capacity in underground conditions. It should be ductile enough to absorb energy from ground movement. These properties contribute to excavation stability during ground movement (Sjölander et al., 2023b).

2.2.3 Shear strength of shotcrete

Shear strength refers to how effectively shotcrete resists forces that try to make it slide or separate along its layers within itself (Zhao et al., 2021). This property is more than just a technical aspect; it plays a crucial role in assessing the stability of rock slopes and underground tunnels. In such environments, shear stresses often contribute most to failure (Zhao et al., 2021). According to American Standard Testing Methods (2012), which provides standards for fibre-reinforced shotcrete, typical shear strengths range from 2 MPa to 5 MPa. The specific value depends on the type and quantity of fibre used, as well as the mix design (ASTM C1550, 2012). The

shear strength of shotcrete can be estimated using the following empirical relationship (Mindess and Young, 2003):

$$\tau = C + \sigma \, tan\phi \quad (2.3)$$

Where τ is the shear strength at failure,

σ is the normal stress,

C is the cohesion intercept, and

ϕ is the angle of internal friction.

Normal weight shotcrete is made with natural aggregates such as crushed stone, gravel, or sand, and typically has a density between 2200 kg/m^3 and 2500 kg/m³ (Neville, 2012; Mindess and Young, 2003). Shear strength plays a crucial role in understanding how shotcrete fails. As shotcrete moves from elastic behaviour into plastic deformation or complete failure, its shear strength defines the limits. Accurate modelling of this behaviour can predict whether shotcrete will deform, crack, or collapse. This is essential for maintaining safe and structurally sound shotcrete linings in underground settings (Zhao et al., 2021).

2.2.4 Elastic response of shotcrete

Elastic modulus, also known as modulus of elasticity, indicates how stiff shotcrete is; it shows how much shotcrete will stretch or compress when a load is applied (Neville, 2012). This is important because shotcrete is expected to withstand heavy stresses while maintaining its integrity (Neville, 2012; Mindess and Young, 2003).

According to the American Concrete Institute, the elastic modulus of shotcrete ranges from 20 GPa to 40 GPa. This range depends on mix design, aggregate size and type, cement content, fibre addition, and curing conditions (American Concrete Institute, 2016; Jolin and Beaupré, 2005). The elastic modulus is defined by the relationship between applied stress and resulting strain as follows (American Concrete Institute, 2016):

$$E = \frac{\sigma}{\varepsilon} \quad (2.4)$$

Where E = elastic modulus of shotcrete (GPa)

σ = applied stress (N/mm² or MPa)

ε = resulting strain (dimensionless)

The elastic modulus describes how shotcrete responds initially under stress in the linear elastic range. With the elastic modulus value, it is possible to estimate how much shotcrete will deform and how stress will be distributed throughout (Neuner et al., 2017). To gain a comprehensive overview of shotcrete's mechanical performance, it is important to understand tensile, shear, and compressive strength. This allows the development of accurate numerical and multivariate models that can help explain shotcrete performance in real-world applications.

2.2.5 Typical shotcrete deformation

Shotcrete used in tunnel linings goes through three key stages as it manages ground pressure; each stage highlights the material's performance. The process starts with elastic deformation, followed by plastic yielding, and ends with a post-yield elastic phase. The ingredients and properties of shotcrete influence its capacity to withstand stress, minimise cracking and retain structural integrity in difficult underground conditions. Figure 2-2 depicts these three phases of shotcrete deformation, adopted from Moritz (2011).

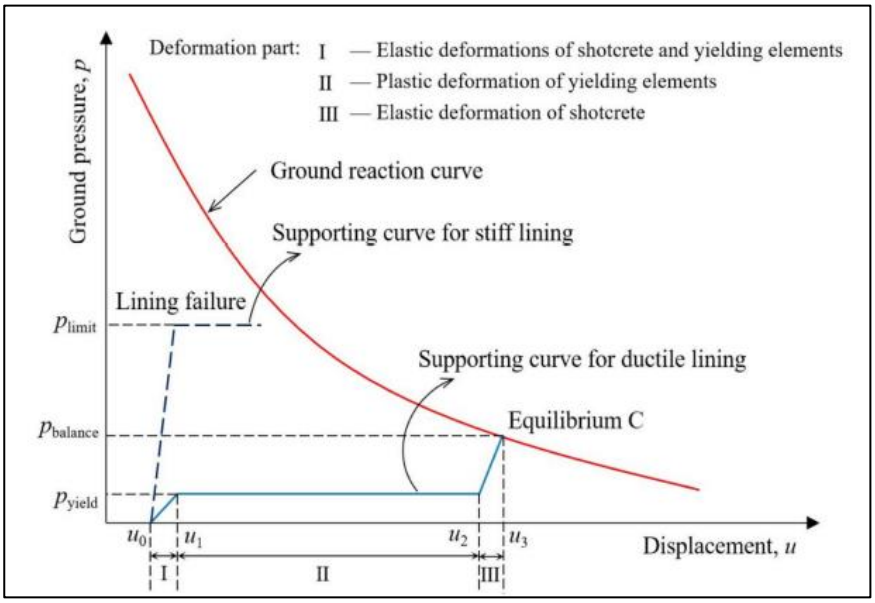


Figure 0-2: Types of shotcrete deformation experienced upon application in underground excavations

During the first phase (I), shotcrete deforms elastically. This simple, reversible process involves only minor, non-permanent changes. At this point, the mix design is critical, as the ingredients can increase the elastic modulus and reduce the risk of early cracking (Liu et al., 2021). If the shotcrete is strong and dense, it resists permanent damage from these initial stresses.

The second phase (II) introduces more complexity. The support structures begin to yield and deform plastically, while the shotcrete may still behave elastically. This phase is particularly challenging for shotcrete in shallow underground tunnels with ground pressure, as it must maintain its cohesion while the environment changes (Beer, 2015). Flexural toughness and ductility are valuable in this phase, allowing the shotcrete to absorb movement without breaking apart or detaching.

In the third phase (III), the supporting structures have fully yielded. The shotcrete lining takes on the load by itself, returning to an elastic response at a higher displacement. At this point, long-term durability and heat resistance become crucial, especially in high-temperature tunnels. Using high-density, thermally stable aggregates, such as dolerite, makes a

significant difference. Dolerite helps to prevent crack formation and propagation (Shah et al., 2021). Residual strength, shrinkage resistance, and a robust microstructure all help prevent spalling and other long-term damage.

Together, these three phases outline how shotcrete behaves as ground pressure and temperature increase. Optimising the mix and mechanical properties at every stage is essential to keep tunnel linings safe and durable, even under difficult geological or thermal conditions. Thermally stable aggregates, fibre reinforcement, and carefully chosen cementitious materials help shotcrete linings perform more effectively. The following section examines the factors that lead to shotcrete deterioration.

2.3 Causes of shotcrete degradation

Several researchers (e.g., Liu et al., 2021; Cui et al., 2019; Dong et al., 2020; and Xie et al., 2024) have spent years exploring the causes of shotcrete deterioration. They have identified two primary factors: mechanical attack and chemical attack (Galan et al., 2019). Loading decreases the critical engineering characteristics of shotcrete. Loading affects compressive, tensile, flexural, shear, and bond strength, especially under high temperatures, stresses, shrinkage, and cracking (Liu et al., 2021). Chemical attack, as described by Galan et al. (2019), involves slow degradation caused by chemical agents such as sulphates, chlorides, and acids that penetrate the cement matrix. This causes expansion, cracking, reduced strength, and a shorter lifespan.

2.3.1 Mechanical attack

Shotcrete is widely recognised as an effective solution for supporting underground tunnels because of its high resistance and durability. However, shotcrete's long-term durability is critical to maintaining tunnel structural integrity and functionality over its service life (Beer, 2015). Field studies

have shown that the service life of shotcrete can be compromised by reductions in shear, tensile, compressive, and flexural strength (Sjölander et al., 2023a; Sjölander and Ansell, 2022). Mechanical failure of shotcrete linings is among the most frequently encountered issues in underground tunnels. This is primarily due to errors in shotcrete application and inherent material deficiencies. Improper mixing or spraying techniques can cause uneven application, while substandard materials, incorrect water-cement ratios, or poorly graded aggregates can significantly undermine strength and durability (Marcher, 2017). Temperature is an even greater challenge in underground environments.

When exposed to high temperatures, the mechanical properties of shotcrete, such as compressive, tensile, and flexural strength, as well as its bond with rock substrate, are negatively affected. This is mainly because heat accelerates hydration, leading to shrinkage, and breaks down hydration products that are responsible for strength development. According to Liu et al. (2021), compressive strength initially rose at curing temperatures from 40°C to 100°C. Nevertheless, compressive strength decreased after one week at these temperatures. In contrast, splitting tensile strength consistently declines as the temperature increases (Beer, 2015).

Bond strength also shows unfavourable behaviour when shotcrete is exposed to elevated temperatures. Cui et al. (2019) found that adhesion between shotcrete and rock improves with moderate heating (< 40°C) but declines again beyond a certain point (> 60°C).

Dong et al. (2020) reported that thermal exposure causes surface cracking in shotcrete. It also forms a powder-like matrix, reducing the mechanical properties of shotcrete. In addition, Pan et al. (2020) reported that high temperatures cause rapid but disorganised hydration reactions. This leads to poor-quality hydration products and shrinkage cracks in shotcrete. According to Xie et al. (2024), temperatures above 150 °C cause extensive

degradation of the shotcrete microstructure. Calcium hydroxide and wollastonite decompose to calcium oxide.

Microstructural analysis supports these findings. Cui et al. (2019) found that larger pores develop in the shotcrete matrix at elevated temperatures, and these pores lower strength. Liu et al. (2021) used Computer Tomography (CT) scans to show particles breaking apart and pores expanding at 40–60°C.

Figure 2-3 shows how temperature plays an important role in shotcrete failure during mechanical loading. As temperature increases, sand shotcrete starts cracking and failing in a brittle manner. Increased temperature causes shrinkage and causes cracking in the matrix. It decreases matrix cohesion. Therefore, sand shotcrete loses its load-carrying ability as temperature increases.

Dolerite aggregates contain dense minerals such as plagioclase, pyroxene, and olivine (Đokić et al., 2020). These aggregates have very low coefficients of thermal expansion (i.e., 6.0 x 10^{-6}/°C and 9.7 x 10^{-6}/°C) and provide thermal stability (Brooks, 2015). Thus, crack formation and propagation become difficult at high temperatures in dolerite aggregates. This ensures matrix cohesion and mechanical strength in shotcretes.

Elevated temperatures severely weaken sand-based shotcrete, making it much more susceptible to damage. In contrast, dolerite-based shotcrete resists both heat and mechanical attack, offering far superior durability and thermal resistance (Shah et al., 2021).



Figure 0-3: Failure form of sand-based shotcrete specimen

Short-term heat exposure may increase shotcrete strength; however, excessive heat can degrade its mechanical properties. Mechanical attack is a major factor in shotcrete breakdown; however, chemical attack is just as significant over time, particularly when it involves corrosion of steel reinforcement. Since this study explores replacing steel fibres with corrosion-resistant fibres, the following section examines steel fibre corrosion and its implications for shotcrete durability.

2.3.2 Steel corrosion

Steel fibre-reinforced shotcrete (SFRC) is essential in underground tunnel construction, where it supports rock faces and helps stabilise openings under challenging conditions. Adding steel fibres increases the resistance of shotcrete to bending, deformation, and cracking, whether the loading is static or dynamic (Nordstrom, 2005). Kaufmann (2014) highlighted a significant drawback of steel fibres: they are susceptible to corrosion. Once corrosion begins, shotcrete durability decreases rapidly, as illustrated in Figure 2-4 (Galan, 2019).



Figure 0-4: Example of steel fibre corrosion that eventually affects the durability of shotcrete lining

Corrosion occurs when steel fibres react with water or environmental chemicals such as chlorides, acids, or even elevated-alkalinity environments. Galan et al. (2019) observed that aggressive chemical conditions, particularly those rich in chlorides, destroy the passive layer that normally shields steel. Over time, this causes microcracking and spalling, and eventually sections of shotcrete begin to delaminate (Liu et al., 2021). As corrosion progresses, the steel fibres lose their reinforcing capability. This ultimately reduces the load-bearing capacity of the shotcrete lining and shortens its service life (Skarżyński and Suchorzewski, 2018).

This problem is especially serious in South African underground mines. Groundwater, acidic mine water, and salinity accelerate steel fibre corrosion. This reduces the mechanical properties of shotcrete layers (Long, 2024). Nitschke and Winternberg (2016) stressed that corrosion cannot be underestimated. They proposed using corrosion-resistant reinforcements, corrosion-protection coatings, controlling crack widths, and proper material choice. Kaufmann (2014) added that using low-absorption

aggregates, such as dolerite, can increase resistance to chemical corrosion. However, this method cannot solve corrosion alone.

Therefore, it is crucial to test non-corrosive fibres to extend the service life of shotcrete (Galan, 2019). The goal is to produce shotcrete that retains its strength and reliability even in the most chemically aggressive underground environments (Alsaif et al., 2019).

2.4 Failure modes of shotcrete

Shotcrete can fail in many ways under mechanical, thermal, or chemical stresses (Uotinen, 2011; Hoek and Brown, 2018). To make shotcrete linings last in underground excavations, it is essential to understand exactly how and why these failures occur. Various factors affect shotcrete performance. These factors include mixture design, aggregate type, fibre type, curing, and the condition of the surface on which it is applied. These aspects affect both shotcrete's energy absorption capacity and its deformation before failure. This study focuses on compressive and tensile failures. These two failure modes are fundamental in defining the mechanical behaviour of shotcrete in underground mining applications (Kong and Garshol, 2015).

2.4.1 Compressive failure

Compressive failure occurs when compressive stress exceeds the compressive strength of shotcrete (Stacey, 2009). Compressive failure is most observed in three specific locations within an underground excavation (Uotinen, 2011), as depicted in Figure 2-5:

1. On the shoulders and roof of the excavation;
2. When there is continuous load bearing on the excavation walls; and
3. At the excavation face.

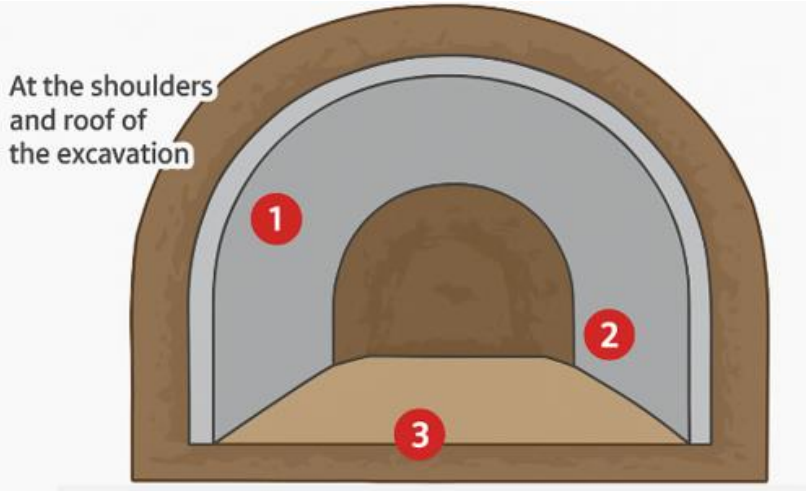


Figure 0-5: Compressive strength failure at three common areas

The components and proportions used in the shotcrete mix directly influence its ability to withstand crushing forces and maintain structural integrity under pressure. The main variables involved are the type and grading of aggregates, the amount of cement, the water-cement ratio, and the inclusion of fibres or admixtures (Kong and Garshol, 2015).

Beyond mix optimisation, proper curing and environmental control are crucial in reducing compressive failure. By curing shotcrete correctly through maintaining consistent temperature and humidity, this minimises early shrinkage and the formation of microcracks. Thermal management is also significant. Methods like selective cooling or dehumidification help prevent issues such as spalling and strength loss caused by high pore pressure (Liu et al., 2021; Luo et al., 2020). Controlling carbonation and porosity is equally important, since increased pores and rapid temperature changes accelerate strength deterioration (Liu et al., 2021). Ensuring appropriate layer thickness, even application, and thorough compaction of shotcrete helps distribute stress more evenly and minimise microcrack development (American Concrete Institute, 2016; Stacey, 2009). Overall, high-performance shotcrete provides the best defence against compressive failure and supports the durability of underground structures (Craw et al., 2025).

2.4.2 Tensile failure

Tensile failure in shotcrete occurs when the material can no longer withstand pulling forces, causing cracks, delamination, or spalling (Uotinen, 2011). This is particularly critical in underground mining where shotcrete faces various stresses and harsh environments. By design, shotcrete has much lower tensile strength than compressive strength, so cracks usually form where stress concentrates. Shrinkage, temperature changes, and poor adhesion to the base enhance the problem. High curing temperatures accelerate hydration, but this often leads to disordered hydration products and reduces tensile strength (Liu et al., 2021; Xie et al., 2024). If shotcrete does not bond sufficiently to the rock substrate, cracks can form rapidly (Cui et al., 2019).

To address this, researchers (Xie et al., 2024; Cui et al., 2019; Galan et al., 2019) have investigated methods to enhance the tensile strength and durability of shotcrete. Incorporating fibres controls cracking in shotcrete by preventing extension and improving resistance to tensile failure (Dong et al., 2020). Supplementary cementitious materials like silica fume and fly ash refine the microstructure, reduce shrinkage, and enhance matrix cohesion (Beer, 2015). High-performance fibres included in shotcrete mix design optimisation can help prevent tensile failure, which in turn improves shotcrete serviceability over longer periods when working underground. Factor of Safety (FoS) is a method used in engineering practice to check the safety and reliability of the support system. FoS is the ratio of resisting forces to driving forces acting on the support system (Das and Sobhan, 2014). The next section discusses the factor of safety as experienced in shotcrete lining.

2.5 Factor of safety in shotcrete lining

Factor of Safety (FoS) is essential for protecting underground excavations. It indicates whether the shotcrete can withstand loads from the surrounding rock mass (Hoek and Brown, 2018). The FoS for shotcrete linings can be

determined from factors such as compressive strength, tensile strength, thickness and the applied loads (Stille and Holmgren, 2015). Most conventional FoS design methods treat shotcrete as a brittle, isotropic, cement-based material, with strength determined almost exclusively by UCS.

The mechanical behaviour of conventional shotcrete indicates that roof FoS increases over time in tunnel linings (Holmgren, 2015). The first week after application is particularly critical, as it determines re-entry into a tunnel (Saw, 2015). At 4 days, the UCS reaches only about 25–30% of the 28-day design strength, leading to a FoS of 1.2–1.4 (Naseri and Bahrani, 2019). At this early stage, shotcrete alone provides little reliability, so additional support is still required. This additional support can be in the form of rock bolts and wire mesh.

By 7 days, the UCS rises to approximately 40–50% of the 28-day value, increasing the FoS to 1.5–1.7 (Vandewalle, 1998). At this point, supplementary supports like rock bolts or lattice girders are still needed because the excavation is not stable enough to support itself (Kompen et al., 2017).

At 28 days, shotcrete is expected to achieve its design strength, which serves as the standard benchmark for structural assurance (American Concrete Institute, 2016). The FoS reaches 2.0–2.3, which is generally sufficient for most tunnel geometries and ground stress conditions (Oreste et al., 2019).

Strength development continues beyond this point; at 56 days, ongoing hydration and microstructural adjustments further increase the UCS, with the FoS reaching about 2.3–2.5 (Thomas, 2018). This later strength gain enhances long-term durability and fracture resistance, which are essential for shallow underground tunnels. Although FoS has been measured for conventional shotcrete, no comprehensive method exists to quantify FoS for dolerite-Xorex fibre shotcrete over short- and long-term periods.

FoS can also be evaluated using Ground Reaction Curves (GRCs). In this research, GRCs were utilised to analyse the final convergence and the corresponding FoS values. Final convergence is discussed because it determines the limits related to the various FoS ranges. Therefore, the next section discusses the GRC in terms of final convergence.

2.5.1 Ground reaction curve of shotcrete

The Ground Reaction Curve (GRC) is fundamental in assessing the interaction between the ground and the shotcrete lining (Hoek and Brown, 2018). At its essence, the GRC illustrates the relationship between ground deformation and the forces experienced by shotcrete linings. This integration is crucial for developing a shotcrete mix design which is suitable for specific geological formations.

Aghchai et al. (2020) demonstrated how the Finite Element Method (FEM) can model the GRC by incorporating material properties such as UCS. FEM can also model loading, including tunnel radius and in situ stresses, used to generate the GRC. FEM simulations improve understanding of shotcrete lining responses. The GRC highlights two important factors: final convergence and FoS (Hwang et al., 2011). FEM can also model loading, including tunnel radius and in situ stresses, used to generate the GRC.

The expected final convergence of shotcrete refers to how much the shotcrete material is expected to deform as it settles and interacts with the surrounding ground (Hwang, 2011). Furthermore, Hwang (2011) showed that numerical models can predict final convergence by considering shotcrete material properties at different curing ages.

At 3 days after application, shotcrete usually shows significant initial convergence because it has relatively low strength at this early stage. Aghchai et al. (2020) reported that expected convergence during the early curing phase ranges from 10 mm to 20 mm. This is because hydration is still ongoing, and early strength is also developing. By day 7, the shotcrete

gains considerable strength, and the expected convergence decreases to around 5 mm–15 mm. Hwang et al. (2011) attributed this to the rapid strength gain in shotcrete.

By 28 days of curing, shotcrete usually reaches a significant portion of its ultimate strength, which is considered the standard curing period in concrete technology. Research by Kwan et al. (2015) indicates that the final convergence stabilises and is expected to fall within the range of around 2 mm to 5 mm. This range is significantly reduced due to the increased stiffness and strength of the material. The stabilisation therefore implies that the shotcrete is effectively supporting the surrounding ground with less deformation.

The existing GRCs are based on input results from shotcrete made with natural sand and steel fibres. The GRC behaviour of shotcrete made from dolerite and Xorex fibre remains largely unknown. Using GRC for this mix design is important to capture strength development and improve tunnel design. Shotcrete failure has adverse effects on a mining operation. The implications of shotcrete failure are discussed in detail in the next section.

2.6 Implications of shotcrete failure in underground mines

Mining is a key driver of global economic growth; it supplies the minerals that support modern society and creates jobs in a wide range of industries (Dikgwatlhe and Mulenga, 2023). Yet the industry continues to struggle with a persistent and often deadly problem: underground accidents, especially falls of ground (FOG). Statistics in South Africa indicate that FOGs account for roughly 37% of all mining deaths (MINCOSA, 2020), making FOG a major threat to miners' safety. This makes dependable ground support critical, with shotcrete playing a central role. Researchers such as Holmgren (1998) and Malmgren and Svensson (2003) highlight the importance of shotcrete in stabilising excavations, maintaining rock stability, and reducing the risk of fatal collapses.

The consequences of mining accidents go well beyond immediate harm or fatalities. A serious incident can bring operations to a standstill. Stacey (2009) lists examples where major ground failures forced mines to shut down permanently. These closures have far-reaching effects, including reduced productivity, lower profit margins, and a poorer long-term outlook for the mine (Stacey, 2009). When shotcrete fails, the danger extends beyond immediate safety concerns. The sustainability of the entire mining operation is at stake, since ground support underpins mine safety.

The financial impact of mining accidents comes in two forms: direct and indirect costs. They both take a heavy toll on the industry. Manuele (2011) classified direct costs as compensation payouts, medical expenses, equipment repairs, and lost production time. Indirect costs run deeper; these include lower morale, lasting disabilities, widespread economic losses, and shaken investor confidence (Manuele, 2011). In many developing regions, entire communities depend on the success of local mines. If shotcrete fails and a mine closes, local economies can be thrown into crisis.

These financial losses are not just hypothetical. Huang et al. (2009) estimate the average cost of a single fatal mining accident at ZAR 2.7 million, not accounting for the longer-term impact of lost productivity. Blumenstein et al. (2011) demonstrate how production losses can render once-promising ore bodies unprofitable. Behm (2009) also noted that equipment damage may force mines to lease replacements; this costly necessity further narrows profit margins.

Mines require shotcrete that can withstand cracking, resist tensile failure, and maintain its strength over time. This is not just about protecting lives; it is about ensuring the ongoing viability of the entire operation. Constitutive models describe the behaviour of shotcrete and the surrounding rock. These models detect weaknesses in the material before failure occurs. Constitutive models help optimise underground support techniques. These tools make decision-making more precise, resulting in safer and more

efficient mines. The next section reviews relevant constitutive models used in shotcrete.

2.7 Constitutive modelling

Schutz (2010) describes constitutive modelling as using mathematical equations to represent how materials such as shotcrete react mechanically, thermally, and chemically. These mathematical models replicate shotcrete behaviour under various loading and environmental conditions. These results are then validated through empirical evidence, giving the designer a sound foundation (Neuner, 2017). Constitutive modelling is an important part of underground excavations. It predicts the stresses, strains, and deformations the shotcrete will experience during its service life (Schutz, 2010). Accurate modelling allows selection of the right shotcrete thickness and material properties.

Shotcrete itself is a dynamic material, constantly evolving due to hydration, chemical reactions, moisture migration, and temperature influences (Paternesi et al., 2016). The mix composition governs how quickly these changes occur, directly affecting early strength, stiffness, and durability. To predict the performance of shotcrete systems, constitutive models must account for this evolving complexity (Neuner et al., 2017).

Despite this, most numerical analyses still rely on simple linear-elastic shotcrete models. These models are computationally efficient but fail to capture the true behaviour of the material. Shotcrete does not behave in a simple linear-elastic way; instead, it exhibits non-linear, viscoelastic, and time-dependent properties. Simplified models overlook these characteristics. To address these gaps, researchers have developed several non-linear constitutive models (Bazzazadeh, 2021). Such models are crucial for analysing stress redistribution within shotcrete and ensuring tunnel stability during excavation and support installation.

Most constitutive models currently target conventional shotcrete with standard sand aggregates and steel fibres (Meschke, 1996; Schutz, 2010; Neuner et al., 2017; Schädlich and Schweiger, 2014; Bazzazadeh, 2021). However, little research examines shotcrete models incorporating recycled aggregates or innovative fibre reinforcements such as Xorex fibres (Guo, 2020; Shah, 2021). This is concerning, given the push by the industry toward more sustainable, high-performance shotcrete formulations.

A recent trend in construction is hybrid shotcrete. This approach combines the standard shotcrete mixture with materials designed to enhance sustainability or performance. Examples include using recycled aggregates or systems that blend a new type of fibre or mix different types of fibres, such as steel and synthetic fibres. The aim of this hybrid shotcrete is to improve toughness, durability, heat resistance, and sustainability simultaneously. However, these enhancements significantly alter the mechanical and flow properties of shotcrete, which current models cannot capture.

This highlights the urgent need for a comprehensive review of non-linear constitutive models. There is a need to determine which existing approaches can address the challenges of hybrid shotcrete and where the deficiencies lie. Only then can we reliably predict the real-world performance of the next generation of similar hybrid shotcrete systems.

2.7.1 Meschke model

Meschke (1996) developed one of the earliest advanced three-dimensional constitutive models for shotcrete. The model significantly improved the simulation of shotcrete performance at early ages and over the long term. The model is based on the multisurface viscoplasticity theory. The theory considers the elastic-plastic and time-dependent behaviour of quasi-brittle materials under various loading conditions. The theory also accounts for changes in stiffness, strengthening, and deformation of shotcrete during its lifetime (Meschke, 1996). One of the main advantages of the model is that

it can simulate compressive hardening and tensile softening. These properties are important to underground shotcrete support structures. The model can simulate non-linear hardening in compression. It can also consider softening, cracking and fracturing of shotcrete under tensile loading (Meschke, 1996; Schädlich and Schweiger, 2014). This dual capability is vital for tunnelling and mining, where shotcrete must withstand shifting loads, seismic events, and the slow relaxation of the surrounding rock mass.

Another strength of the model is its treatment of time-dependent deformation. Shrinkage, creep, and viscoplasticity are dominant factors affecting shotcrete linings over both short and long durations. Meschke's formulation decomposes total strain (ε^{total}) into elastic (ε^{el}) shrinkage (ε^{shr}), creep (ε^{cr}), and viscoplastic (ε^{vp}) components, enabling independent tracking of each mechanism (Jia et al., 2024; Liu et al., 2022). This mirrors the ongoing evolution of shotcrete microstructure as hydration progresses, moisture content shifts, and microcracks develop.

Figure 2-6 represents this process in three steps. Initially, immediate elastic deformation and early shrinkage occur, triggered by rapid chemical and thermal reactions after shotcrete application. As loading persists, creep and viscoplastic strains develop, driven by microstructural changes and stress relief. The system attains equilibrium. The strain rates become lower. Deformation eventually reaches a steady state. Residual stresses, the environment, and boundary conditions control this behaviour (Neuner et al., 2017; Paternesi et al., 2016).

Meschke's constitutive model remains a foundational tool for simulating shotcrete in underground engineering. Its ability to simultaneously address stiffness changes, tensile softening, creep, and shrinkage makes it essential for reliably predicting shotcrete support.

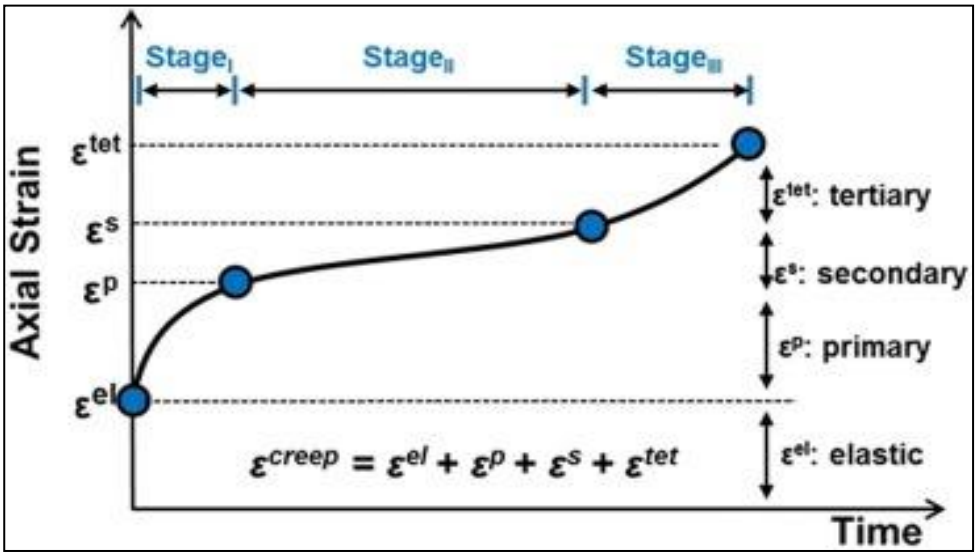


Figure 0-6: The creep constitutive model associated the viscoplastic multisurface theory after Meschke (1996)

The evolution of stiffness in shotcrete is modelled using hyper-elastic constitutive relations that dynamically represent changes in Young's modulus. Equations (2.6) and (2.7), referred to as Meschke's model, capture the changes in the properties of shotcrete over time and their impact on Young's modulus (Meschke, 1996):

$$E(t) = E^{(28)}\,\beta_E^I(t) \tag{2.6}$$

$$\beta_E^I = \begin{cases} \beta_E^{II} = c_E t + d_E t^2, & if\ t \le t_E, \\ \beta_E^{II} = \left(a_E + \frac{b_E}{t - \triangle t_E}\right)^{-0.5}, & if\ t_E < t \le 672h, \\ \beta_E^{II} = 1, & otherwise, \end{cases} \tag{2.7}$$

where $E^{(28)}$ represents Young's modulus at 28 days

β_E^{II} is the flow constant (dimensionless)

t stands for time (h)

a_E, b_E, c_E, and d_E represent smooth time transition parameters (dimensionless).

The flow constant β_E^{II} in Equation (2.7) controls the rate of time-dependent stiffness development in shotcrete. It governs changes during curing, creep, or viscoplastic deformation. This parameter plays a critical role in modelling the time-dependent mechanical behaviour of the material.

The flow constant in Equation (2.7) controls the rate of time-dependent stiffness development in shotcrete. It governs changes during curing, creep, or viscoplastic deformation. This parameter plays a critical role in modelling the time-dependent mechanical behaviour of the material.

The smooth time transition parameters a_E, b_E, c_E, and d_E control the smooth evolution of material properties. They describe the transition from early-age state to the long-term condition. This enables accurate prediction of stiffness development over time using Equation (2.6).

The Meschke model has been widely used in various studies to capture the behaviour of shotcrete, particularly its time-dependent creep and shrinkage (Meschke, 1996; Khalili et al., 2010). This model has been instrumental in numerically modelling tunnel linings and the complex mechanical behaviour of shotcrete under varying loading conditions. It is particularly useful for accounting for time-dependent phenomena like curing, creep, and viscoplastic deformation. This provides a robust tool for predicting the long-term behaviour of shotcrete under real-world conditions. The model considers the development of important mechanical parameters, such as strength and stiffness, during curing, creep, and viscoplastic behaviour. It allows an overall evaluation of shotcrete performance over time (Neuner et al., 2017; Naseri and Bahrani, 2019).

Despite its advantages, Meschke's model has some notable limitations. A major problem is that it tends to overestimate the development of the compressive strength of shotcrete after 7 days. Figure 2-7 clearly illustrates this overestimation of prediction. As a result, predictions of shotcrete's long-term performance can be inaccurate, which is more than a trivial issue. If maintenance schedules depend on these forecasts, there is a risk of underestimating stiffness loss or how damage accumulates over time. This poses a real threat to the safety and reliability of structures supported by shotcrete.

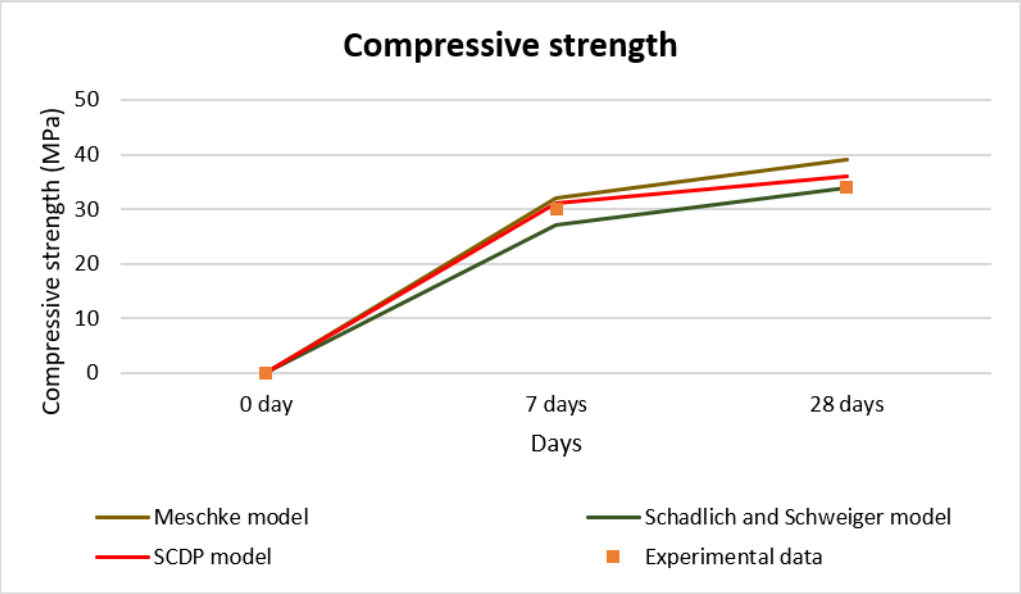


Figure 0-7: Predictive ability of the Meschke Model against experimental data and similar models (after Meshcke, 1996; Schädlich and Schweiger,2014; Neuner et al., 2017)

The following section introduces the Schädlich and Schweiger model and explore its application in greater detail.

2.7.2 Schädlich and Schweiger model

Schädlich and Schweiger (2014) developed a viscoelastic-plastic material model for shotcrete that captures time-dependent behaviours pertaining to strength, stiffness, creep, shrinkage, and plasticity. The model accounts for both hardening and softening properties under different loading conditions. The evolution of material stiffness and strength is primarily governed by changes at 28-day curing, as expressed below (Schädlich and Schweiger, 2014):

$$E(t) = E^{(28)}\, exp\left[S_{stiff}\left(1 - \sqrt{28/t}\right)\right] \qquad (2.8)$$

Where E^{28}= Young's modulus at 28 days (in GPa)

S_{stiff}= stiffness parameter of shotcrete (dimensionless or in GPa, depending on calibration)

t = time (in days).

The evolution of the stiffness of concrete, S_{stiff}, can be expressed as follows (Schädlich and Schweiger, 2014):

$$S_{stiff} = \frac{-\ln[E^{(1)}/E^{(28)}]}{\sqrt{28}-1} \quad (2.9)$$

Where $E^{(1)}$ and $E^{(28)}$ represent Young's modulus at 1 day and 28 days of curing respectively.

Compared with the Meschke model, the Schädlich and Schweiger model has shown superior performance in certain areas, particularly in predicting the compressive strength behaviour of shotcrete at late age. The predictions align closely with experimental data, as shown in Figure 2-8. The ability of the model to capture these time-dependent behaviours makes it particularly useful for simulating the long-term performance of shotcrete in applications such as tunnel linings, where compressive strength is a significant factor (Schädlich and Schweiger, 2014).

The Schädlich and Schweiger (2014) model often falls short in predicting creep in shotcrete, particularly during the first 24 hours and at later stages, as illustrated in Figure 2-8.

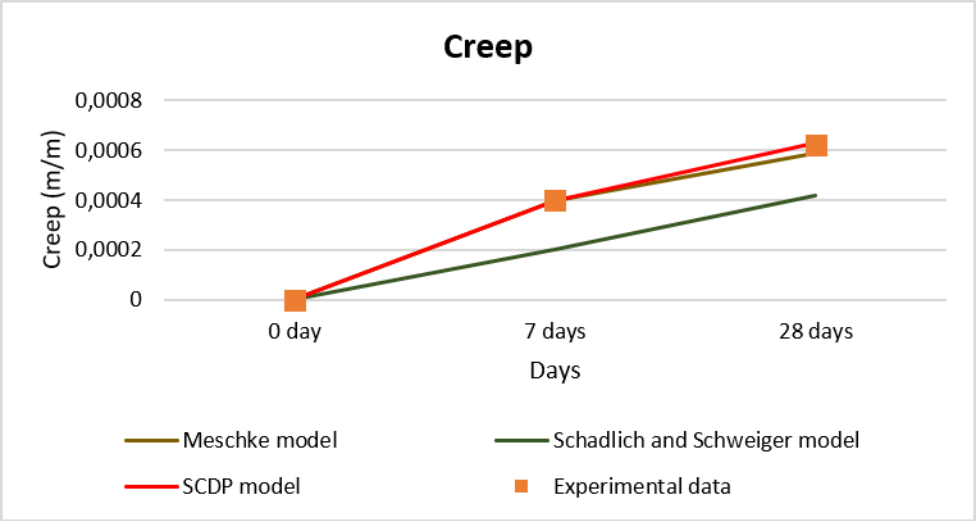


Figure 0-8: Predictive ability of the Schädlich and Schweiger model against experimental data and similar models (after Meshcke, 1996; Schädlich and Schweiger, 2014; Neuner et al., 2017)

Underestimating creep is more than a technical issue; it directly affects how engineers assess the safety and performance of shotcrete used in underground mines. When the model fails to predict early-age creep correctly, the load-bearing capacity of new shotcrete may be overestimated. Such an overestimation increases the risk of failure. Additionally, underestimating creep can compromise worker safety, lead to early crack development, and threaten the long-term stability of the tunnel or excavation (Schädlich and Schweiger, 2014).

To further improve understanding of shotcrete behaviour, the Simplified Concrete Damage Plasticity model has been proposed. This section discusses the model.

2.7.3 Shotcrete damage plasticity model

Neuner et al. (2017) introduced the Shotcrete Damage Plasticity (SCDP) model as a comprehensive constitutive model that reflects how shotcrete behaves over time under demanding, variable loads. Rather than relying on a single theory, this model integrates several theories, each addressing a specific aspect of shotcrete behaviour.

At its centre is the plasticity theory, which explains what happens when shotcrete is deformed past its yield surface and does not return to its original shape. This allows the model to simulate how shotcrete responds to elevated compression and shearing stresses in underground mines before application.

The model also incorporates isotropic continuum damage theory to monitor how shotcrete gradually loses stiffness and strength as its internal structure deteriorates. This refers to micro-cracks, small voids, and other imperfections that develop and expand over time. By tracking this damage with internal variables, the model links microscopic changes to the overall material response and describes how stress and strain evolve. This allows for predictions of stiffness reduction and the progression toward failure.

Shrinkage theory is also included, accounting for the volume changes shotcrete undergoes during drying and cement hydration. These changes create internal stresses that can cause cracking, affecting both early and long-term performance. In addition, a modified solidification theory describes how shotcrete stiffens and creeps with time, covering early-age hardening and stress relaxation as the material cures. Together, these elements enable the SCDP model to simulate the complex interplay of plastic deformation, damage, shrinkage, and creep. The result is a more detailed and realistic prediction of shotcrete performance underground (Neuner et al., 2017). The relationship between these variables and the response of the material is mathematically captured as follows (Neuner et al., 2017):

$$E(t) \cong \{q_1 + [\ln(1 + \Delta^{0.1})]\,[q_2\,\tau\,t^{-0.5} + q_3]\}^{-1} \quad (2.10)$$

Where $E(t)$ = Young's modulus at time t(in GPa)

q_1 = material compliance (in GPa)

q_2, q_3 = short-term creep evolution parameters (dimensionless or in GPa depending on calibration)

t = time (in days)

Δ = change in stiffness (dimensionless or as a ratio of moduli, e.g., $E(t)/E_0$)

τ = creep time constant (in days).

However, the SCDP model has its drawbacks. One significant issue is its tendency to overpredict shrinkage-related deformation in early and late ages (see Figure 2-9).

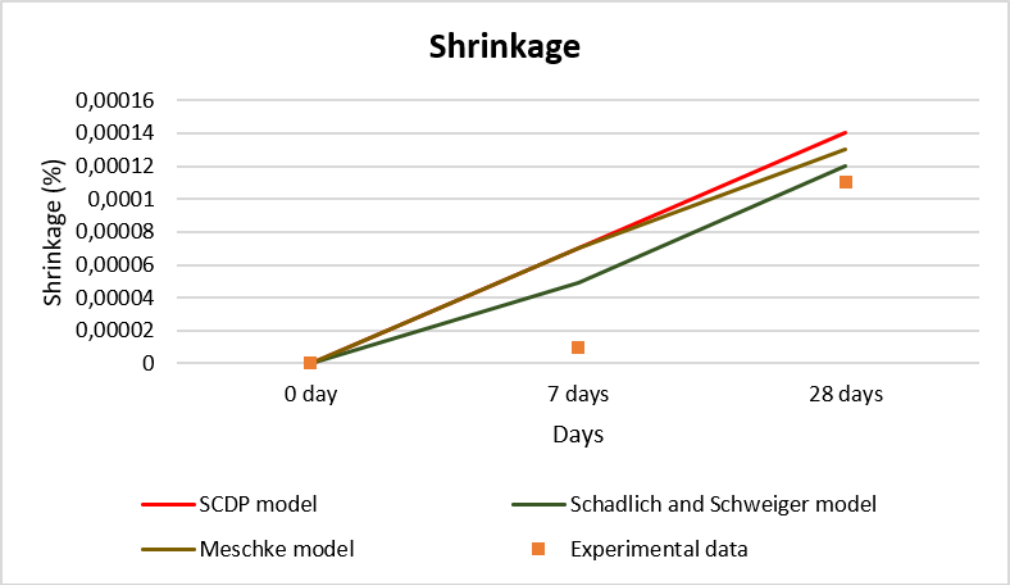


Figure 0-9: Predictive ability of the SCDP Model against experimental data and similar models (after Meshcke, 1998; Schädlich and Schweiger, 2014; Neuner et al., 2017)

Despite including shrinkage theory to address time-dependent volume changes, Neuner et al. (2017) observed that the models forecast higher shrinkage strain than field measurements. As a result, the model may overestimate internal stresses and the likelihood of early cracking, suggesting structural risks that may not actually exist. This can lead to overly conservative designs and unnecessary maintenance in mining and tunnelling operations.

Furthermore, the shortcomings of the approaches were identified. In particular, the available models proposed by Meschke (1996), Schädlich and Schweiger (2014), and Neuner (2017) provide different predictions of Young's modulus and strength development. However, these approaches do not adequately describe the behaviour of the proposed shotcrete. The Meschke model significantly overpredicted the evolution of Young's modulus, while the Schädlich and Schweiger model underestimated it as presented in Figure 2-10.

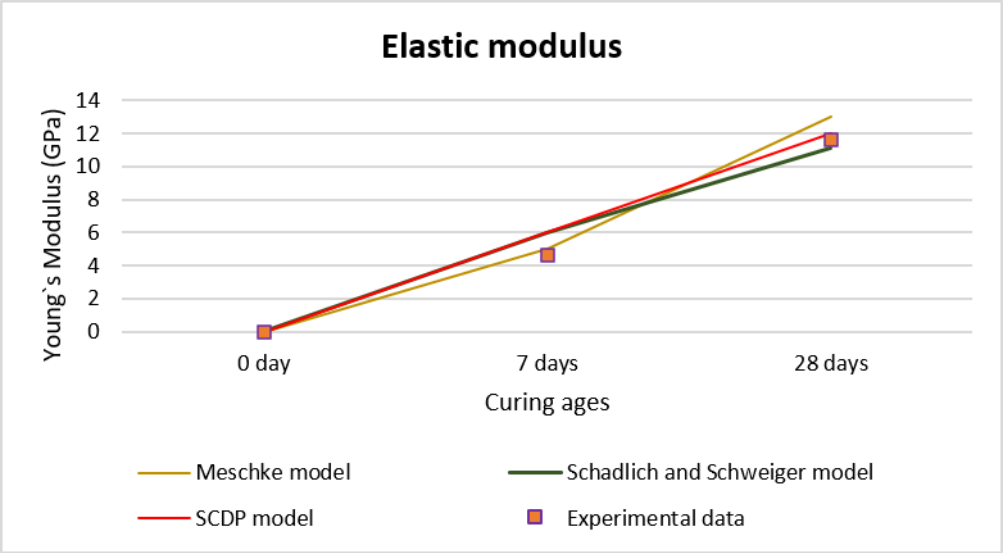


Figure 0-10: Evolution of elastic modulus depicted from various models.

This misprediction can increase project costs and lead to inefficient use of the shotcrete support system. Numerical and multivariate regression models are needed that specifically incorporate sustainable materials such as dolerite aggregates and Xorex fibres. Developing this type of model enables more accurate prediction of shotcrete performance and supports a transition toward greener construction methods in underground tunnelling.

2.7.4 Need for multivariate regression modelling

Underground tunnel excavation is increasingly complex, multivariate regression modelling is needed to design the performance of shotcrete. Shotcrete performance is influenced by multiple variables, including fibre dose, aggregate properties, curing age, water-cement ratio, in situ stresses, environmental factors, and application procedures. The existing constitutive models do not account for all variables acting simultaneously. Therefore, existing constitutive models still have limited ability to predict shotcrete behaviour. Additionally, multivariate models are used to predict performance. The challenge is that most were formulated for conventional concrete, not shotcrete. This presents a serious challenge since shotcrete displays unique characteristics related to its spraying and rebound process,

fibre distribution and orientation, variability in compaction, and underground conditions.

Therefore, a multivariate regression model is urgently needed to integrate experimental laboratory testing, numerical modelling, and field performance into a predictive platform. Using such a model will improve prediction accuracy and reliability while reducing uncertainty. More importantly, current models do not account for sustainable materials such as dolerite aggregates and Xorex fibres, despite the growing importance of sustainable construction materials in shotcrete. Developing a multivariate regression model that incorporates these sustainable materials will greatly improve the predictability of these shotcrete mixes.

2.8 Research gaps and motivations

The declining availability of natural sand is becoming a significant challenge in the construction industry, particularly for underground support applications where shotcrete is often used. Regions such as Mpumalanga are often adjacent to mining areas that produce substantial volumes of dolerite by-products. However, little research has examined the use of waste dolerite as an alternative aggregate for shotcrete, representing a gap in the existing research. Using dolerite as an alternative aggregate could leverage waste aggregates and reduce the over-extraction of natural sand, while improving waste management and addressing the environmental issues associated with dolerite waste. Although dolerite has potential, little research has investigated the mechanical and durability performance of shotcrete designed with dolerite as an aggregate source to replace natural sand. In addition to alternative aggregates, fibre reinforcement is widely adopted in shotcrete applications to improve tensile strength, ductility, and crack resistance. Traditional steel fibres are prone to corrosion, which increases the risk to long-term durability in underground conditions. Emerging replacement fibres, such as Xorex fibres, have shown potential

for corrosion resistance and durability. Limited studies have examined these fibres in shotcrete mix designs intended for underground excavation.

Most predictive models have been developed using shotcrete made from natural sand reinforced with conventional steel fibres. Consequently, the modelling scope is limited to natural sand and steel fibres.

Several reasons support addressing these gaps. Environmentally, using dolerite as a shotcrete aggregate is a more sustainable option because it reduces reliance on limited natural sand reserves and decreases negative environmental impacts. Economically, using locally sourced dolerite may reduce shotcrete material costs and lower mine-closure liability associated with waste-rock dump treatment.

In terms of performance, using Xorex fibres may resolve the durability shortcomings of traditional steel fibres and extend the service life of underground support systems. Strong experimental results increase the precision of multivariate regression models and numerical calculations, allowing predictive models to more accurately simulate real-world conditions. This study bridges the gap between theory and practice by combining experimental and computer modelling to assess the performance of shotcrete containing dolerite aggregate and Xorex Fibres. In this way, the outcomes support improvements of safer, more resilient, and more environmentally friendly underground infrastructure.

2.9 Concluding remarks

The current state of the art in modelling sustainable shotcrete systems is far from satisfactory. Most published work focuses on predicting and analysing the performance of conventional shotcrete mixtures. These are typically characterised by a combination of natural sand and steel fibres. Studies focusing on dolerite aggregates and recycled materials, as well as Xorex fibres, are scarce, which constitutes a serious limitation. This work is motivated by this knowledge gap, and its contribution is the proposed

integrated framework, which aims to comprehensively account for variability.

In this paper, laboratory tests, numerical simulations, and multivariate regression analyses are used to account for the complex physico-chemical processes involved. This integrated approach, which merges experimental, analytical, and numerical methodologies, is expected to provide accurate estimates of the mechanical performance and durability characteristics of the dolerite–Xorex fibre shotcrete mixture. Moreover, the proposed framework bridges the gap between laboratory findings and real-world applications by accounting for the range of mechanisms typically encountered in underground structures. Finally, the method introduced herein is expected to become a valuable tool for designing sustainable support systems.

To conclude, the present study was conducted within the scope of developing durable and ecological shotcrete mixtures, which are mainly used in underground construction. The proposed methodology integrates laboratory investigations and numerical simulations with multiple regression analysis. This approach allows not only accurate prediction of the mechanical performance of the mixture, but also consideration of sustainability aspects.

Chapter 3: Collection of experimental data and research methodology

3.1 Introduction

The chapter details the research design, experimental programme, testing procedures, instrumentation, and analytical methods used to evaluate shotcrete performance. The methodology was designed to meet the research objectives set in Chapter 1 and address the research gaps identified in Chapter 2.

The study employed a mixed-methods approach, as described by several authors. Laboratory experimentation was used to obtain measured values of shotcrete performance, while numerical simulation was used to examine the engineering implications of the experimental findings. Predictive modelling was applied to establish relationships between the investigated variables. Collectively, these approaches provide multiple lines of evidence and strengthen the research findings.

Shotcrete specimens were made using a controlled mixture of dolerite aggregates, Xorex fibres, cementitious materials, water, and water-reducing superplasticiser. In total, 48 specimens were fabricated and cured for 4, 7, 28, and 56 days.

At each curing age, 12 specimens were tested: 3 specimens for TCS, UCS, tensile strength, and shrinkage tests. Thus, the 48 specimens were allocated to the experimental programme as described in the preceding section. The number of repetitions was considered sufficient to allow statistical inference on the influence of shotcrete curing age on its performance.

The study focused on a single proposed shotcrete mix with Xorex fibres and dolerite aggregates. This decision maintained experimental control and avoided additional variables arising from other mix designs. This decision

also allowed the study to focus on the effect of curing age on the selected shotcrete mix without additional sources of variability.

The study did not reproduce a conventional shotcrete mix experimentally because its performance is already well established in the literature. The study relied on published findings to represent the operational characteristics of conventional shotcrete for comparison. The authors avoided unnecessary replication of effort and focused on the proposed shotcrete mix.

The experimental findings provided the basis for the numerical and predictive modelling components of the study. The measured material properties formed the foundation for the numerical simulation, which interpreted the engineering implications of the experimental results. The predictive modelling component relied on the numerical simulation findings to establish relationships between the variables investigated in the study. Thus, the 3-stage experimental, numerical simulation and predictive modelling approaches were integrated to advance the research objectives.

The procedures used in specimen preparation, curing, testing, and numerical modelling, statistical inference, and data interpretation were followed in accordance with the details provided in the preceding sections.

3.2 Mix ingredients

The selection of shotcrete ingredients plays a crucial role in shotcrete performance and durability for underground applications. A traditional shotcrete mix design typically consists of cement, sand aggregates, water, fibres and superplasticiser. Each mix design component affects critical properties such as setting time, early-age strength, long-term durability and workability. The following sections document the characteristics of these constituents in detail.

3.2.1 On-site collection of bulk aggregates

Dolerite aggregates used in this study were sourced from AfriSam's Rooikraal Quarry, situated near Brakpan in Gauteng, South Africa. The precise coordinates of the sampling locations are presented in Figure 3-1. Although dolerite is readily available across South Africa from various quarries and dumps, this investigation used material specifically obtained from Rooikraal Quarry. AfriSam voluntarily contributed dolerite aggregates from their existing stockpiles to support this research. The mechanical properties of dolerite, coupled with its availability as a by-product of coal mining, make it a viable substitute for sand aggregate for use in shotcrete.



Figure 0-1: Geographical location of the Rooikraal quarry sampling site (Coordinates: 6°00'0.0"N, 12°00'0.0"E)

The collected materials comprised coarse aggregates with a grain size of 10 mm and fine aggregates measuring less than 5 mm. This grading was purposefully selected to comply with the requirements outlined in American Standard Testing Methods (2018b), which specifies that aggregates suitable for shotcrete applications should range from fine particles (< 5 mm) up to a maximum size of less than 10 mm. Following the guidelines

stipulated in American Standard Testing Methods (2018b) ensures that the shotcrete mix achieves adequate workability, pumpability, and mechanical performance. Aggregate size cannot be underestimated in shotcrete work. It ensures good compaction, prevents rebound, and increases strength and durability during hardening. The dolerite aggregates collected are depicted in Figure 3-2.



Figure 0-2: (A) Stockpile of coarse dolerite aggregates (10 mm); (B) Collected 10 mm dolerite aggregates; (C) Stockpile of fine dolerite aggregates (5 mm) and; (D) Collected 5 mm dolerite aggregates

Typical properties of dolerite aggregates are presented in Table 3-1, as documented by Chaudhry et al. (2021). These properties indicate that dolerite aggregates have favourable physical characteristics that can provide sufficient mechanical strength and durability when incorporated into shotcrete.

Table 0-1: Engineering properties of dolerite aggregates

Parameter	Standard	Value
Flakiness (%)	ASTM C-4791	17
Specific gravity (%)	ASTM C-128-93	3.0
Water absorption (%)	ASTM C-128-93	0.2
Soundness (%)	ASTM C-88	3.2
Los Angeles (%)	ASTM C-33-90	9
Aggregate Crushing Value (%)	BS 812: Part 112 and 110	4
Adhesion (%)	IS 6241-1971	98

Cement is an essential component in shotcrete design, mainly responsible for binding the constituents. The next section describes the type of cement chosen and the reason for the selection.

3.2.2 Selection of cement

The Blast Furnace Slag Cement (BFSC) used in this study was locally sourced from a Builders Warehouse outlet in South Africa. Blast Furnace Slag Cement (BFSC) is made by mixing Portland cement with Ground Granulated Blast-Furnace Slag (GGBFS), which is a product of steelmaking. Chemically, BFSC has high amounts of calcium, silica, and alumina, which facilitate pozzolanic reactions that form additional C-S-H gel, filling pores, reducing permeability, and creating a denser matrix (Alsadey and Mohamed, 2020). BFSC also offers performance benefits in shotcrete. The slow hydration of slag makes BFSC heat-resistant and less likely to cause cracks due to heat in massive shotcrete sections (Chen and Wei, 2021).

Furthermore, it increases workability and long-term durability while also improving compressive strength as the slag hydrates over time (Onyekaa et al., 2023). With fibre additions, this mix will have both delayed thermal

stress development and enhanced crack control, improving early-age performance (Brodd et al., 2024).

The binder contributes to overall strength; however, fibres control cracking. The next section discusses fibre selection.

3.2.3 Xorex fibre reinforcement

Fibres are a vital part of shotcrete mixes for underground excavations because they provide additional ground support and improve mechanical performance (Thomas, 2018). Fibres dosage and geometry affect tensile strength and crack control (Schutz, 2010). Performance assessment of fibre-reinforced shotcrete is based on mechanical test methods such as compressive strength, tensile strength, shear strength, and Young's modulus. This study uses Xorex fibres produced by Fibre Reinforcing Solutions (Fibsol, 2023), a South African-based company that specialises in concrete reinforcement systems. Xorex fibres are made by shaving cold-drawn steel wire, which is bent into a waved shape; see Figure 3-3. They have a nominal diameter of 1 mm, a length of 40 mm, and a tensile strength of 700 N/mm² (Fibsol, 2023). They improve shear and flexural strength, fatigue resistance, and impact resistance, and limit crack propagation in shotcrete. Shotcrete is reinforced with Xorex fibres for improved durability. They make maintenance unnecessary. They also replace traditional steel fibres, especially when used in small quantities underground.



Figure 0-3: Xorex fibres

Adding fibre helps prevent cracking and improves durability. Water is necessary to hydrate cement and affects strength. This next section looks into water and its importance in shotcrete mix design.

3.2.4 Mixing water used in the preparation of shotcrete

Water is an essential element in shotcrete because it directly influences cement hydration, workability, setting time, strength gain, and durability. This study used potable water in accordance with American Standard Testing Methods (2018a). Potable water is expected to be free of deleterious substances that could affect cement hydration, setting time, strength gain, or durability (Neville, 2012; Twort, 2002). It is important to ensure that both water quality and quantity meet the intended level of pumpability, adhesion, and overall shotcrete performance. Water-reducing agents further improved the shotcrete mix performance, allowing the w/c ratio to decrease without sacrificing workability. The next section describes the superplasticiser used in this study and its effects on the overall shotcrete mix design.

3.2.5 Characteristics of the superplasticizer used

For this study, we used a superplasticiser called CHRYSO® Fluid Optima 206. It is a high-range water-reducing admixture used principally to increase workability whilst limiting the water in the mix. This superplasticiser conforms to the American Standard Testing Methods (2019a), ensuring the admixture meets performance criteria and delivers consistent water reduction, compatibility with cementitious materials, and controlled setting time.

This admixture was chosen to aid shotcrete performance, especially with dolerite aggregates used as a replacement for natural sand. Dolerite aggregates are dense and more angular, which can reduce workability and increase the potential for segregation during application (Alsadey and Mohamed, 2020). CHRYSO® Fluid Optima 206 addresses these issues by increasing the cohesiveness and fluidity of the fresh mix without increasing the water-to-cement (w/c) ratio, thus ensuring that the strength and long-term durability of the hardened shotcrete are retained. The following section outlines the laboratory procedures for casting, curing, and testing of the shotcrete specimens.

3.3 Experimental design

The mix design of each shotcrete ingredient is detailed in Table 3-2. The weight fraction of each component is defined as the ratio of its mass to the total mass of all components in one cubic metre of the mix. The corresponding mass in a 25 kg batch is calculated by multiplying the weight fraction by the total batch mass (25 kg). To ensure reproducibility in laboratory evaluations, the mix proportions were normalised by expressing the mass of each constituent as a fraction of the total mix weight, providing a consistent basis for sample preparation across all tests.

Table 0-2: Shotcrete mix design ingredients

Component	Quantity (kg/m^3)	Weight fraction (wt)	Mass in batch (kg)
Blast furnace slag cement	400	0.2134 wt	5.34 kg
Fine Aggregate (≤ 5 mm)	850	0.4537 wt	11.43 kg
Coarse Aggregate (≤ 10 mm)	400	0.2134 wt	5.34 kg
Water	180	0.0960 wt	2.40 kg
Superplasticizer	4	0.0021 wt	0.05 kg
Xorex Fibres	40	0.0213 wt	0.53 kg
Total	**1874**		**25.09 kg**

The mix design in Table 3-2 was informed by the American Concrete Institute (2006), which provides guidance for specifying underground shotcrete mix design. This standard collectively informed the compositional requirements, performance characteristics, and application criteria for wet-mix shotcrete.

The cumulative mass of the mix components was 1874 kg/m^3. To facilitate reproducibility in laboratory evaluations, the mix proportions were normalised by calculating the mass fraction of each constituent relative to the total mix weight. The resulting weight fractions were 0.2134 for both cement and coarse aggregate, 0.4537 for fine aggregate, 0.0960 for water, 0.0213 for Xorex fibres, and 0.0021 for superplasticiser. Figure 3-4 depicts the mix design constituents.

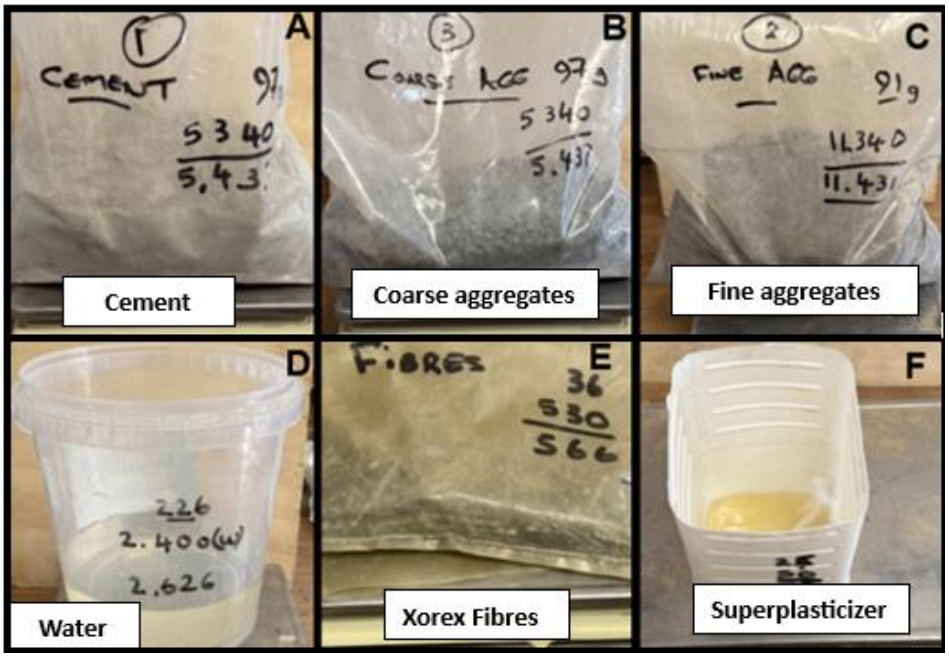


Figure 0-4: The mix design ingredients – (A) Cement; (B) Coarse dolerite aggregates; (C) Fine dolerite aggregates; (D) Water; (E) Xorex fibres; and (F) Chryso® superplasticizer

Each experimental batch consisted of 5.34 kg cement, 11.34 kg fine aggregate, 5.34 kg coarse aggregate, 2.40 kg water, 0.53 kg Xorex fibres, and 0.05 kg superplasticiser. This ratio was maintained throughout preparation.

In total, 48 specimens were produced. Thirty-six cylindrical specimens were produced, from a cylinder that had a diameter of 50 mm, and a height of 100 mm. Twelve specimens were set aside for each of the UCS, TCS and shrinkage tests. The length-to-diameter ratios ranged from 2.3 to 2.4. This is acceptable for compressive testing, reducing end effects (Mindess et al., 2003; ASTM, 2023).

The remaining 12 specimens were made ready for direct tensile testing. These specimens were cast using a multi-cavity mould made from 5 mm thick Perspex (polymethyl methacrylate). The cavities were designed to produce the required geometry for direct tensile testing. Perspex was chosen for this application because it is dimensionally stable when cast and relatively easy to demould compared with other materials. Using a multi-

cavity mould allowed us to produce specimens under identical conditions. Figure 3-5 below shows the specimen configurations used.

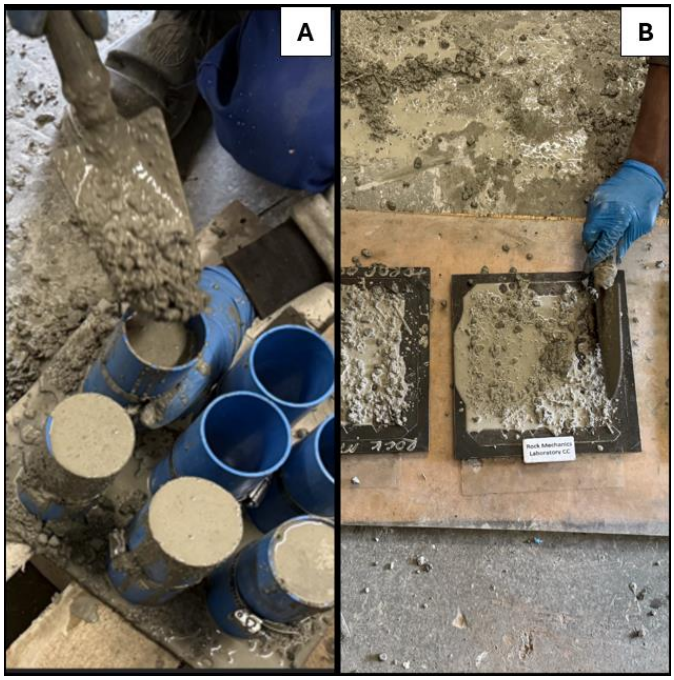


Figure 0-5: Casting of specimens – (A) Cylinder and (B) thick Perspex

The cylindrical moulds were filled in three layers, and after placing each layer, manual rodding was done using a 25 mm diameter tamping rod. This method ensured proper compaction, reduced air voids, and simulated typical field practices in a controlled lab setting. The compaction process followed the standards of the American Society for Testing and Materials (2022) and was essential for achieving good bonding between aggregates and ensuring consistent results across specimens (Neville, 2012).

To assess the early and long-term strength development of the shotcrete, all specimens were cured in air for 4, 7, 28, and 56 days. Open-air curing was utilised as depicted in Figure 3-6 in accordance with the American Society for Testing and Materials (2021). Open-air curing was chosen because it closely replicates the actual site conditions where shotcrete is exposed to varying humidity, ventilation, and temperature.



Figure 0-6: Air curing of specimen in a sealed vacuum desiccator

Four curing ages of 4, 7, 28, and 56 days were selected to characterise the development of shotcrete strength from early to later ages. The 4- and 7-day periods represent the early-age response relevant to the initial development of underground support capacity. The 28- and 56-day periods capture later-age strength development and provide a basis for assessing longer-term structural performance (Papworth and Banthia, 2000).

All specimens were demoulded after 24 h and subsequently maintained under the prescribed curing conditions until their designated testing ages. Mechanical testing was then conducted at 4, 7, 28, and 56 days. The following section describes the procedures used for each mechanical test.

3.4 Mechanical tests

The mechanical properties of the shotcrete mixes were determined by conducting various mechanical tests. The samples were prepared using dolerite aggregates as the fine and coarse aggregate materials in the shotcrete mixes. The shotcrete specimens were air-cured for 56 days, with

evaluations at four key intervals: 4, 7, 28, and 56 days. The mechanical tests included triaxial compressive strength to determine strain and Poisson's ratio, along with assessments of tensile strength, shrinkage, cohesion, and internal friction angle. These tests were designed to comprehensively assess the effects of aggregate type and curing duration on the mechanical behaviour of shotcrete. Additionally, these test findings were used to develop numerical and multivariate regression models. The sections below provide a detailed discussion of how each test was conducted.

3.4.1 Triaxial compressive strength and shear strength test

The triaxial compressive strength (TCS) of 12 cylindrical specimens was evaluated in accordance with the ASTM procedure D2664-67 (ASTM, 1997a). For each specimen, the peak axial load was recorded under the prescribed confining pressure. The TCS was calculated as the maximum axial load divided by the specimen's initial cross-sectional area.

The experimental strength data were plotted against the corresponding confining pressures to establish the shotcrete strength envelope. Confining pressure was plotted on the horizontal axis, while the corresponding peak strength was plotted on the vertical axis. The resulting envelope characterised the shotcrete response under increasing confinement.

A best-fit relationship was established from the experimental data. Where the response was approximately linear, a single linear regression was fitted to the representative data range. Where nonlinear behaviour was observed, multiple linear segments represented the envelope to capture changes in the material response. Each linear segment was defined by its gradient (m) and y-intercept (c), over a specified range of confining pressure.

The resulting gradient and intercept were subsequently used to derive the Mohr–Coulomb shear-strength parameters. The internal friction angle, (ϕ),

and apparent cohesion, (C), were determined from the fitted strength envelope using Equation 3.1 (ASTM, 1997a).

$$\phi = arcsin\frac{m-1}{m+1} \tag{3.1}$$

While the apparent cohesion, interpreted in accordance with Coulomb's failure criterion, was determined by Equation 3.2 (American Society for Testing and Materials, 1997a):

$$C = b\frac{1-\sin\phi}{2\cos\phi} \tag{3.2}$$

The above values formed the basis for studying the shear strength behaviour, confinement effect, and failure mode of the shotcrete specimens at various confining pressures. The shear strength can also be deduced from Coulomb's failure criterion using Equation (2.3).

Through plotting the failure points from multiple triaxial tests at different confining pressures, the strength envelope can be derived. The envelope is a good predictor of shotcrete behaviour in actual in-situ loading conditions. The envelope is best suited for tunnel liners and shallow underground excavations.

The experimental setup consisted of three main components: a triaxial pressure cell, a servo-controlled universal testing machine, and a confining pressure system. The universal testing machine was calibrated in accordance with the American Society for Testing and Materials ASTM D 2664-67 (1997a) to ensure accurate load application. The shotcrete specimen was first placed inside the triaxial cell and enclosed in a flexible latex jacket to prevent water or oil from the cell from entering the specimen. The specimen was positioned between two lightly lubricated steel plates to minimise friction and ensure even load distribution during testing. Figure 3-7 depicts this setup. This ensured uniform stresses on the specimen, reducing the chance of premature failure from uneven loading (Golser, 1991).



Figure 0-7:Triaxial compressive strength sample testing setup. (A) Mold assembly with ports and sleeve for sample preparation. (B) Compressive strength testing machine

During testing, axial stress and confining pressure are applied simultaneously until the target confinement level (σ_3) was reached. This initial phase created hydrostatic stress conditions, which means the specimen was evenly compressed from all sides. Once this pressure was stable, the axial load was increased at a constant rate of 0.5 MPa/s to 2.0 MPa/s, following the American Society for Testing and Materials (1997a). The specimen was continuously loaded to failure, which occurred within 5 min to 15 min. Additionally, Mohr-Coulomb parameters such as cohesion (C), internal friction (ϕ), and strengthening coefficient (β) were measured. These parameters were used to evaluate shear strength evolution, failure modes, and to serve as input data for numerical simulations.

3.4.2 Tensile strength tests

The tensile strength of 12 dog-bone specimens was tested using the method recommended by the American Society for Testing and Materials (ASTM D638) (1997). Tensile strength testing measures how much force shotcrete can resist before breaking when pulled apart. It is very important

in determining the tensile strength of shotcrete. Tensile strength is vital in underground support systems under tensile stress and strain conditions.

Although the American Society for Testing and Materials (2023) was not specifically created for shotcrete, researchers such as Tannant et al. (1999) and Archibald (2001) have adapted the method for testing shotcrete and Thin Spray-on Liners (TSLs) by modifying key parameters like the specimen dimensions and loading rate. This adaptation stems from the lack of a dedicated tensile testing standard for shotcrete, making the American Society for Testing and Materials (2023) a practical alternative.

The testing process began by slowly increasing the load at 2.5 N/s until it reached 100 N, which took about 40 s. After that, there was an increase of force increased at a steady rate of 5 N/s until the sample broke (American Society for Testing and Materials, 2023). Figure 3-8 depicts the shotcrete sample test.



Figure 0-8: Tensile strength testing

3.4.3 Shrinkage tests

Shrinkage was measured on twelve cylindrical specimens in accordance with ASTM C1581 standards (American Society for Testing and Materials, 2009). Cylindrical specimens maintained uniform geometry and eliminated shape inconsistencies. Each specimen was oven-dried at 105 ± 5°C for 24 h to remove all moisture content, as specified by ASTM D2216-19. After drying, the specimens were cooled in a desiccator to prevent immediate reabsorption of ambient moisture. Once cooled, high-precision electrical resistance strain gauges were securely bonded axially along the longitudinal surface of each specimen using a suitable adhesive, as depicted in Figure 3-9.

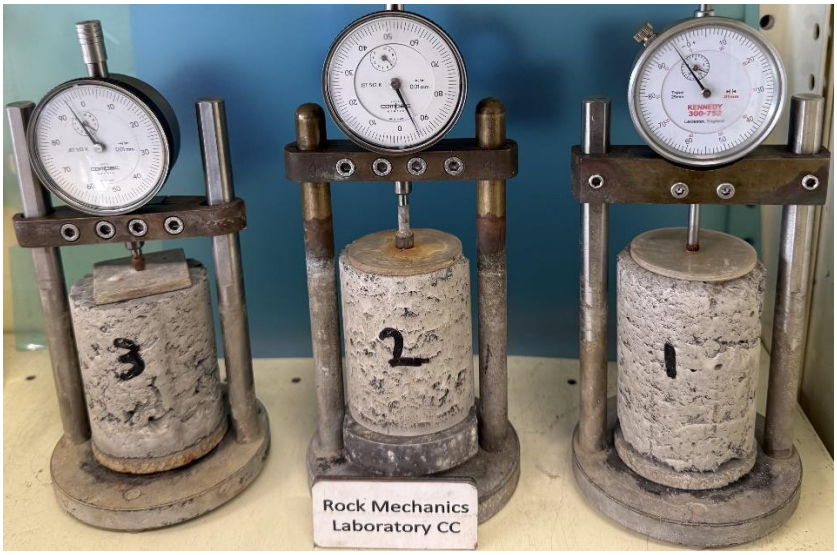


Figure 0-9: Shotcrete cores with strain gauges

The strain gauges were calibrated and connected to a data acquisition computer system that could capture micro-strain changes in real time. We recorded the initial zero reading (baseline) immediately after installation. The specimens were then placed in a climate-controlled chamber maintained at 23 ± 2°C and 50 ± 4% relative humidity to simulate standard laboratory drying conditions. Axial shrinkage strain was continuously monitored and recorded at predetermined intervals, typically at 3, 7, 28, and 56 days. The recorded strain (ε_s) over time was numerically evaluated as follows (Meschke,1997):

$$\varepsilon_s = \frac{\Delta L}{L_0} \quad (3.3)$$

where ΔL is the change in length and L_0 is the original length of the shotcrete specimen.

3.4.4 Uniaxial Compressive strength tests

Poisson's ratio and Young's modulus were determined through standard UCS tests. These tests were conducted on 12-cylinder specimens in accordance with the American Society for Testing and Materials (ASTM D 3148-72) (1997b). Cylindrical rock specimens were instrumented with both axial and lateral strain measurement devices to capture deformation behaviour under loading. Axial strain was recorded using Linear Variable Differential Transformers (LVDTs) affixed longitudinally along the specimen surface. Lateral strain was measured simultaneously using LVDTs positioned perpendicularly around the mid-height of each specimen. The specimens were carefully aligned between hardened steel plates within a servo-controlled loading frame to ensure concentric loading and avoid eccentric stress distribution. Axial load was applied continuously at a constant stress rate of 0.5 MPa/s to 1.0 MPa/s until failure, as shown in Figure 3-10.



Figure 0-10: Shotcrete specimen instrumented with both axial and lateral strain

During the loading phase, we continuously recorded stress and strain. Young's modulus (E) was subsequently determined as the slope of the linear-elastic portion of the axial stress–strain curve and was calculated as follows by Equation 3.4 (American Society for Testing and Materials, 1997b):

$$E = \frac{\Delta\sigma}{\Delta\varepsilon_a} \tag{3.4}$$

Where $\Delta\sigma$ represents the change in axial stress and $\Delta\varepsilon_a$ the corresponding change in axial strain within the elastic region.

Poisson's ratio (ν) was evaluated by calculating the negative ratio of lateral to axial strain over the same linear-elastic portion of the stress-strain curve (Kruger and van der Westhuizen, 2023):

$$\upsilon = -\frac{\varepsilon_l}{\varepsilon_a} \tag{3.5}$$

Where ε_l denotes lateral strain and ε_a denotes axial strain.

3.5 Development of multivariate regression models

Experimental and field data were initially imported into MATLAB from Microsoft® Excel® spreadsheets as tables, then transformed into numeric matrices to enable statistical analysis. Appendix G depicts this stepwise process. The next step involved a systematic preprocessing approach that entailed cleaning and validating missing and inconsistent data. Lastly, data were normalised and classified into two groups: short-term and long-term shotcrete performance. Data sets were well organised to reflect the relevant independent and dependent variables for shotcrete performance behaviour.

After data preprocessing, a correlation matrix was generated to measure relationships among variables using two approaches: Pearson correlation and Spearman correlation. Pearson correlation tested linear relationships between two variables, while Spearman correlation identified monotonic relationships when the data distribution was not normal. The correlation

coefficients were calculated using MATLAB statistical functions, producing symmetric matrices in which each entry reflects the strength and direction of relationships between pairs of variables. Alongside, statistical significance testing was conducted in the form of p-value calculations.

This statistical analysis produced the Pearson correlation heatmap to provide a detailed graphical depiction of the magnitude and nature of the factors driving the behaviour of dolerite–Xorex fibre-reinforced shotcrete over extended periods. It included a thorough analysis of both laboratory experiment findings and numerical simulation results from the previous analyses. The chosen set of input variables for this exercise encompassed curing time, tensile strength, modulus of elasticity (E), Poisson's ratio (ν), maximum stress, failure load, maximum shear, shear strength, strength factor in tension, total displacement, volumetric strain, and convergence.

Before visualisation, the data set was carefully filtered to check whether the data was complete, consistent, and appropriate for statistical analysis. The Pearson correlation coefficient (r) was computed to determine the strength of the linear relationship between all pairs of variables. Correlation coefficients ranged from −1 to +1. Positive values suggested a direct relationship, while negative values suggested an inverse relationship. Values near zero suggested no linear correlation between the variables. This correlation matrix was later visualised as a heatmap, using colours to show the intensity and direction of correlations.

The heatmap offered a brief graphical representation of the relationships between several variables. It helped identify the major parameters affecting shotcrete behaviour. The correlation analysis helped identify the variables with the greatest effect on shotcrete performance. This set of variables served as the foundation for developing prediction models. Only variables with the greatest effect on shotcrete performance were considered for model development. A multi-dimensional approach for variable selection was used. Experimental and field data in raw form were initially imported into MATLAB from Microsoft® Excel® spreadsheets as tables, then

transformed into numeric matrices to enable statistical analysis. Appendix G depicts this stepwise process. The next step involved a systematic preprocessing approach that entailed cleaning and validating missing and inconsistent data. Lastly, the data was normalised and classified into two groups: short-term and long-term shotcrete performance. Data sets were well organised to reflect the relevant independent and dependent variables for shotcrete performance behaviour.

3.6 Numerical simulations under static and dynamic loads

This section examines the numerical simulations used to understand how the rock mass around the tunnel and the Xorex fibre shotcrete support perform. For the simulation, several Rocscience software packages were used for the analysis, including Unwedge, RocSupport, and RS2. Numerical simulations were conducted using RocScience support software, including Unwedge, RS2, and GRC. The subsequent sections explain each software simulation in detail.

3.6.1 Simulations using Unwedge Deterministic analysis tool

Unwedge stability analysis is deterministic, meaning it does not explicitly account for variability and uncertainty in the input parameters. Kinematic and limit equilibrium analyses were carried out. Potential wedges were established through stereographic projections of intersecting joints. Stability was determined through evaluation of the ratio of driving to resisting forces to calculate the Factor of Safety FoS (Duncan, 2000):

$$FoS = \frac{\sum Resiting\ forces}{Driving\ forces} \tag{3.6}$$

Where FoS > 1 correspond to stable conditions, and FoS < 1 correspond to unstable conditions.

For each scenario, the software analysed potential wedges and calculated weight and FoS. After adding shotcrete support, Unwedge recomputed wedge stability and compared the unsupported and supported conditions.

For each kinematically valid wedge, the program calculates one key output variable: the Factor of Safety (FoS). An FoS value significantly greater than 1.0 suggests stability, whereas values near or below 1.0 indicate potential instability. These outputs provide a direct, quantitative assessment of shotcrete performance.

Rock Wedge Stability and the performance of dolerite-Xorex fibre-reinforced shotcrete were analysed using Unwedge software provided by Rocscience. The study evaluated the efficiency of fibre-reinforced shotcrete in minimising wedge failure and increasing stability during mining using the FoS. The numerical analysis followed laboratory and field-testing methods to produce realistic results. The model geometry was formulated based on the dimensions of the tunnel cross-section. The surface excavation dimensions (tunnel height and width) were specified as shown in Figure 3-11.

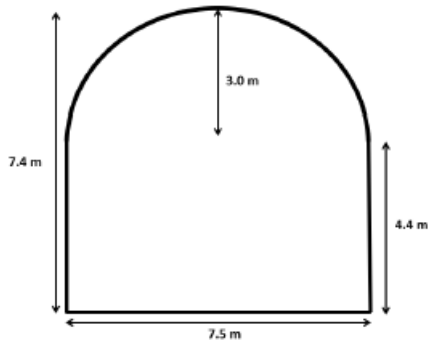


Figure 0-11:Cross-section dimensions used in this study

For each scenario, the software analysed potential wedges and calculated weight and FoS. After adding shotcrete support, Unwedge recomputed wedge stability and provided comparison between the unsupported and supported condition. For each kinematically valid wedge, the program calculates one key output variable which is the Factor of Safety (FoS). An FoS value significantly greater than 1.0 suggests stability, whereas values

near or below 1.0 indicate potential instability. These outputs provide a direct and quantitative assessment of the performance of shotcrete.

Rock Wedge Stability and the performance of dolerite-Xorex fibre-reinforced shotcrete were analysed using Unwedge software provided by Rocscience. The study evaluated the efficiency of fibre-reinforced shotcrete in minimizing wedge failure and increasing stability during mining using the FoS. Numerical analysis conducted was in line with laboratory and field-testing methods to create realistic analysis results. The geometry of the model was formulated by considering the dimensions of a tunnel cross-section. The dimensions of surface excavation in terms of height and width of the tunnel were specified as depicted in Figure 3-11.

Three joint sets were used to model the tunnel excavation with moderate stress. Every joint set indicates a primary direction where the supported rock is weak. Using three joint sets ensures a better understanding of how wedges might develop and fail around the tunnel. These joints were plotted on a stereonet to study any formation of wedge formation among them. This helps in understanding the overall geological structure (refer to Figure 3.12).

Parameters needed for the analysis include joint orientation (dip and dip direction), tunnel dimensions, rock unit weight, groundwater conditions, and in-situ stress conditions. It is also necessary to know joint shear strength parameters such as cohesion and friction angle. The parameters used for Unwedge simulation are listed in Table 3.3.

Table 0-3: Input parameters used for Unwedge simulations

Input parameter	
Unit weight rock	2.5 t/ m^3
Groundwater conditions	-
In situ stresses	4.5 MPa
Joint 1	66°/130°
Joint 2	87°/143°
Joint 3	85°/262.1°
Internal friction angle	As per each curing period (i.e., 46.6°, 49.5°, 51.6° and 49.3°)

Input parameter	
Cohesion	As per each curing period (i.e., 3.5, 3.8. 4.6 and 5.3)
Tensile strength	As per each curing period (i.e., 1.67, 2.63, 3.57 and 4.21)
Model	Mohr-Colomb model

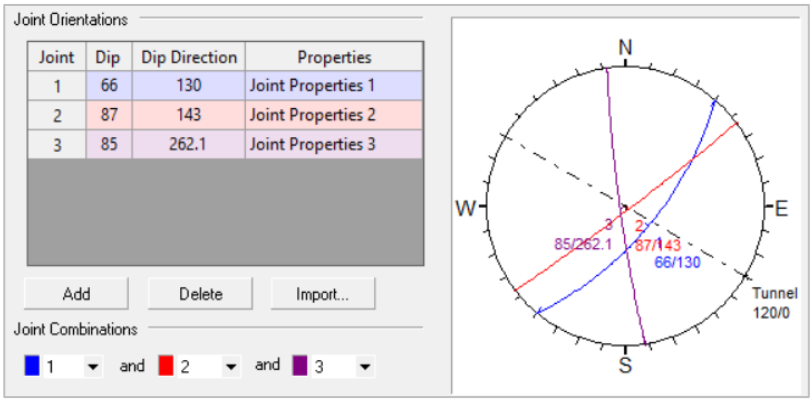


Figure 0-12: Stereonet of the simulated underground situation using Unwedge

Simulation modelling began with a control model assuming no shotcrete. Next, various scenarios involving the use of dolerite-Xorex fibre-reinforced shotcrete were generated by varying the input data depending on the curing age. The material properties such as cohesion, tensile strength, and angle of internal friction were modified based on the curing age through experimental values obtained from laboratory tests. A constant shotcrete layer thickness of 50 mm was applied in all simulation cases. Wedge geometry, weight of the wedge, and FoS values were computed by the simulations.

3.6.2 Simulation of Ground Reaction Curve

RocSupport software by Rocscience Inc. was used to simulate Ground Reaction Curves (GRC), analysing tunnel deformation behaviour based on stress redistribution due to tunnelling. The simulation provided a way of understanding how the rock mass interacted with the support system in the rock environment. The Hendrik Tunnel, located in Limpopo Province, South

Africa, was chosen as the case study because it lies in a sedimentary basin with sandstone formations (Figure 3-13). This study adopted the geomechanical data for the Hendrik Tunnel from a well-documented study by Madanda et al. (2025). The model requires field parameters such as the Geological Strength Index (GSI), intact uniaxial compressive strength, rock material and rock disturbance factor (see Figures 3-13 to 3-16).



Figure 0-13: Tunnel entry for the first and second tunnel

Figure 3-13 provides basic information for assessing the mechanical behaviour of the sandstone encountered in the Hendric tunnel. Figure 3-13(a) shows the intact UCS of sandstone, which is expected to be between 50 MPa and 100 MPa. This range relates to rock specimens that fracture after more than one strike with a geological hammer, suggesting moderate to high strength. These UCS values are crucial for determining bearing capacity, excavation methods, and tunnel support needs. Figure 3-13 (b) depicts the disturbance factor of 0.8. This factor is critical for adjusting intact rock strength in empirical models like Hoek-Brown, ensuring realistic rock predictions.

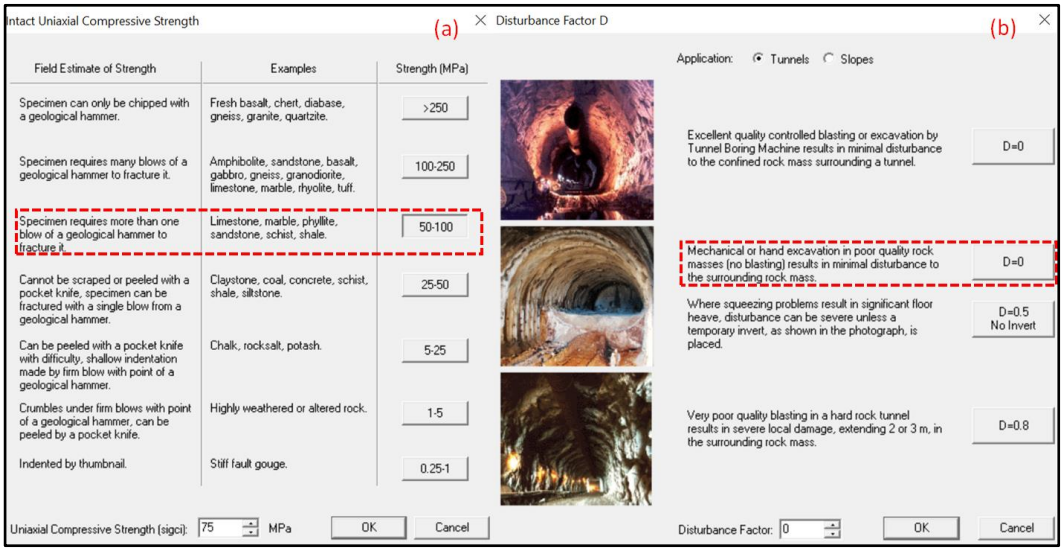


Figure 0-14: Estimation of rock mass properties – (a) intact uniaxial compressive strength of sandstone and (b) disturbance factor of the tunnel

Figure 3-14 shows additional rock mass characteristics. The Geological Strength Index (GSI) as seen in Figure 3-14(a), is an indication of the quality and structural condition of the rock mass. The GSI varies from well-structured intact rock masses to highly fractured and disintegrated rocks. Figure 3-14 (b) depicts the selection of the value. The value is a material parameter that is applied to the Hoek-Brown failure criterion for determining the strength behaviour of confined rock masses. The value of (m_i) is chosen from the 'Pick' instruction interface of the software, where specific values of (m_i) for rock masses are defined according to Hoek-Brown empirical data. Figure 3-14 shows additional rock mass characteristics. The Geological Strength Index (GSI), shown in Figure 3-14(a), indicates the quality and structural condition of the rock mass. The GSI varies from well-structured intact rock masses to highly fractured and disintegrated rocks. Figure 3-14(b) depicts the selection of the value. The value is a material parameter that is applied to the Hoek-Brown failure criterion for determining the strength behaviour of confined rock masses. The value of (m_i) is chosen from the 'Pick' instruction interface of the software, where specific values of (m_i) for rock masses are defined according to Hoek-Brown's empirical data.

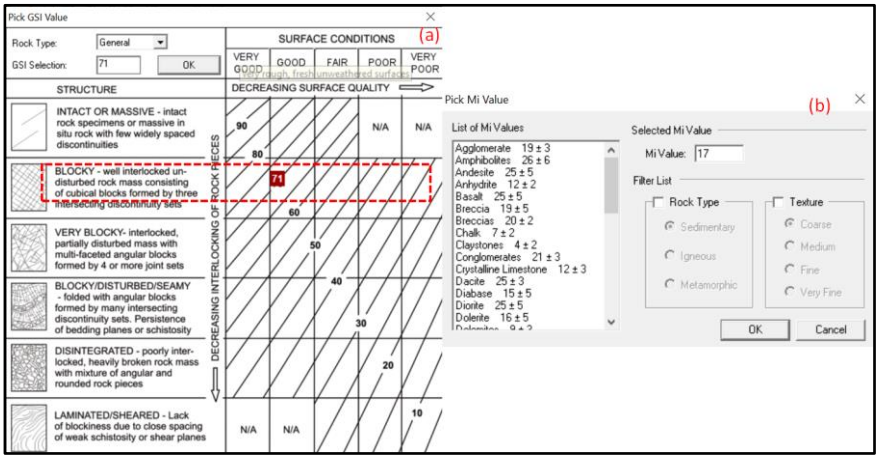


Figure 0-15: Estimation of rock mass properties – (a) Geological Strength Index of sandstone and (b) Maximum peak strength of the rock

Figures 3-15 (a) and (b) show the important stress relationships for modelling tunnel stability and shotcrete performance. Figure 3-15(a) shows the non-linear relation between the major (σ_1) and minor (σ_3) principal stresses. This relation describes the rock mass strength envelope and calibrates the Hoek-Brown failure criterion for modelling. Figure 3-16 (a) and (b) depict the shear versus normal stress envelope, which captures the combined effects of friction and cohesion while revealing probable failure planes around the excavation.

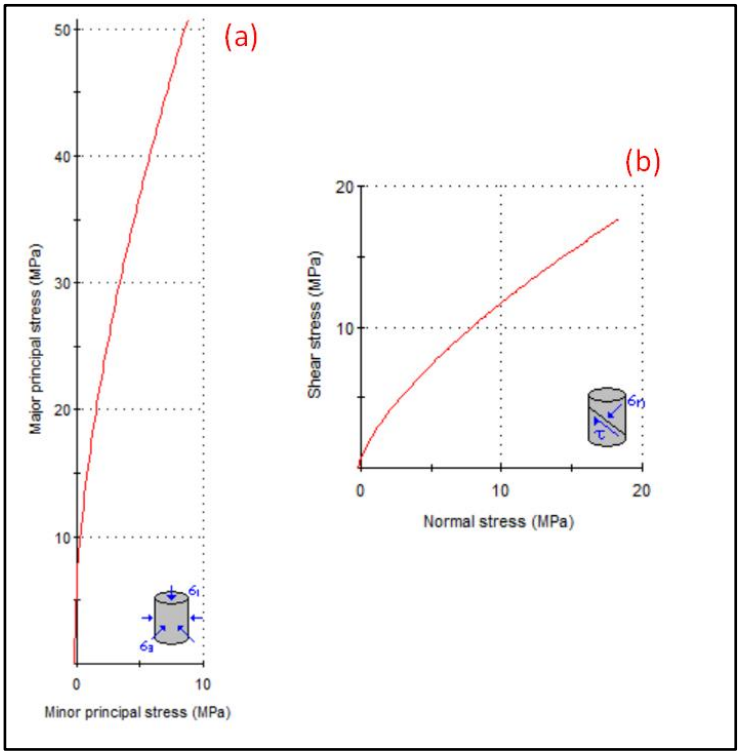


Figure 0-16: Estimated stresses of the rock mass – (a) Plot showing major and minor stress and (b) Shear stress and Normal stress of the rock unit

The rock mass properties of sandstone used for this study are documented in Table 3-4.

Table 0-4: Input parameters for the simulation of Ground Reaction Curve

RocLab input	**Description**	**Symbol and (units)**
σ_{ci} (MPa)	Uniaxial compressive strength of intact shotcrete material	As per data collected
GSI	Geological Strength Index	69
m_i	Hoek–Brown material constant for intact material	17
D	Disturbance factor	-
m_b	Reduced Hoek–Brown material constant for the rock mass/shotcrete mass	5.61853
S	Hoek–Brown rock mass constant	0.031923
A	Hoek–Brown exponent	0.501463
C (MPa)	Cohesion	As per data collected
ϕ (°)	Internal friction angle	As per data collected

RocLab input	Description	Symbol and (units)
σ_t (MPa)	Tensile strength	As per data collected
σ_c (MPa)	Rock mass compressive strength	6,22197
σ_{cm} (MPa)	Rock mass/global compressive strength	11,8895
E_m (GPa)	Deformation modulus (Young's modulus) of the rock mass / shotcrete mass	As per data collected

The shotcrete evaluated for this study included several critical parameters, such as shear strength, compressive strength, Young's modulus, and Poisson's ratio, all monitored throughout the curing process. Chapter 4 provides details about the estimation of these mechanical properties. These properties were incorporated into numerical simulations to analyse the behaviour of the material under various conditions. The comprehensive material characteristics of the shotcrete applied within the tunnel are provided in Table 3-5.

Table 0-5: Material properties of shotcrete applied for the tunnel

Curing period (days)	Young's Modulus (E)	Poisson ratio (υ)	Shear strength (τ)	UCS σ_c (MPa)	Tensile strength σ_t (MPa)
4	12.47	0.18	8.75	10.85	1.67
7	15.36	0.17	9.65	12.33	2.63
28	18.98	0.35	10.75	19.91	3.57
56	20.34	0.37	11.10	22.07	4.21

3.6.3 Simulations of the selected tunnel in RS2 software

Numerical analysis for a shallow underground mine tunnel lined with fibre-reinforced shotcrete was performed using Phase2 (RS2) finite element modelling software. The modelling exercise aimed to examine deformation characteristics, stress redistribution, and overall tunnel stability at shallow depths under in-situ stress conditions.

A geometric model of the tunnel was created using actual measurements obtained from the shallow underground mining environment. This model consisted of the actual tunnel parameters to simulate realistic ground behaviour. The finite element grid was carefully set near the tunnel edges to enable realistic analysis of stress concentrations and deformation areas, as shown in the modelled geometry.

Before the analyses, the boundary conditions, convergence criteria, and solver settings were determined to ensure stable numerical computation and accurate solutions. The model boundary was set to impose in-situ confining stresses while allowing deformation near the excavation.

The initial stress state represented a shallow in situ stress state. This was because the model considered the overburden depth and the horizontal-to-vertical stress ratio in the underground environment. Experimental results described the rock mass and fibre-reinforced shotcrete characteristics. The input parameters listed in Tables 3-4 and 3-5 were used to define the material properties for the numerical simulation. The corresponding input parameter interface is presented in Figure 3-17.

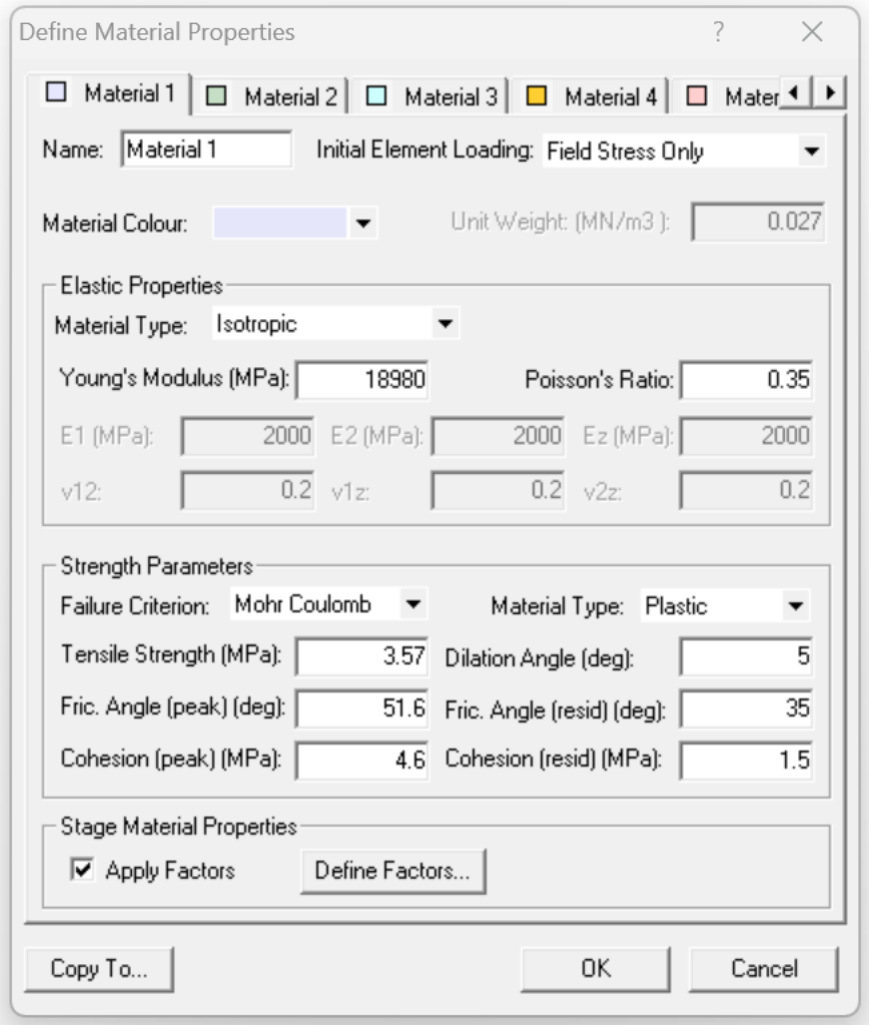


Figure 0-17: Input material parameters for the Mohr–Coulomb model of dolerite–Xorex fibre-reinforced shotcrete.

The results obtained included total displacement, strength ratio, maximum shear strain and volumetric strain. These results were used to evaluate tunnel stability, deformation behaviour and the performance of the dolerite-Xorex fibre-reinforced shotcrete.

3.7 Limitation of the work and challenges encountered

The study investigated a single shotcrete mix comprising Xorex fibres, BFSC, dolerite aggregates, water, and a high-range water-reducing admixture. This controlled the experimental variables but limits the generalisability of the findings to other mix designs, fibre contents,

aggregate types, and binder systems. The results therefore characterise the performance of the investigated formulation rather than shotcrete generally.

Creep was not evaluated because the required laboratory equipment was unavailable. Consequently, the experimental and numerical analyses do not account for time-dependent creep deformation. This limits the interpretation of long-term support behaviour and prevents direct comparison with constitutive models that explicitly incorporate creep.

The specimens were air-cured. The study therefore did not assess the effects of alternative curing regimes on hydration, strength development, and shrinkage. Consequently, the findings should not be extrapolated directly to shotcrete exposed to substantially different curing environments.

The numerical model was not independently validated against field measurements. Although the experimentally determined material properties informed the numerical simulations, no field-scale application or monitoring was undertaken to verify the predicted support response. The model results are therefore numerical predictions rather than field-validated performance estimates. Their accuracy also depends on the reliability of input parameters such as the Geological Strength Index, disturbance factor, in-situ stress state, discontinuity properties, and shotcrete mechanical properties.

The proposed mix was also not evaluated under actual underground spraying conditions. Its sprayability, pumpability, rebound, placement behaviour, and in-situ performance therefore remain to be established. Future research should address these limitations through creep testing, alternative curing regimes, evaluation of multiple mix designs, and field-scale trials with independent monitoring and model validation.

Chapter 4: Effect of dolerite aggregates and Xorex fibres on shotcrete properties

4.1 Introduction

The chapter gives the mechanical properties of the shotcrete reinforced with dolerite aggregates and Xorex fibres after curing periods of 4, 7, 28, and 56 days. The data collected through UCS, TCS, tensile strength, shear strength, Young's modulus and shrinkage tests will be carefully analysed to establish the process of strength increment. For convenience and conciseness throughout this thesis, shotcrete with dolerite aggregates and Xorex fibres is termed dolerite-Xorex fibre-reinforced shotcrete.

4.2 Evolution of the Uniaxial Compressive Strength with time

This section presents a detailed analysis of the results associated with UCS tests presented earlier in Chapter 3. In addition to this, the results for Young's modulus and Poisson's ratio are discussed; the raw data are depicted in Appendix D.

4.2.1 Uniaxial Compressive strength of the fibre-reinforced shotcrete

Table 4-1 depicts test results obtained for the UCS, Poisson's ratio and Young's modulus. All tests were performed on a servo-controlled electromechanical loading machine. The data acquisition system used was a computer linked to the electromechanical loading machine, as shown in Figure 3-10.

Table 0-1: Mean and standard deviation of UCS, Young's modulus, and Poisson's ratio at various curing ages

			Uniaxial Compressive Strength (MPa)			Young's modulus (GPa)			Poisson's ratio (-)		
Specimen No	**Curing time (days)**	**Mass (g)**	**UCS (MPa)**	**Average UCS (MPa)**	**Standard deviation UCS**	**E (GPa)**	**Average $\overline{E}$ (GPa)**	**Standard deviation E_σ**	**υ (-)**	**Average $\overline{\upsilon}$ (-)**	**Standard deviation υ_σ**
1	4	447.7	11.04	10.85	0.44	13.50	12.47	1.181	0.24	0.18	0.07
2	4	407.8	11.17			11.18			0.09		
3	4	379.8	10.35			12.74			0.20		
4	7	441.9	12.36	12.33	0.48	13.86	15.36	1.315	0.15	0.17	0.05
5	7	344.5	12.80			15.80			0.18		
6	7	440.1	11.84			16.43			0.17		
7	28	414.8	19.48	19.91	0.71	18.78	18.98	0.223	0.34	0.35	0.04
8	28	411.5	20.73			18.96			0.26		
9	28	321.9	19.53			19.21			0.44		
10	56	419.7	21.37	22.07	1.25	20.57	20.34	0.206	0.64	0.37	0.20
11	56	408.7	21.33			20.29			0.26		
12	56	374.9	23.52			20.17			0.26		

The UCS data in Table 4.1 show steady growth in compressive strength over the curing period. At day 4, samples showed an average UCS of 10.85 MPa with very low variation (σ = 0.44 MPa), indicating high reliability and uniformity in curing. At day 7, UCS was 12.33 MPa (σ = 0.48 MPa), showing the mix has adequate strength to provide initial underground support. The most significant changes occurred at higher ages; at day 28, UCS was 19.91 MPa (σ = 0.71 MPa), and at day 56, UCS was 22.07 MPa (σ = 1.25 MPa). This steady growth is primarily attributed to cement hydration, as C-S-H gel is a fundamental component in the development of any cementitious material (Liu et al., 2021).

Variations at lower ages were consistently small (≤ 0.5 MPa), suggesting well-controlled curing. As curing age increased, variability rose moderately (σ = 1.25 MPa), likely due to the heterogeneity of fibre-reinforced shotcrete, where aggregate and fibre orientation play an important role. The angular shape and density of the dolerite aggregates (specific gravity 2.8–3.0) increased interlocking, internal friction, and load-dispersion properties of the materials (Michael et al., 2013).

Compared with international benchmarks, the mixture does not fully meet the UCS requirements at the curing times tested. According to the American Shotcrete Institute of Concrete 506R (2016), the UCS values needed for standard shotcrete mixes range from 15 MPa to 25 MPa after 7 days and from 20 MPa to 40 MPa after 28 days. The dolerite-Xorex fibre-reinforced shotcrete mix yielded 12.33 MPa at 7 days and 19.91 MPa at 28 days, thus failing to match the UCS values.

This variation may be explained by the relatively low fibre content of 0.02 wt% Xorex used in the mix, compared with standard shotcrete mixes, which normally use 2 wt% fibres to improve early-age strength and performance after cracking (Liu et al., 2021). This suggests the possibility of increasing the fibre dosage to meet international standards while remaining economically viable.

The sample mass decreased from about 411.7 g on day 4 to 374.4 g on day 56 due to the hydration reaction and moisture loss from the sample matrix. However, despite the decrease in the mass of the samples, there was an increase in the UCS and Young's Modulus because of curing.

4.2.2 Stress-strain relationship under Uniaxial Compressive Strength testing conditions

The axial and radial stress-strain results in Figure 4-1 evaluate the compressive performance of dolerite-Xorex fibre-reinforced shotcrete at 4, 7, 28, and 56 days of curing. Figure 4-1 clearly illustrates the development of UCS.

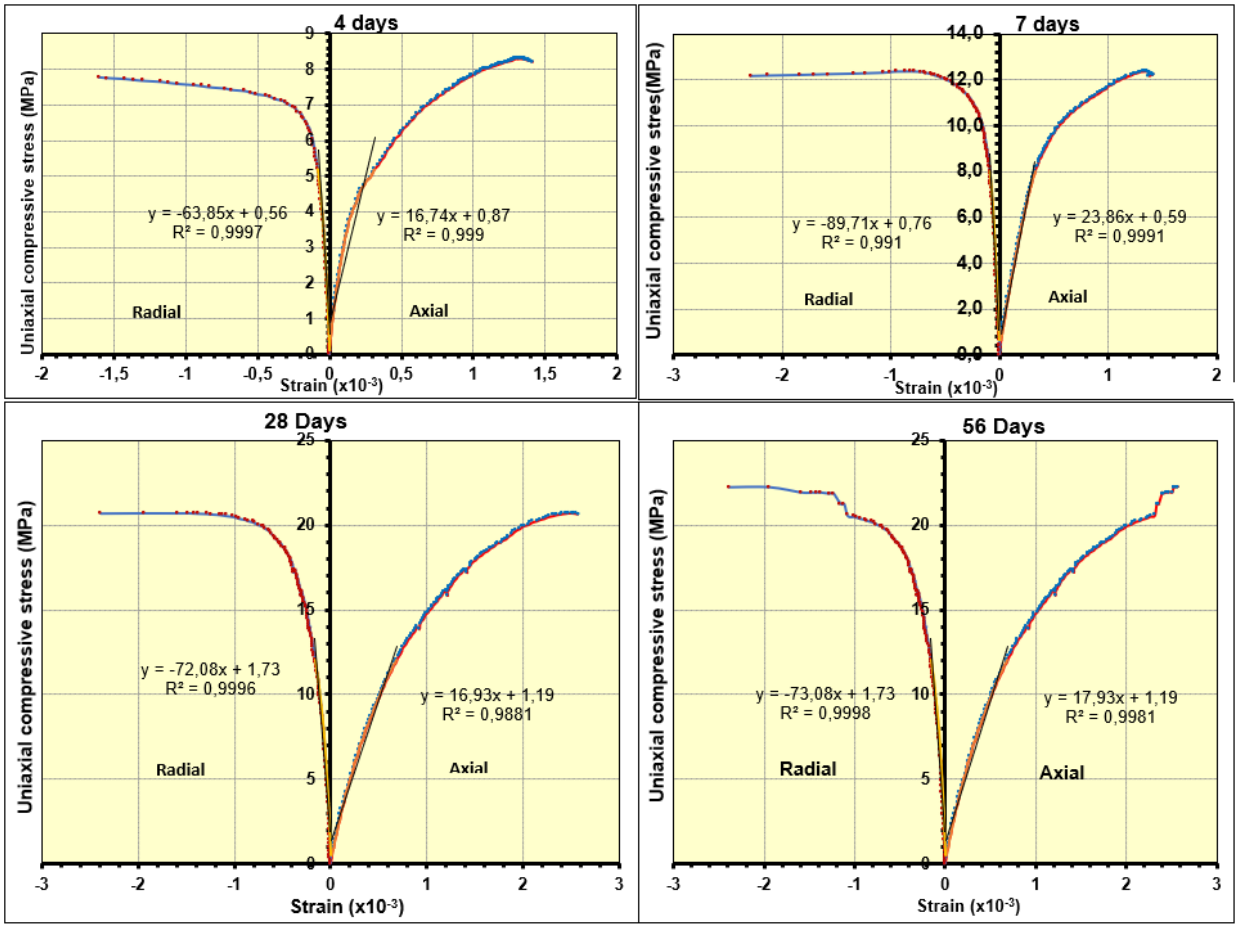


Figure 0-1: Stress-strain relationships for axial and radial deformation under uniaxial compression at varying curing durations (4, 7, 28, and 56 days)

At 4 days, the axial stress–strain curve has a moderate elastic slope. This indicates the early stiffness of the shotcrete matrix. At this stage, the hydration process is still in its early stages. Yet the dense dolerite aggregates help create a high elastic modulus of 12.47 GPa (Zhou et al., 2025). The axial curve moves into a nonlinear zone as microcracks begin to form. The rounded peak and slow post-peak drop suggest that Xorex fibres already help bridge cracks and increase ductility. Radial strain at this age starts to grow earlier in the loading sequence. This proves that the young matrix allows expansion at lower stress levels. Still, the radial curve stays smooth, which indicates that fibres help control microcrack growth. The high regression coefficients ($R^2 \approx 0.999$) for both axes show steady early-age behaviour despite limited matrix maturity.

At 7 days, the axial stress–strain curve becomes noticeably steeper, indicating that the material is getting stiffer as hydration progresses and the bond between paste and aggregate strengthens. Peak uniaxial compressive strength rises to around 12–13 MPa, showing a sharp early increase in strength. The axial curve still shows a rounded peak, indicating that the fibres are working as intended by enhancing ductility and reducing brittleness (Thomas, 2018). Radial strain does not appear until later in the loading process, unlike at 4 days. This happens because the matrix is further developed and the dolerite aggregate is stiffer than the matrix. Dilation becomes significant only as the curve approaches the nonlinear region, and even then, it remains well controlled due to the crack-bridging effect of Xorex fibres. The linear elastic region still shows a very strong correlation, with R^2 remaining above 0.99. At 7 days, the mechanical response remains highly consistent.

At 28 days, the axial stress–strain curve becomes noticeably steeper in the elastic region, indicating that the shotcrete matrix is fully developed and well bonded. Compressive strength peaks at about 20 MPa to 21 MPa, meaning the shotcrete reaches its elevated strength. After this peak, the curve is smoother than at earlier ages; the fibres play a bigger role here, increasing ductility (Bernard, 2015). For most of the loading, radial strain remains low,

with dilation only appearing near peak stress. This limited expansion shows the confining effect of dolerite aggregates and fibres, which keep cracks tight. The stress–strain data are consistent and reliable, with regression values close to 0.99. By 28 days, the results demonstrate clear maturity and stability.

At 56 days, the axial stress–strain curve is very similar to the curve at 28 days; however, it is slightly stiffer, with peak compressive strength reaching about 22 MPa to 23 MPa. This increase in stiffness shows that the shotcrete has completed the hydration process and reached its maximum strength. The axial curve still shows a rounded peak, meaning the Xorex fibres keep the shotcrete ductile and help prevent brittle failure, even at this stage (Thomas, 2018).

Radial strain remains low for most of the loading, increasing only as stress aggregates. This pattern indicates strong confinement from the dense dolerite aggregates and a mature matrix, along with strong fibre bridging across any developing cracks (Bernard, 2010). The R^2 values for both axial and radial fits show consistent, reliable shotcrete behaviour. This shotcrete mix performs well in terms of crack control and stress–strain behaviour.

The dense dolerite aggregates give the structure rigidity, making shotcrete resistant to deformation. Xorex fibres act early, bridging microcracks before they expand, so the material fails gradually rather than breaking suddenly. As the shotcrete cures, the stress–strain curves become steeper and the mix gains strength. However, the curves remain rounded with no sharp, brittle peaks, and the fibres maintain ductility, keeping cracks under control.

This stress-strain curve indicates resilient mechanical performance. Unconfined compressive strength (UCS) indicates how much load a material can withstand before failing. However, to fully understand its behaviour, it is important to examine its stress-strain response. This relationship shows the peak strength given by the UCS and reveals how shotcrete deforms under compression. The next Section discusses the stress-strain relationship associated with uniaxial compressive strength.

Besides the deformation associated with UCS, other factors such as Young's modulus and Poisson's ratio indicate the mechanical resilience of shotcrete.

4.2.3 Role of fibre type and dosage in the development of the Uniaxial Compressive Strength

Results from the UCS tests clearly show significant differences between the fibre-reinforced shotcretes reported in the literature and the dolerite-Xorex fibre-reinforced shotcrete proposed in this research after 28 days. In the literature, the mixes (Zhou et al., 2025; Khosh and Atapour, 2024) incorporated a fibre content of 1 wt. However, this study used a fibre dosage of 0.02 wt%, as shown in Figure 4-2. Furthermore, error bars efficiently represent the variation in uniaxial compressive strength measurements for fibre-reinforced shotcrete. The short error bars across all fibre types show consistency in the experimental findings, meaning the results deviate little from the mean values.

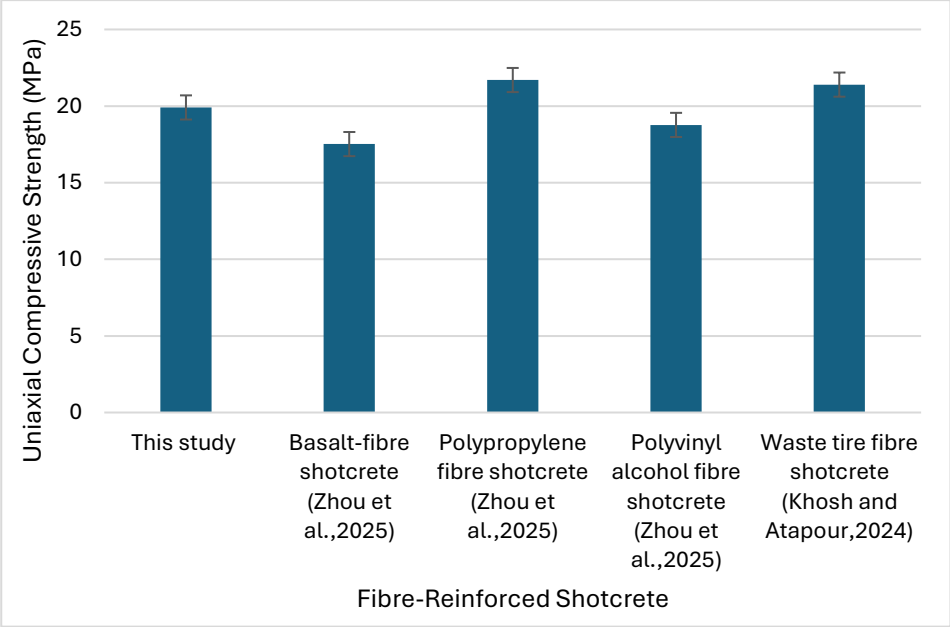


Figure 0-2: UCS values of shotcrete at 28 days for this study and published literature with error bars representing 95% confidence range

In comparisons of various sets of data, basalt-fibre shotcrete always has the lowest compressive strength, standing at approximately 17-18 MPa, while PVA-fibre systems slightly surpass it at around 19 MPa. In this regard, polypropylene-fibre shotcrete (≈21-22 MPa) and waste textile fibre systems (≈21 MPa) show better performance.

The current mix design produced a UCS of 19.9 MPa with an extremely small fibre addition of 0.02 wt%. While this result is insufficient to meet the minimum standards outlined by EFNARC (2019), it is important to compare it with other fibre-reinforced shotcrete systems described in the literature. The following Sections will address Young's modulus and Poisson's ratio; these two parameters are crucial for characterising elastic deformation.

4.2.3.1 Poisson's ratio of the reinforced shotcrete

Table 4-1 presents the measured values of Poisson's ratio, averaging 0.18 to 0.37 with a standard deviation ($\sigma \leq 0.20$). During the early stages of curing (4-7 days), the average value was about 0.18 with a very small variance (σ = 0.05-0.07). Thus, at early curing stages, specimens displayed constant behaviour in terms of lateral strains. At 28 days, the average Poisson's ratio increased to 0.35 (σ = 0.04), and at 56 days it reached 0.37 (σ = 0.20), indicating an increased lateral deformation capacity as the matrix matured.

This study used static Poisson's ratios, measured under controlled laboratory load conditions. The difference between static and dynamic Poisson's ratios comes from differences in loading rate and material responses. Static Poisson's ratio is measured when slow and gradually applied loads are used, while dynamic Poisson's ratio is measured by rapid loads using the wave propagation approach to measure the instantaneous elasticity of the material. Measured values of Poisson's ratio in this study are 0.18 on day 4; 0.17 on day 7; 0.35 on day 28; and 0.37 on day 56.

The increment in Poisson's ratio over time is related to continuous hydration, densification of the shotcrete matrix, and better bonding, among

other factors. According to Ahmed (2018), Poisson's ratio for shotcrete ranges from 0.21 to 0.25 at 7 and 28 days. However, Byfors (1980) noted greater variation in static Poisson's ratio, ranging from 0.13 to 0.68 depending on test conditions and material type. The dynamic range was narrower, at around 0.21- 0.25, according to Mesbah (2002).

Table 4-2 depicts the Poisson's ratio of this mix design compared with the Poisson's ratio documented in the literature (EFNARC, 2019). The mechanical validity of shotcrete relies on Poisson's ratio to predict deformation patterns and assess the ability of the material to redistribute stresses, which is crucial for anticipating cracking or structural failure.

Table 0-2: Comparison of Poisson's ratio (ν) ranges between EFNARC (2019) and Xorex-dolerite reinforced shotcrete

Source / Mix composition	**Poisson's ratio (υ) (7 and 28 days)**
7 days	
European Federation of National Associations Representing Concrete (EFNARC, 2019)	0.18
This current study	0.18
28 days	
European Federation of National Associations Representing Concrete (EFNARC, 2019)	0.25
Current study	0.35

The Poisson ratio in this study ranged from 0.18 to 0.37 at 7 days and 28 days, respectively. EFNARC (2019) and Bernard (2020) reported typical values between 0.18 and 0.25 for 7 days and 28 days, respectively. These figures are attributed to the limited lateral strain capacity resulting from the rounded and smooth surface of natural sand.

The Poisson's ratio recorded at 7 days is consistent with the one reported by EFRNAC (2019). Conversely, at later stages of curing, this study reports 0.37, which is higher than 0.25. This indicates that this mix design can

absorb and redistribute stresses laterally as curing advances (Xie et al., 2024). As Kim et al. (2021) reported, incorporating rough, angular aggregates enhances interparticle friction and mechanical interlock.

The observed trend in this study underscores the noticeable influence of aggregate shape and surface texture on the elastic properties of fibre-reinforced shotcrete. Angular dolerite aggregates promote greater interlock and improve lateral stress transfer under compression. Additionally, introducing Xorex fibres enables more effective crack bridging and stress redistribution within the matrix at a low dosage of 0.02wt%.

4.2.3.2 Development of Young's modulus over time

Young's modulus (E), or modulus of elasticity, is a vital mechanical property that defines the stiffness of a material. This development of stiffness in shotcrete, as indicated by Young's modulus (E), plays a critical role in understanding its elastic response under uniaxial loading.

At 4 days, E was measured at 12.44 GPa, rising to 15.36 GPa at 7 days, 18.98 GPa at 28 days, and reaching 20.34 GPa by 56 days. This trajectory is consistent with ongoing hydration and densification processes typical of cement-based materials, where microstructural development leads to increased stiffness over time (Liu et al., 2021).

The measured Young's modulus values for fibre-reinforced shotcrete with Xorex fibres were evaluated at curing ages of 4, 7, 28, and 56 days. Table 4-3 presents the Young's modulus results of this study and compares them with previously published data on shotcrete incorporating natural sand and steel fibres, allowing for an assessment of how both curing time and fibre reinforcement impact the stiffness of the material.

Table 0-3: Comparative table of Young's modulus for shotcrete with sand and steel fibres

Curing age (Days)	**Young's modulus E (GPa) for a type of shotcrete with references**	
	Natural sand + Steel fibres	**Crushed dolerite + Xerox fibres (This study)**
4	12.5 – 18.0 (Kim et al., 2018)	12.44
7	18.0 – 22.0 (Kim et al., 2018)	15.36
28	28.0 – 33.0 (Lee et al., 2016)	18.98
28	21,537 (Neuner et al.,2017)	
56	30.0 – 34.0 (Lee et al., 2016)	20.34

The dolerite-Xorex fibre-reinforced shotcrete mixes demonstrated an increasing Young's modulus, which improved from 12.44 GPa at 4 days to 20.34 GPa at 56 days. Nonetheless, the observed Young's modulus remained significantly lower than in other studies using conventional shotcrete mixes containing natural sand and steel fibres, where the minimum value ranged from 27.9–28.9 GPa (Kim et al., 2018; Lee et al., 2016). The reduced stiffness of dolerite mixes may be linked to factors such as the lower fibre content used in the mixture (0.02 wt% Xorex fibres compared to 2 wt% steel fibres).

Additionally, the mineralogical nature of dolerite aggregates and the microstructure of dolerite mixes hindered their elastic performance. While dolerite aggregates produced better compressive strength, the observed elastic stiffness was lower than that recorded in mixes with sand. In conclusion, the results show an important balance between strength and stiffness, and the importance of mix optimisation to meet international shotcrete requirements. The next section assesses the triaxial compressive

strength of the shotcrete. This characteristic is very important in determining how well it resists cracking and how durable it is in underground settings.

4.2.4 Triaxial Compressive Strength of dolerite-Xorex fibre-reinforced shotcrete

The TCS tests were conducted with three different confining stresses (σ_3), which were applied to get different values of the major principal stress (σ_1) depending on the confining stress. The results of this test are shown in Appendix B. The confining stresses (i.e., 0.5, 1 and 2) were used because they are standard in triaxial testing for tunnel support materials, as they reflect the real-world rock mass confinement acting on an initial shotcrete support layer. The results produced graphs showing the correlation between confining stress and the material's strength at different confining levels, as shown in Figure 4-3.

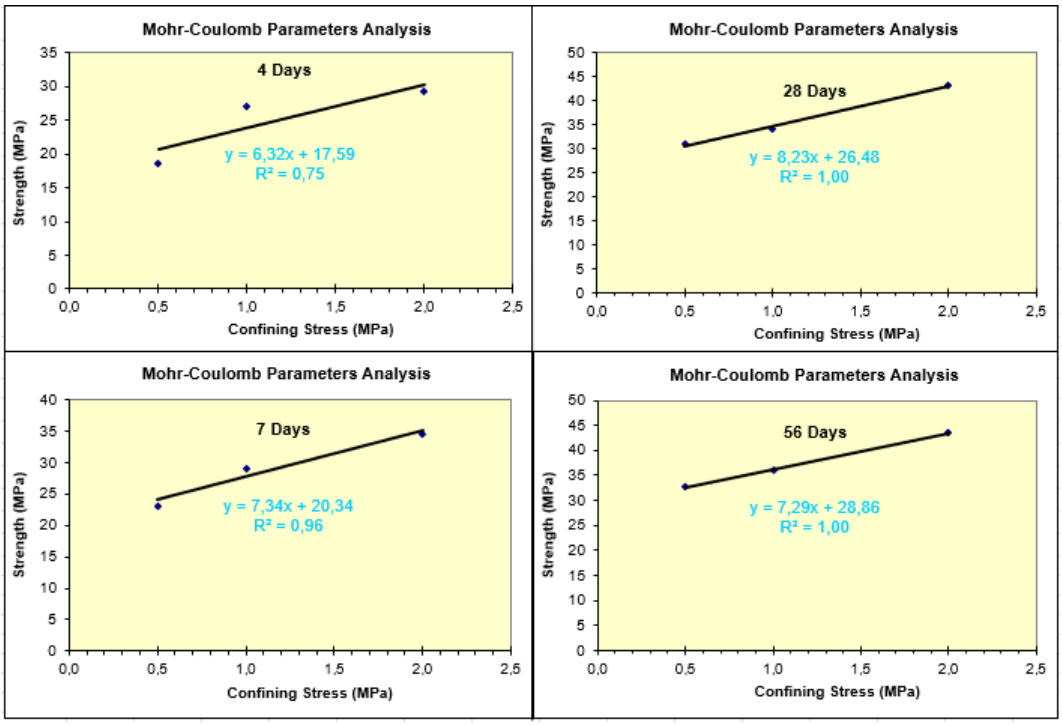


Figure 0-3: Variation of Mohr-Coulomb shear strength parameters of fibre-reinforced shotcrete over different curing ages

At the lowest value of σ_3 = 0.5 MPa, there is a strength gain from 18.7 MPa at 4 days to 23.1 MPa at 7 days, followed by an appreciable increase to 30.9 MPa at 28 days. A small increase to 32.6 MPa at 56 days suggests that strength development tends to level off after 28 days.

In the case of σ_3 = 1.0 MPa, strength gain occurs from 27.1 MPa at 4 days to 29.0 MPa at 7 days, 34.2 MPa at 28 days, and 36.0 MPa at 56 days. These observations are due to continuous hydration and densification of the matrix, which enhances crack-bridging capability under moderate confinement (Thomas, 2018).

For the highest level of confinement (σ_3 = 2.0 MPa), the strength gain is maximum, as it increases from 29.2 MPa at 4 days to 34.6 MPa at 7 days and reaches 43.1 MPa at 28 days. Thereafter, strength shows no significant change at 56 days, and it remains 43.5 MPa, indicating a nearly fully matured material. This behaviour is characteristic of compacted geomaterials under high triaxial stresses, as strength becomes more dependent on particle friction, aggregate locking, and confinement-induced restriction of crack expansion (Zhou et al., 2025). The behaviour at 56 days shows that the microstructure has fully matured.

Overall, these trends show that initial hardening relates to rapid cement hydration and pore refinement, whereas the steady period after day 28 reflects microstructure stabilisation accompanied by slower formation of hydration products (Neville, 2012; Mehta and Monteiro, 2014). The low gains during later periods may also indicate an approach to a quasi-stable state, characterised by insignificant curing influence on mechanical properties. Although the dolerite–Xorex fibre shotcrete did not meet the UCS criteria, the TCS results showed a progressive increase in strength with increasing curing age and confining pressure.

The results indicate the ability of the shotcrete mix to achieve high strength under confinement. The next section discusses the Mohr-Coulomb parameters that were assessed as part of the TCS testing.

4.3 Mohr-Coulomb parameters

This study assessed the Mohr-Coulomb parameters, including the strengthening parameter (β), cohesion (C), and internal friction angle (ϕ) of the reinforced shotcrete. Table 4-4 summarises the results for these parameters.

Table 0-4: Development of cohesion (C), internal friction angle (ϕ) and strengthening parameter (β) with curing duration for the shotcrete specimens

Curing duration (days)	Cohesion C (MPa)	Internal friction angle ϕ (°)	Strengthening parameter β (-)
4	3.5	46,6	6.32
7	3.8	49.5	7.34
28	4.6	51.6	8.23
56	5.3	49,3	7.29

4.3.1 Determination of cohesion and friction angle of reinforced shotcrete

Cohesion (C) and internal friction angle (ϕ) increase consistently as curing time progresses. This is important when assessing how shotcrete will perform in tunnel support. Cohesion rose from 3.5 MPa at 4 days to 5.3 MPa by 56 days, clearly indicating improved matrix bonding and effective fibre reinforcement, which aligns with the typical strength gain of cement-based materials during hydration (Neville, 2012; Mindess et al., 2003).

Dolerite-Xorex fibre-reinforced shotcrete demonstrated significantly higher cohesion values starting at 3.5 MPa at early curing stages and reaching approximately 5.3 MPa after extended curing periods. This improvement in cohesion is primarily attributed to two factors: initially, the angularity and hardness of dolerite aggregates, which enhance particle interlock. Second, Xorex fibres improve crack-bridging capacity and enable more effective stress distribution. Notably, recent research corroborates that replacing

natural sand with crushed, hard rock aggregates such as dolerite or granite can elevate cohesion values beyond 4.5 MPa (Ghasemalizadeh and Khoshnazar, 2024).

The internal friction angle increases from 46.6° after 4 days to 49.5° after 7 days, reaching a peak of 51.6° after 28 days. This indicates that shear strength evolves during hydration, resulting in a denser matrix structure. These behaviours are due to better particle interlocking, stronger bond strength between the aggregates and matrix, and higher shear-sliding resistance of the mature cementitious matrix. The decrease in the friction angle from 49.8° to 49.3° at 56 days shows microstructural stability and little additional curing effect on shear strength development.

Conventional shotcrete mixtures made from natural river sand and steel fibres usually have friction angles that range from 35° to 45° (Beer, 2015). This is because river sand particles are round or sub-round, providing moderate inter-particle friction (Beer, 2015). Adding steel fibres mainly affects ductility and crack resistance, not the friction angle.

4.3.2 Strengthening parameter relative to the reinforced shotcrete

The strengthening effect (β) given in Table 4-6 rises from 6.32 at 4 days to 8.23 at 28 days. This is due to higher confinement efficiency, a denser matrix, and greater interlocking of aggregates with age. This rise indicates better stress transmission and the formation of a cohesive, load-carrying matrix. At 56 days, it falls to 7.29, indicating microstructural stabilisation and entry into the maturity stage of hydration. Beyond this stage, hydration contributes little to strength gain. Confinement efficiency peaks at 28 days, and beyond this period, performance remains stable.

Altogether, these findings highlight how combining high-friction, angular aggregates like dolerite with Xorex fibres can substantially enhance the strengthening parameter. Tensile strength is another key mechanical

property for assessing shotcrete. This aspect is discussed in detail in the following section.

4.4 Tensile strength development

Tensile strength determines the ability of the shotcrete to resist the initiation and propagation of cracking under tensile stress. Appendix C provides the raw data used to plot the tensile strength relationship in Figure 4-4.

The findings indicate a clear, incremental increase in tensile strength over time: 1.67 MPa at 4 days, 2.63 MPa at 7 days, 3.57 MPa at 28 days, and reaching 4.21 MPa at 56 days. This progression can be attributed to cement hydration and enhanced fibre–matrix bonding in cementitious composites.

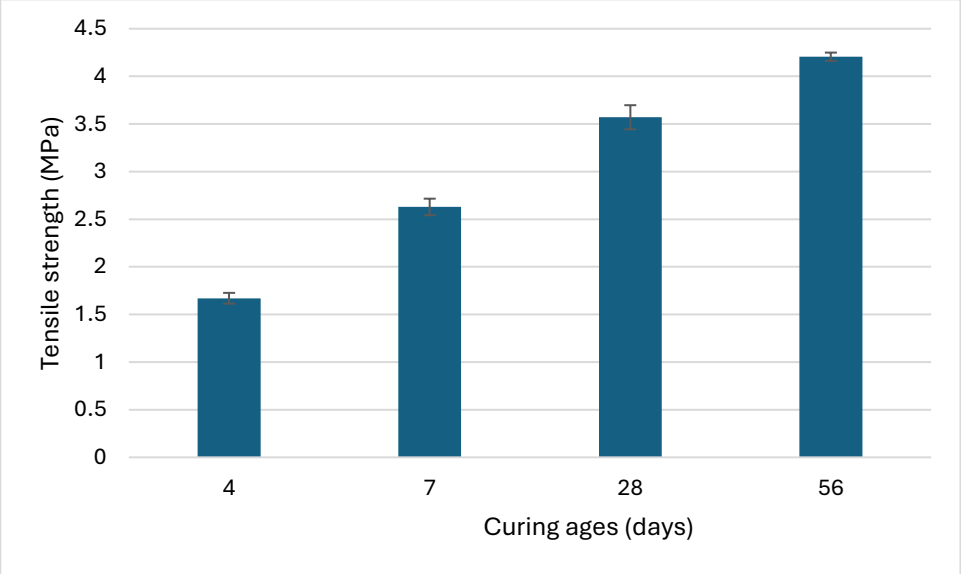


Figure 0-4: Development of the tensile strength of the reinforced shotcrete over various curing days with error bars representing 95% confidence range

At 7 days, the tensile strength was recorded at 2.63 MPa, which is within the range of 2.5-3.5 MPa recommended by EFNARC (2006) as being suitable for early-age shotcrete application. This indicates good early hydration and adequate strength development. The tensile strength was recorded at 3.57 MPa at 28 days, slightly below the minimum of the 3.5-5.0 MPa range recommended by EFNARC (2006). Tensile strength of 4.21 MPa was attained at 56 days, which is within the range of 4.0-5.5 MPa as

suggested by Shah et al. (2022). These results show that there is satisfactory tensile strength development at 7, 28, and 56 days due to the use of Xorex fibres and dolerite aggregates.

4.4.1 Effect of fibre dosage and fibre type on tensile strength

Zhou et al. (2025) assessed the effect of fibre type and content on the tensile properties of shotcrete used in mining applications. In the investigation, shotcrete was mixed using polypropylene, basalt and PVA fibres at 1 wt% content. After 28 days of curing, the highest tensile strength (2.17 MPa) was observed for shotcrete reinforced with polypropylene fibres, followed by basalt fibres (1.37 MPa) and PVA fibres (0.90 MPa).

Whereas Zhou et al. (2025) applied fibres at 1 wt%, the current research achieved a higher tensile strength of 3.57 MPa at 28 days (Figure 4-5) using 0.02 wt% Xorex fibres. This suggests that low fibre content can achieve better reinforcement efficiency by transferring load effectively.

Similarly, Khosh and Atapour (2024) obtained a tensile strength of 4 MPa for shotcrete with 1 wt% waste textile fibres. The type of fibre affects tensile performance because fibres differ in interfacial bonding, stiffness, and crack-bridging ability.

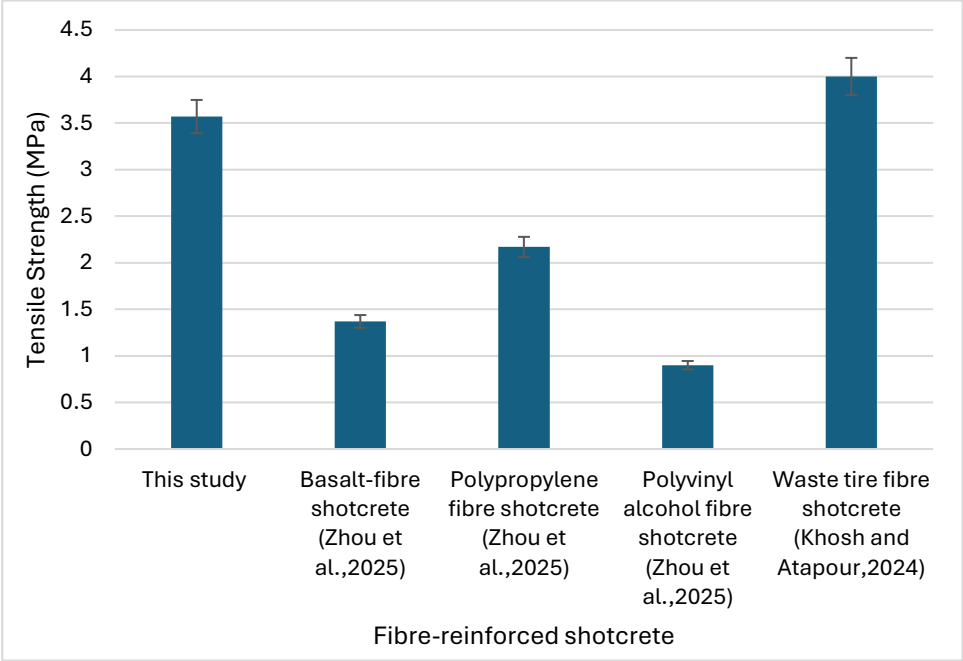


Figure 0-5: Comparison of 28-day tensile strength of shotcrete in this study and published literature with error bars representing 95% confidence range

Zhou et al. (2025) investigated the effect of fibre type and dose on composite materials. From an economic point of view, Xorex fibre reinforcement offers a distinct cost advantage because it requires an extremely low application dose (0.02 wt%). Although tensile strength is an important parameter, shrinkage behaviour of shotcrete is equally important. The next Section discusses the shrinkage behaviour of the dolerite-Xorex fibre-reinforced shotcrete.

4.5 Time-dependent shrinkage behaviour

The mean and standard deviations of the values at each age are shown in Table 4-5. Appendix A includes the actual shrinkage values. Figure 4-6 graphically depicts the observed progression. The shrinkage value increases continuously with curing age, with an almost linear pattern. The recorded shrinkage values range from around 0.021% at day 4 to 0.053% at day 7, 0.064% at day 28, and 0.070% at day 56. These values increase because of continued hydration and tension created by capillaries.

Table 0-5: Average shrinkage (%) of fibre-reinforced shotcrete over different curing ages

Days for curing	Mean value of shrinkage (%)	Standard deviation of shrinkage (%)
4	0.0210	0.0178
7	0.0533	0.0085
28	0.0643	0.0101
56	0.0700	0.0111

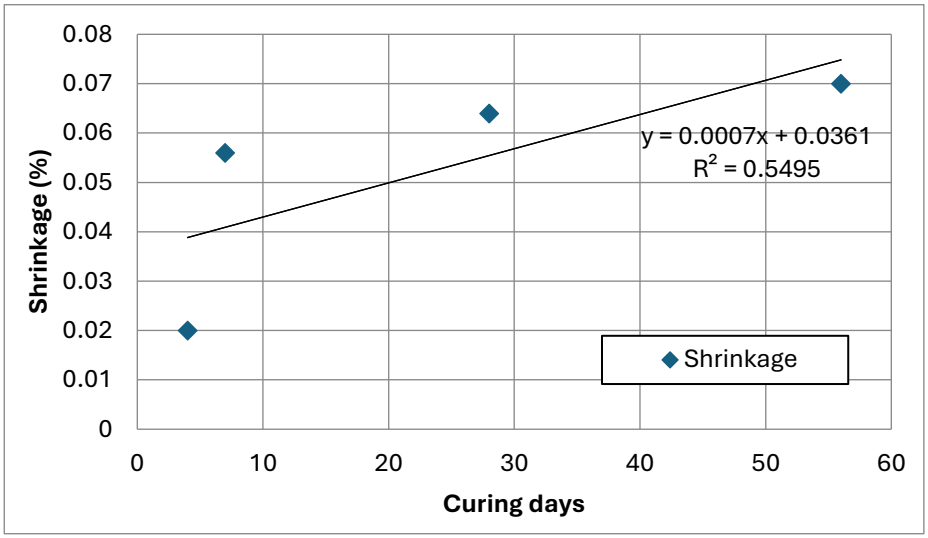


Figure 0-6: Shrinkage development of the reinforced shotcrete over various curing days

The findings show a significant link between shrinkage development and curing time, influenced by hydration progress and moisture loss. At day 4, shrinkage remains low at 0.0210%, reflecting the matrix's instability during hydration. However, after 7 days, shrinkage rises significantly to 0.0533%, indicating matrix stability and uniform shrinkage distribution. After 28 days, shrinkage rises again to 0.0643%, recording a peak shrinkage of 0.0700% at 56 days. Beyond 56 days, shrinkage stabilises as moisture loss is governed by long-term drying processes. Low shrinkage values in dolerite-Xorex fibre-reinforced shotcrete imply good dimensional stability and matrix densification. The next stage focuses on developing shear strength.

4.6 Shear strength of shotcrete

The results of shear strength were derived using Equation (3.1) presented in Section 3.3.1. Table 4-6 summarises the performance of shotcrete samples reinforced with angular dolerite aggregates, tracked across curing periods of 4 days, 7 days, 28 days, and 56 days.

Table 0-6: Shear strength of shotcrete specimens with dolerite aggregates at different curing ages

Curing (Days)	Shear Strength (τ) (MPa)
4	8.75
7	9.65
28	10.75
56	11.10

An examination of the data in Table 4-6 reveals a clear, progressive increase in shear strength as the curing period extends. For instance, samples cured for 4 days exhibited a shear strength of 8.75 MPa, whereas samples cured for 56 days reached 11.10 MPa. Hu (2024) reported that conventional shotcrete had a shear strength of 4.66 MPa after 28 days of curing in a granite interface, whereas Zhu et al. (2024) obtained 0.01323 MPa for the modified mixture with doped glass fibres. At the same time, the dolerite–Xorex fibre shotcrete demonstrated a value of 10.75 MPa, which is about 131% higher than that of conventional shotcrete (Hu, 2024) and 81,100% higher than the mixture reported by Zhu et al. (2024). The high shear-resistance capacity of the proposed composition was found, which can be beneficial for reinforcing underground excavations.

4.7 Comparison of experimental results with existing constitutive models

The difference between experimental outcomes and conventional mix design is evident in material properties as presented in Figures 4-7 to 4-9. Current shotcrete practice uses sand aggregates with steel fibres.

Constitutive models such as Meschke (1996), Schädlich and Schweiger (2014), or Shotcrete Damage Plasticity (1998) assume the hydraulic mechanism of Portland cement, standardised shrinkage, and strength-gain processes.

The experimental dolerite–Xorex fibre shotcrete mix used angular dolerite aggregates and corrosion-resistant Xorex fibres. First, the shrinkage values were indicated a significant difference as presented in Figure 4-7. The conventional mix design rarely shows shrinkage over time, as shown by the flat shrinkage prediction line in the models mentioned above. In comparison, the experimental shotcrete mix peaked at seven days and reduced at day 28 due to the inhibitive action of Xorex fibres and the different hydraulic mechanism of dolerite fines.

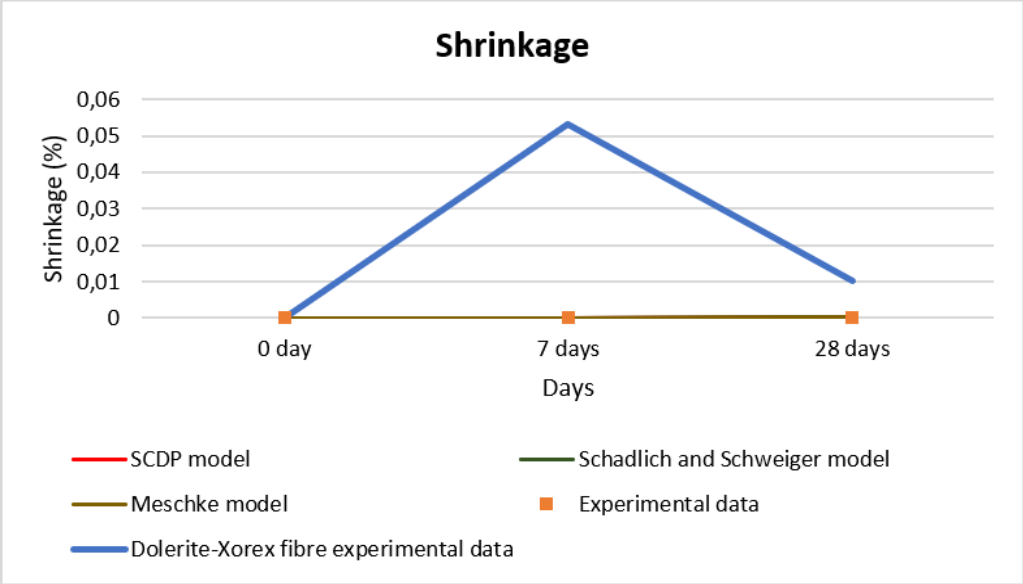


Figure 0-7: Shrinkage comparison with constitutive models

Further differences are reflected in compressive strength and elastic modulus. The conventional mix design demonstrated higher compressive strength at day 28 of curing it reached 40-45 MPa compared to 30 MPa for the experimental mix as presented in Figure 4-8. The dolerite–Xorex fibre shotcrete attained lower strength due to a higher volume of hydraulic binder with lower pozzolanic activity and a lower fibre percentage (0.02 wt%). It can be assumed that the strength gain of the experimental mix follows a

similar pattern to the conventional sand–steel fibre shotcrete mix, but at a lower level due to slower pozzolanic activity of dolerite fines.

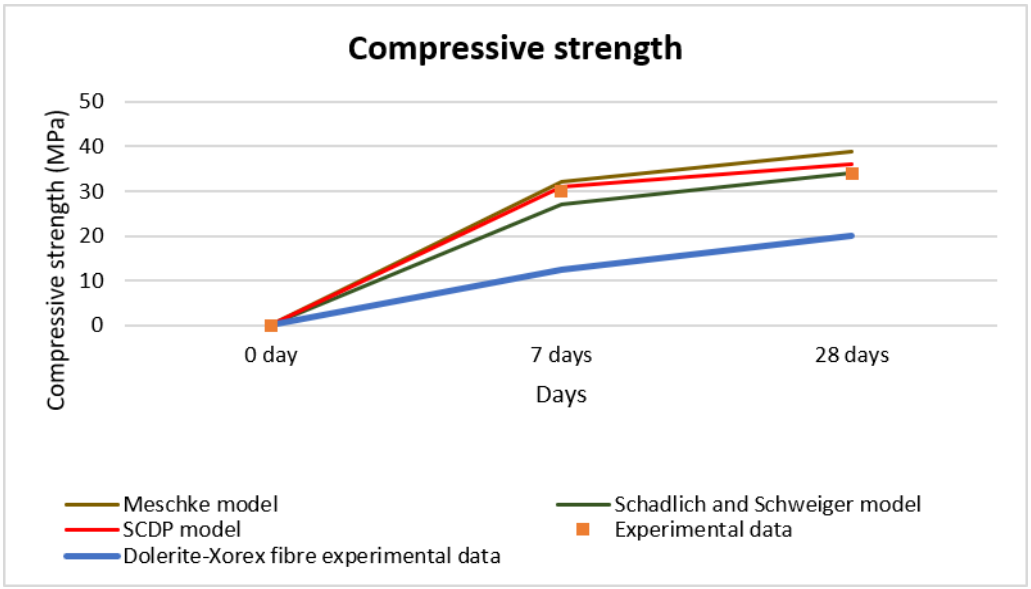


Figure 0-8: Compressive strength comparison with constitutive models

Additional differences were also found in the modulus of elasticity, as presented in Figure 4-9. The conventional mixes demonstrated a lower stiffness at 28 days of curing. In contrast, the experimental mix had a higher stiffness of 18 GPa. This outcome can be explained by the higher percentage of fibre reinforcement and the larger grain size of dolerite compared to sand in conventional mixes.

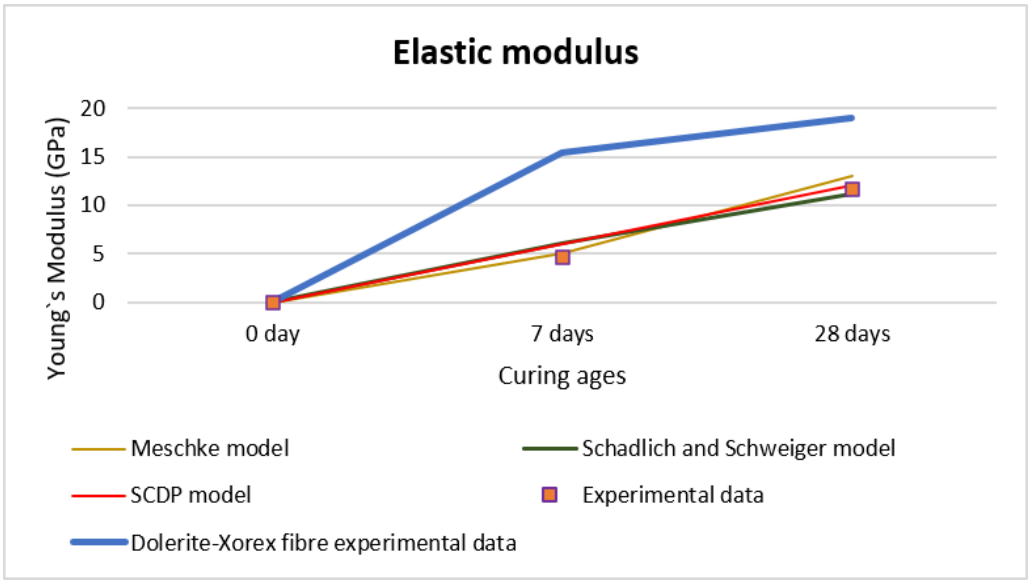


Figure 0-9:Elastic Modulus comparison with constitutive models

It can be concluded that conventional shotcrete mixes properties and their prediction models do not apply to dolerite–Xorex fibre shotcrete because of its sustainability features and dosages of mix design. The use of dolerite aggregates and Xorex fibres in the experimental mix resulted in noticeable differences in stiffness, shrinkage, and strength-gain patterns. This experimental mix showed unique characteristics that constitutive models applied to conventional sand–steel fibre shotcrete cannot predict. The findings of this study can help develop the constitutive models specific to sustainable shotcrete mixes with synthetic fibres.

4.8 Significant findings from the study

The mechanical strength properties of the dolerite–Xorex fibre-reinforced shotcrete mix show a clear tendency to increase with age, indicating the role of hydration, matrix densification, and aggregate interlocking. Despite the strength gains, the UCS values did not meet the requirements of ASTM D 3148-72 (1997) at 7 and 28 days, mainly due to the low fibre dosage of 0.02 wt%. This finding is particularly valuable from an economic point of view, as it illustrates a trade-off between the cost-benefit of fibre addition and meeting standard specifications for the initial strength of shotcrete.

The triaxial compressive strength performance further underscores the importance of confinement in the functional properties of shotcrete. Strength gains were most notable up to 28 days, followed by a stabilisation trend, signifying a shift in the dominant failure mechanisms from hydration and matrix densification to frictional resistance and aggregate interlocking. This means that in confinement-dominated engineering applications, shotcrete strength should be attributed primarily to aggregate characteristics rather than matrix hydration processes.

The Mohr-Coulomb relationship further supports this point by showing that the cohesion and angle of friction of the mix are significantly higher than those of the conventional sand–steel fibre mix. This can be explained by the higher shear resistance attributed to the angularity of the dolerite

aggregates and crack-bridging properties of the Xorex fibres. Similarly, the tensile strength performance confirms the high fracture resistance of the shotcrete at all stages of cure, with values comparable to some international standards, which in turn ensures crack-initiation resistance. The shrinkage capacity of shotcrete also remained within acceptable limits at all curing stages, further supporting its potential applicability in underground construction.

Overall, the study demonstrated several key findings valuable to both scientific and engineering communities. The key research contribution of this study is illustrating the mechanisms that govern the mechanical properties of shotcrete with alternative aggregates and synthetic fibres. Indeed, the comparison between conventional and experimental shotcrete revealed that, in many cases, shotcrete strength development is governed not by the hydration process but by aggregate characteristics and the degree of fibre-induced confinement. This is particularly evident when comparing the study results with constitutive models in the literature (Meschke, 1996; Schädlich and Schweiger, 2014; Shotcrete Damage Plasticity, 1998).

Constitutive models in the literature generally rely on assumptions about Portland cement hydration, mix shrinkage capacity, and corresponding strength development. For instance, Meschke (1996) demonstrated that the degree of cement hydration significantly impacts the autogenous shrinkage and mechanical properties of shotcrete. The same study showed that sand–cement mixtures exhibit lower shrinkage than the gravel–cement mixtures with a similar liquid-to-solid ratio. In contrast, the experimental shotcrete showed a peak in shrinkage at seven days, followed by a reduction at 28 days, which can be attributed to the inhibitory pressure of the fibres and the hydration characteristics of the dolerite fines.

Similarly, the compressive strength development of the experimental mix was lower than the conventional sand–steel fibre shotcrete in most cases (≈30 MPa for the experimental mix versus 40–45 MPa for the conventional

mix at 28 days), which can be explained by the differences in the pozzolanic properties of the binder and the absence of significant fibre dosage. Finally, the elastic modulus was also higher for most experimental mixes (≈18 GPa for dolerite–Xorex versus 15–16 GPa for conventional mixes) due to the angularity and larger grain size of the dolerite aggregates. Therefore, it can be asserted that the constitutive models commonly used in practice are not directly applicable to sustainable shotcrete solutions due to the significant differences in the mechanical properties of alternative binders, aggregates, and fibres.

Chapter 5: Static and dynamic mechanical performance of dolerite-Xorex fibre-reinforced shotcrete

5.1 Introduction

This chapter contains the results of the numerical modelling of dolerite–Xorex fibre-reinforced shotcrete under static and dynamic loading conditions. The main goal of the study was to assess the strain response and performance of the shotcrete support under the influence of the modelled excavation.

The input parameters were selected based on the findings of the laboratory tests described in Chapter 4. Particularly, the rock strength properties, including uniaxial compressive and tensile strengths, Poisson's ratio, cohesion, friction angle, and Young's modulus, were used as inputs for the numerical models. This way, the actual mechanical properties of the tested material were used instead of theoretical values.

Three Rocscience software programs were used for the numerical simulations: Unwedge, RocSupport, and RS2. The first program was used to assess the possibility of wedge formation due to the intersection of discontinuities around the excavation. With the given input parameters, Unwedge was used to estimate the contribution of shotcrete support to the wedge stability.

RocSupport was used to estimate ground response characteristics and develop Ground Reaction Curves (GRC). The analysis allowed us to estimate the interaction between rock-mass deformation and the support system's pressure response. In addition, the FoS was evaluated to determine how sufficient the support was for the given ground conditions. Thus, the analysis provided information on the correlation between the ground response and the support characteristics.

RS2 was used to estimate rock mechanics around the excavation under the given loads. Finally, the performance of shotcrete under static and dynamic

loading was evaluated and compared to the conventional shotcrete using the criteria given in Appendix G. The criteria were selected based on the review of the scientific literature, including such properties as UCS, modulus of elasticity, shear strength, Poisson's ratio, and tensile strength. As a result, the numerical simulations allowed us to analyse the behaviour of the dolerite–Xorex fibre-reinforced shotcrete under the actual field-like conditions.

5.2 Findings from the numerical simulations with Unwedge

The Unwedge analysis was performed on an unsupported tunnel geometry and a fibre-reinforced shotcrete-supported tunnel. In the case of a fibre-reinforced shotcrete tunnel, the strength parameters of the shotcrete were selected based on the different periods of curing. We later plotted and analysed these results. The discussion focused on variations in the FoS. Appendix E provides the raw data used for the analysis.

5.2.1 Unsupported tunnel case

The unsupported tunnel case wedge stability analysis reveals that there is the creation of several rock wedges. The rock wedges result from intersections between discontinuities in the tunnel profile. Factors of safety (FoS), along with the weights of different wedges, have been provided in Table 5-1, whereas a 3D illustration of the geometry of these wedges is given in Figure 5.1 below.

Table 0-1: Factor of safety and weights of unsupported tunnel

Wedge ID	Location	Factor of Safety (FoS)	Weight (t)
4	Lower-Right wedge	4.598	0.787
5	Upper-Left wedge	1.691	0.985
6	Roof wedge	2.643	3.104

From Figure 5-1, the top-left wedge (Wedge 5) is a zone of instability. This is because this wedge has a Factor of Safety (FoS) of less than 2. Despite the large mass associated with the roof wedge (FoS = 2.64), it may become unstable if environmental conditions change.

A low factor of Safety (FoS) indicates poor joint orientation, small joint spacing, and large wedges, which reduce excavation stability (Liu et al., 2024). These factors strongly promote wedge failure, as shown in simulation studies by Liu et al. (2021), where poor joint orientation, small joint spacing, and large wedge geometry usually led to FoS values below 1.5. FoS values less than 1.5 indicate an unstable wedge; therefore, extra reinforcement is needed. According to Hoek (2023), stable underground excavations normally have FoS values ranging from 1.3 to 1.5 to cater for uncertainties of geology, modelling, and construction. The results from the current study include FoS values within and above the required range, with the upper-left wedge having the highest FoS of 1.693.

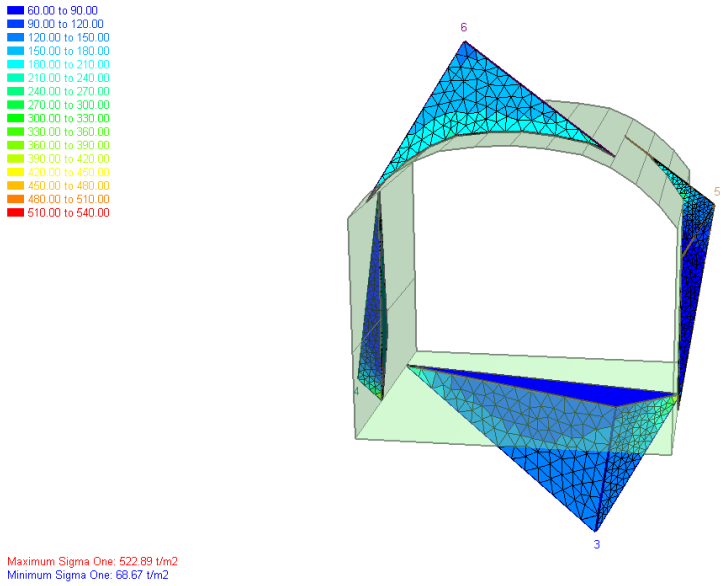


Figure 0-1: 3D visualisation of rock wedge geometry under unsupported excavation conditions

As illustrated in Figure 5-1, the upper-left wedge (Wedge 5) represents the critical instability zone. It exhibits a Factor of Safety (FoS) below 2, indicating unstable behaviour under the existing in-situ stress conditions.

Despite the large mass associated with the roof wedge (FoS = 2.64), it may become unstable if environmental conditions change.

Low factor-of-safety (FoS) values typically indicate poor joint orientation, a high frequency of discontinuities, and larger wedge volumes (Liu et al., 2024). In unsupported tunnels, the excavation remains unstable because adverse geological structures govern wedge formation. Previous research results state that wedges whose FoS value is below 1.5 are classified as unstable wedges and thus need to be supported (Li et al., 2025).

5.2.2 Supported tunnel with dolerite-Xorex fibre-reinforced shotcrete

Numerical modelling results for the supported tunnel show that tunnel support enhances wedge stability. The FoS of the various wedges improved after implementing support with 100 mm-thick dolerite Xorex fibre-reinforced shotcrete. Table 5-2 gives the FoS of the wedges and their weights.

Table 0-2: FoS values for floor, lower right, upper left, and roof wedges at curing ages of 4, 7, 28, and 56 days.

Curing days	Wedge ID	Location	FoS	Weight (t)
28 days of conventional shotcrete	4	Lower-Right wedge	16.063	0.787
	5	Upper-Left wedge	4.508	0.985
	6	Roof wedge	3.458	3.104
4 days	4	Lower-Right wedge	39.589	0.787
	5	Upper-Left wedge	11.572	0.985
	6	Roof wedge	2.827	3.104
7 days	4	Lower-Right wedge	43.188	0.787
	5	Upper-Left wedge	12.746	0.985
	6	Roof wedge	3.118	3.104
28 days	4	Lower-Right wedge	47.586	0.787
	5	Upper-Left wedge	14.181	0.985
	6	Roof wedge	3.474	3.104
56 days	4	Lower-Right wedge	48.986	0.787
	5	Upper-Left wedge	14.638	0.985
	6	Roof wedge	3.587	3.104

The effectiveness of the 50 mm-thick dolerite-Xorex fibre shotcrete combination as a tunnel lining system was investigated on days 4, 7, 28, and 56 of curing. Numerical analysis was carried out under the tunnel excavation conditions as shown in Figures 5-2 to 5-5. The Factor of Safety (FoS) shows that stability increases with curing age. All wedges considered exhibit FoS greater than 1 at all curing ages.

For example, the most stable condition in terms of FoS is the Lower Right wedge (Wedge 4), which shows an increase in FoS from 39.589 to 48.986. The increased stability in this case is due to increased support mobilisation as the shotcrete stiffens and strengthens, even though its self-weight is lower (0.787 t). Another important stabilisation finding is in the Upper Left wedge (Wedge 5), where FoS increases from 11.572 to 14.638. Although it is lower than that of Wedge 4, this condition is very stable because it involves time-dependent stabilisation of the lining systems. The Roof wedge (Wedge 6), showing the highest self-weight (3.104 t), also shows the least stable conditions, with FoS values increasing from 2.827 to 3.587.

The significant increase in FoS can mainly be attributed to stress redistribution due to the gradual stiffening of the shotcrete liner during curing (Nie et al., 2021). As stiffness increases, the efficiency of stress transfer from the rock mass to the liner improves. This process redistributes stress away from the joints and edges of excavations. Stress redistribution will reduce the driving stresses acting on wedges, while increased mobilisation resistance improves stability.

According to Kong et al. (2022), FLAC3D modelling showed that gradual rock mass degradation would greatly reduce the FoS. This can result in an 85% drop due to higher rock pressure, which in turn causes the shotcrete lining to degrade and eventually leads to tunnel instability. Conversely, the current study investigates the performance of fibre-reinforced shotcrete from early to late ages and its importance in providing greater excavation stability. The findings show that the rate at which shotcrete strength

develops is highly important, as greater stiffness promotes better load distribution and stress redistribution.

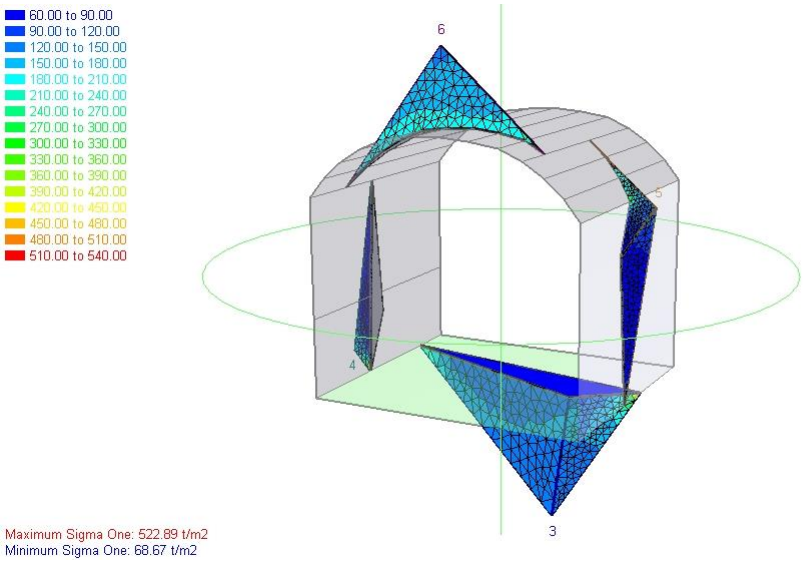


Figure 0-2: Simulated tunnel response using 50 mm of shotcrete at 4 days

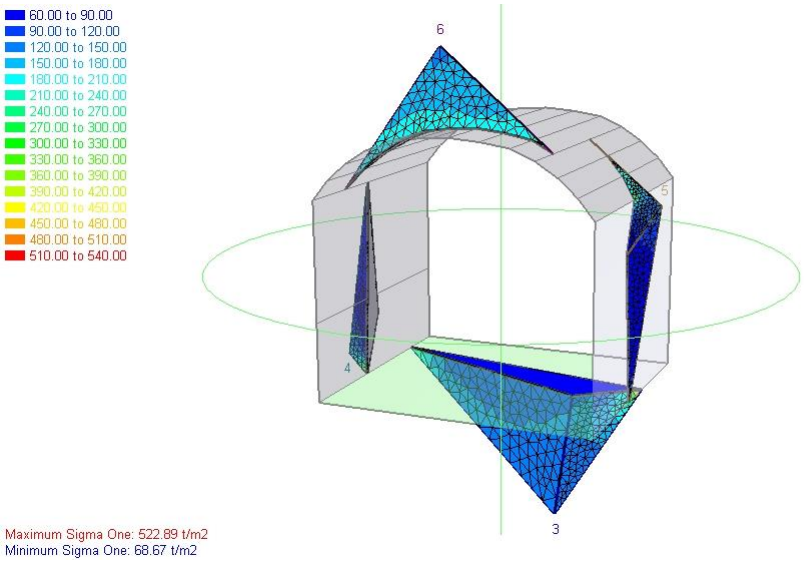


Figure 0-3: Simulated tunnel response using 50 mm of shotcrete at 7 days

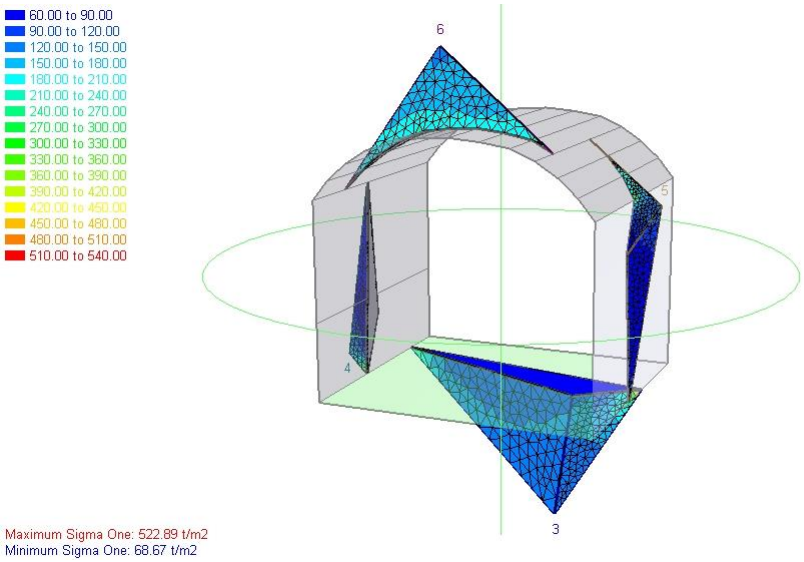


Figure 0-4: Simulated tunnel response using 50 mm of shotcrete at 28 days

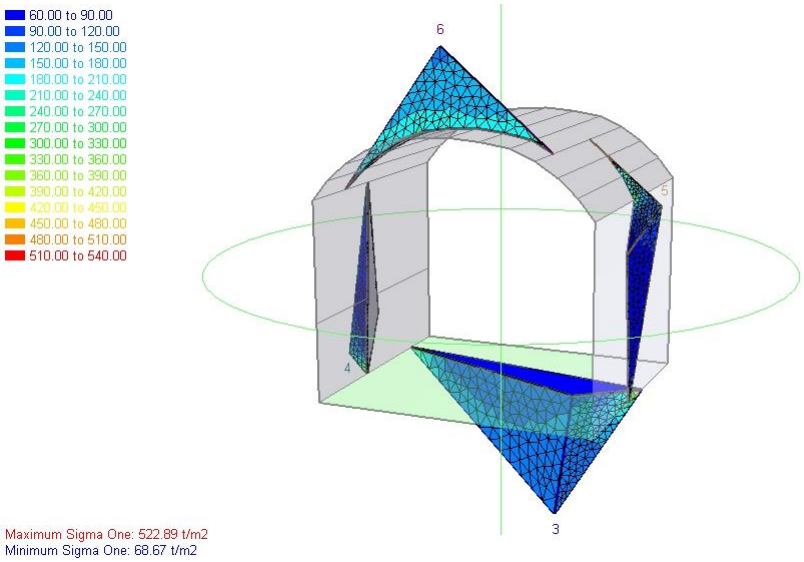


Figure 0-5: Simulated tunnel response using 50 mm of shotcrete at 56 days

The wedge stability analysis results for 28 days show that FoS varies with wedge position and configuration, as shown in Figure 5-6. In this regard, the lower right wedge had the greatest FoS of 16.063 despite its light weight of 0.787 t, indicating good confinement and a high level of difficulty for mobilisation. However, the roof wedge was the most critical zone of instability, with a minimum FoS of 3.458 and a maximum wedge weight of 3.104 t. In this regard, the upper-left wedge is considered a relatively risky section, with an FoS of 4.508.

Comparative analysis shows that the alternative mix design outperforms the conventional shotcrete mixture in wedge stability and safety margin factors. The wedge at the bottom right side showed a significant increase in FoS from 16.063 to 47.586, indicating improved strength and confinement. Likewise, the wedge at the top left saw a marked increase from 4.508 to 14.181, implying improved support efficiency and stability.

In contrast, the roof wedge revealed just a slight improvement in FoS, increasing from 3.458 to 3.474. This minimal difference suggests that the mass of the wedge is the most significant factor affecting roof stability.

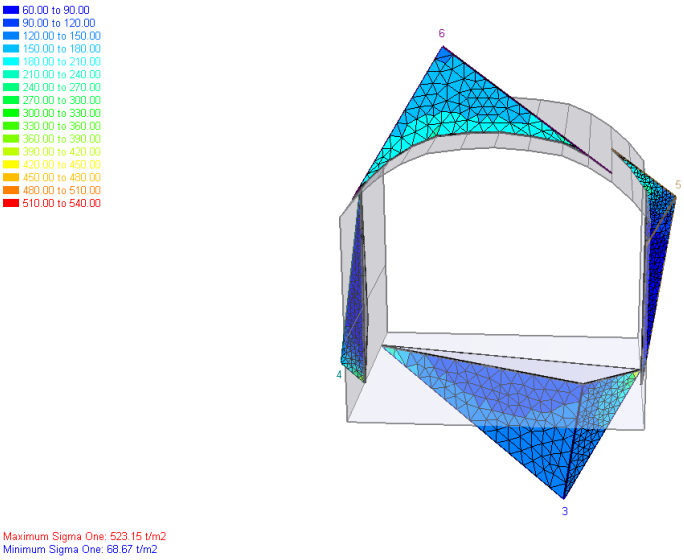


Figure 0-6: 3D visualisation of rock wedge geometry supported with conventional shotcrete

5.2.3 Comparison between supported and unsupported tunnels

A comparison between the unsupported and supported tunnelling scenario illustrates the effect of fibre-reinforced shotcrete in stabilising wedges (see Table 5-3). The system contributes to stable excavation by minimising the possibility of wedge movement.

Table 0-3: Wedge Stability (FoS) across wedges – Unsupported conventional shotcrete and dolerite–Xorex fibre shotcrete

	Wedge ID	***Wedge***	***FoS***
Unsupported	6	Roof wedge	2.643
4 days	6	Roof wedge	2.827
7 days	6	Roof wedge	3.118
28 days	6	Roof wedge	3.474
56 days	6	Roof wedge	3.587
Unsupported	4	Lower-Right wedge	4.598
4 days	4	Lower-Right wedge	39.589
7 days	4	Lower-Right wedge	43.188
28 days	4	Lower-Right wedge	47.586
56 days	4	Lower-Right wedge	48.986
Unsupported	5	Upper-Left wedge	1.691
4 days	5	Upper-Left wedge	11.572
7 days	5	Upper-Left wedge	12.746
28 days	5	Upper-Left wedge	14.181
56 days	5	Upper-Left wedge	14.638

The unsupported tunnel case study showed FoS values above 1 for all identified wedges, indicating marginal stability in the natural state. However, the small safety factor, especially regarding the upper-left wedge whose FoS was 1.691, shows the risk associated with this wedge.

Installing 50-mm reinforced shotcrete will improve wedge stability, with all wedges achieving an FoS greater than required. The lower-right wedge exhibits the greatest improvement, where the FoS of 4.598 in an unsupported condition increases to a range between 39.589 and 48. 986. The upper-left wedge, which is unstable with an FoS of 1.691 in an unsupported condition, becomes stable with values for FoS varying between 11.572 and 14.638. The roof wedge is more stable, with FoS values ranging between 2.827 and 3.587. In all cases, reinforced shotcrete improved stability.

Although the unsupported excavation meets the stability criteria, the fibre-reinforced shotcrete lining provides a considerable improvement in FoS for all wedge types. This suggests that the shotcrete lining not only meets the required stability but also provides a margin of safety beyond the requirements. This is accomplished through improved confinement, better load distribution, and strength gain from curing time. The next section examines the Ground Reaction Curve more closely and discusses how it is used to evaluate support performance.

5.3 Ground Reaction Curves (GRC) of shotcrete support

The Unwedge simulation results were further verified using the GRC analysis technique. The GRC method assesses the relationship between tunnel convergence and the support pressure developed by the shotcrete lining. This technique is a well-known approach for evaluating rock-support interaction in underground tunnels. The simulations were carried out using the parameters given in Tables 3-4 and 3-5.

GRCs were analysed employing the elastic-plastic and elastic visco-plastic approaches to simulate the behaviour of the rock mass around the tunnel. The Hoek-Brown yield criterion was used as the constitutive approach because it can simulate the nonlinear strength behaviour of a jointed rock mass. Hoek-Brown yield criterion is considered one of the best constitutive models in underground rock engineering. It was supposed that the rock mass would behave elastically up to yielding and plastically beyond yielding.

The GRC was used to analyse how tunnel deformation reacts to stress redistribution from excavation activities. The simulations effectively captured the interplay between the rock mass and the support systems across different curing ages. Appendix F provides the output parameters from the GRC analysis, and Figures 5-7 to 5-11 show the corresponding graphs.

The GRCs illustrated in Figures 5-7 to 5-11 show a gradual increase in tunnel stability as the shotcrete curing period increases. As the shotcrete gains strength, it becomes more effective at stabilising the rock structure over time. This phenomenon confirms support mechanics theory on tunnel stability, which relies on the interaction between the rock mass and support structure rather than on their individual resistance (Cui et al., 2019).

The behaviour of a tunnel without support is shown in Figure 5-7. For such tunnels, stability depends solely on rock mass strength. Stress redistributes immediately after excavation, causing tunnel deformation to rise from 0.88% at the tunnel face to 1.16% at the support, and eventually to 2.32%. Consequently, the tunnel becomes very unstable, with a Factor of Safety of 0.28.

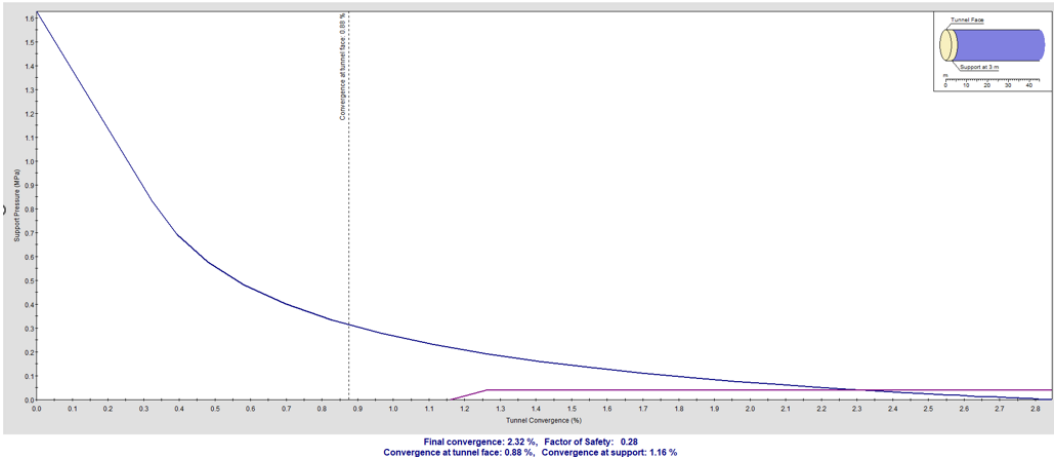


Figure 0-7: Ground Reaction Curves of an unsupported tunnel

The tunnel reaction after conventional shotcrete application at 4 days of curing is presented in Figure 5-8. Shotcrete initially improves deformation resistance, but its performance is limited. Convergence reduces to 0.62% at the tunnel face and 0.88% at the support point compared with the open tunnel. Short-term convergence increases to 1.35%, while long-term convergence reaches 2.49%.

The factor of Safety rises to 0.57 when fibre-shotcrete spraying is applied but drops to 0.33 in the long term. This shows that early-age shotcrete can provide some confinement but cannot withstand increasing rock loading.

This phenomenon is consistent with Adhikari & Roy (2023), which states that early-age shotcrete is prone to failure due to its lower strength.

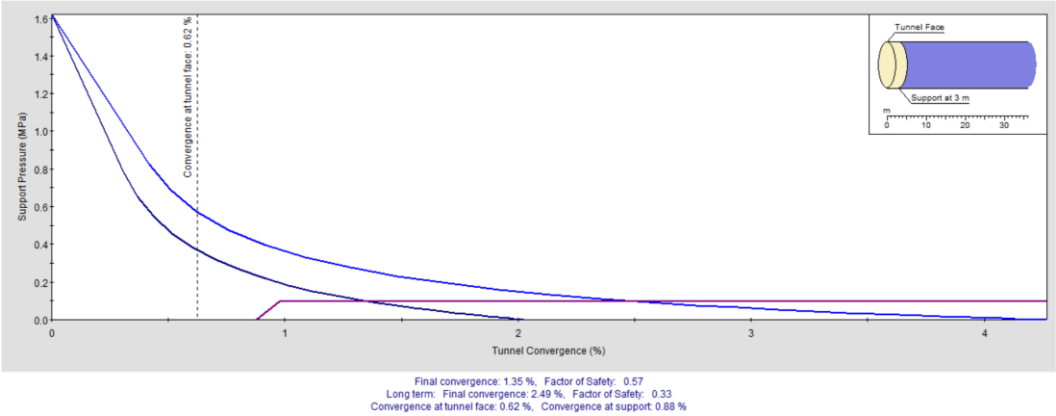


Figure 0-8: Ground Reaction Curve with the application of shotcrete cured for 4 days

After 7 days of curing (Figure 5-9), the rock and support system improves in stability as shotcrete stiffness increases. Tunnel convergence reduces to 0.94% in the short term and increases slightly to 1.11%in the long term. The Factor of Safety (FoS) rises to 1.56 in the short term, indicating that the support system is sufficient to resist the loads applied by the excavation process. However, FoS in the long-term case drops to 0.89 as stress redistribution continues to affect tunnel stability, regardless of the increased shotcrete strength. This clearly emphasises the importance of early shotcrete strength in improving support performance. These results are also supported by Lohar et al. (2024), who observed that curing time is a crucial parameter controlling the strength behaviour of shotcrete.

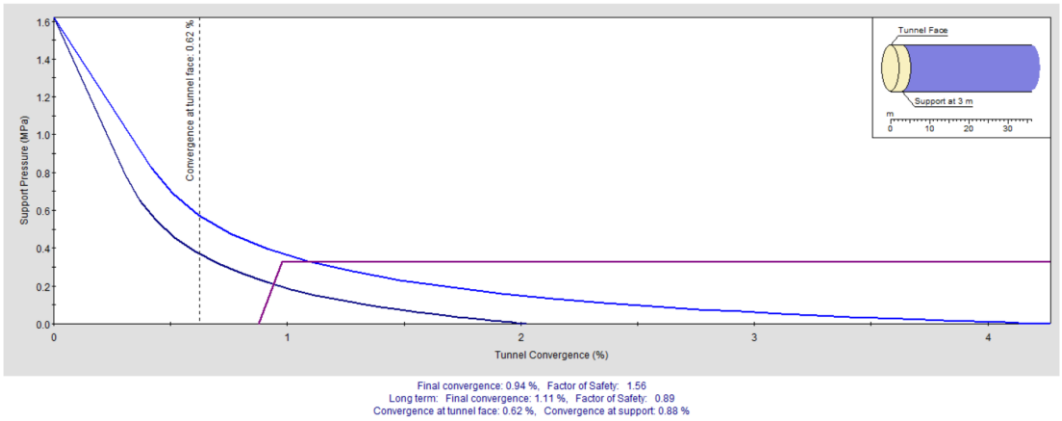


Figure 0-9:Ground Reaction Curve with the application of shotcrete cured for 7 days

By day 28 (Figure 5-10), the shotcrete has developed sufficiently to ensure proper confinement, leading to greater tunnel stability. Convergence in the short term is stabilised at around 0.91%, and the factor of safety climbs up to 2.92. These results demonstrate a strong and effective support system that can adequately resist ground pressures. While long-term convergence rises slightly to 0.94%, the FoS remains above 1 at 1.65, indicating stable performance. The rock-support system is well-matched, and load transfer is effective due to stiffness and confinement.

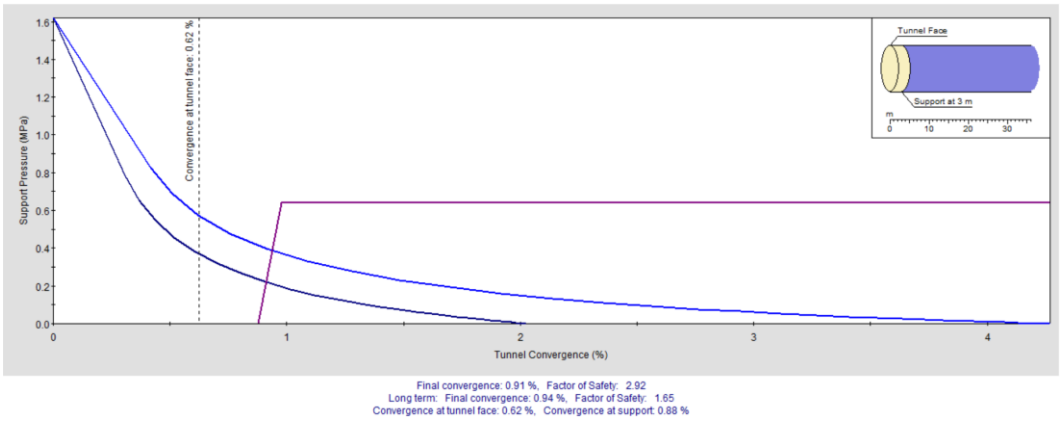


Figure 0-10: Ground Reaction Curve with the application of shotcrete cured for 28 days

The 56-day curing time (Figure 5-11) shows the optimum support performance. Tunnel convergence in the short- and long-term decreases to 0.90% and 0.92%, respectively. Meanwhile, the corresponding factors of

safety (FoS) increase to 4.26 and 2.41, respectively. This indicates very stable excavation under immediate and progressive loads. The small variation in the short-term and long-term convergence values shows that the rock support system is close to reaching equilibrium. This is because the fully developed shotcrete lining distributes stress successfully.

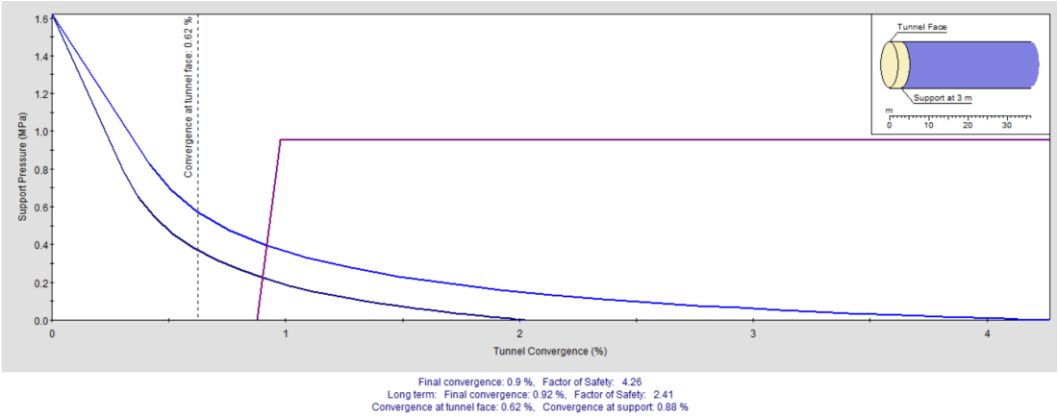


Figure 0-11:Ground Reaction Curve with the application of shotcrete cured for 56 days

From the above, shotcrete curing and stiffness development are critical to maintaining tunnel stability. More curing time improves the support system's load-bearing capacity and reduces the risk of failure. This conclusion is supported by studies by Hoek and Martin (2023), who found that shotcrete thickness, stiffness, and curing improve excavation stability. Adhikari and Roy (2023) also support this, stating that strength development is an important factor in increasing stress resistance and reducing the likelihood of failures. The findings indicate that tunnel stability depends on more than installing the support system. It additionally relies on the continuous interaction between the rock mass and the shotcrete lining.

5.4 Shotcrete performance in RS2 tunnel analysis

RS2 was used for numerical modelling to further validate the performance of the designed excavation using shotcrete support. Strength factor, total displacement, maximum shear strain, and volumetric strain were the parameters that were evaluated at various depths in the excavation. The

strength factor is the ratio of available shear strength to the shear stress. This factor shows the stability of the rock-shotcrete interface. Higher strength factor values indicate greater safety against instability.

Total displacement measures the total deformation of the excavation caused by the applied load. It directly measures the efficacy of the shotcrete liner in restraining the ground movement. Maximum shear strain measures the shear deformation in both the rock mass and shotcrete liner. Volumetric strain measures volume change in the ground during excavation. Numerical simulation results are presented in Table 5-4 and Figures 5-12 to 5-16.

Conventional shotcrete performance decreased progressively with increasing excavation depth, as observed after a 28-day period. Volumetric strain increased from 7.05×10^{-4} at 50 m depth to 9.0×10^{-4} at 200 m depth. This indicates increased compressive deformation from high overburden pressures, suggesting poor adaptability to deep excavation depths. The maximum shear strain value increased even more significantly, reaching 2.0×10^{-4} and 4.5×10^{-4} at depths of 50 m and 200 m, respectively. This means the shear strain was higher, resulting in greater difficulty for the lining to compensate for deformation. The total displacement also increased, reaching 2.20×10^{-3} m and 4.80×10^{-3} m at depths of 50 m and 200 m, respectively.

Strength factor values also increased consistently with depth, rising from 2.34 at 50 m to 4.39 at 200 m. The strength parameter increased with excavation depth because the support structure mobilised under higher loading conditions. Nonetheless, the strength parameters were always lower compared to those of the fibre-reinforced shotcrete support system. This indicates that normal shotcrete provides little strength under increasing excavation loads. The low strength of shotcrete makes it vulnerable to tensile stress.

Table 0-4:Output parameters for dolerite-Xorex fibre-reinforced shotcrete at varying depths and curing periods

Shotcrete thickness	Curing period (days)	Depth (m)	Volumetric strain (-)	Strength factor	Total displacement (m)	Maximum Shear strain
100 mm	28 days (conventional shotcrete)	50	7.05×10^{-4}	4.34	2.20×10^{-3}	2.0×10^{-4}
		100	8.1×10^{-4}	3.80	2.40×10^{-3}	2.5×10^{-4}
		150	8.5×10^{-4}	2.83	3.60×10^{-3}	3.50×10^{-4}
		200	9.0×10^{-4}	2.39	4.80×10^{-3}	4.50×10^{-4}
100 mm	4	50	5.0×10^{-6}	5.54	5.0×10^{-5}	1.2×10^{-5}
		100	5.7×10^{-6}	4.58	6.0×10^{-5}	1.3×10^{-5}
		150	7.0×10^{-6}	3.61	6.5×10^{-5}	1.4×10^{-5}
		200	8.0×10^{-6}	3.63	7.0×10^{-5}	1.5×10^{-5}
100 mm	7	50	4.0×10^{-6}	5.70	4.0×10^{-5}	1.23×10^{-5}
		100	5.0×10^{-6}	4.83	4.5×10^{-5}	1.25×10^{-5}
		150	5.7×10^{-6}	4.77	5.1×10^{-5}	1.34×10^{-5}
		200	6.0×10^{-6}	3.80	6.0×10^{-5}	1.40×10^{-5}
100 mm	28	50	4.5×10^{-6}	7.86	3.0×10^{-5}	1.30×10^{-5}
		100	5.5×10^{-6}	6.90	4.9×10^{-5}	1.35×10^{-5}
		150	5.3×10^{-6}	5.95	5.1×10^{-5}	1.32×10^{-5}
		200	5.0×10^{-6}	4.01	5.0×10^{-5}	1.45×10^{-5}
100 mm	56	50	4.0×10^{-6}	9.10	2.0×10^{-5}	1.02×10^{-5}
		100	4.8×10^{-6}	6.25	3.0×10^{-5}	1.1×10^{-5}
		150	5.2×10^{-6}	6.15	3.5×10^{-5}	1.2×10^{-5}
		200	6.3×10^{-6}	6.10	4.0×10^{-5}	1.3×10^{-5}

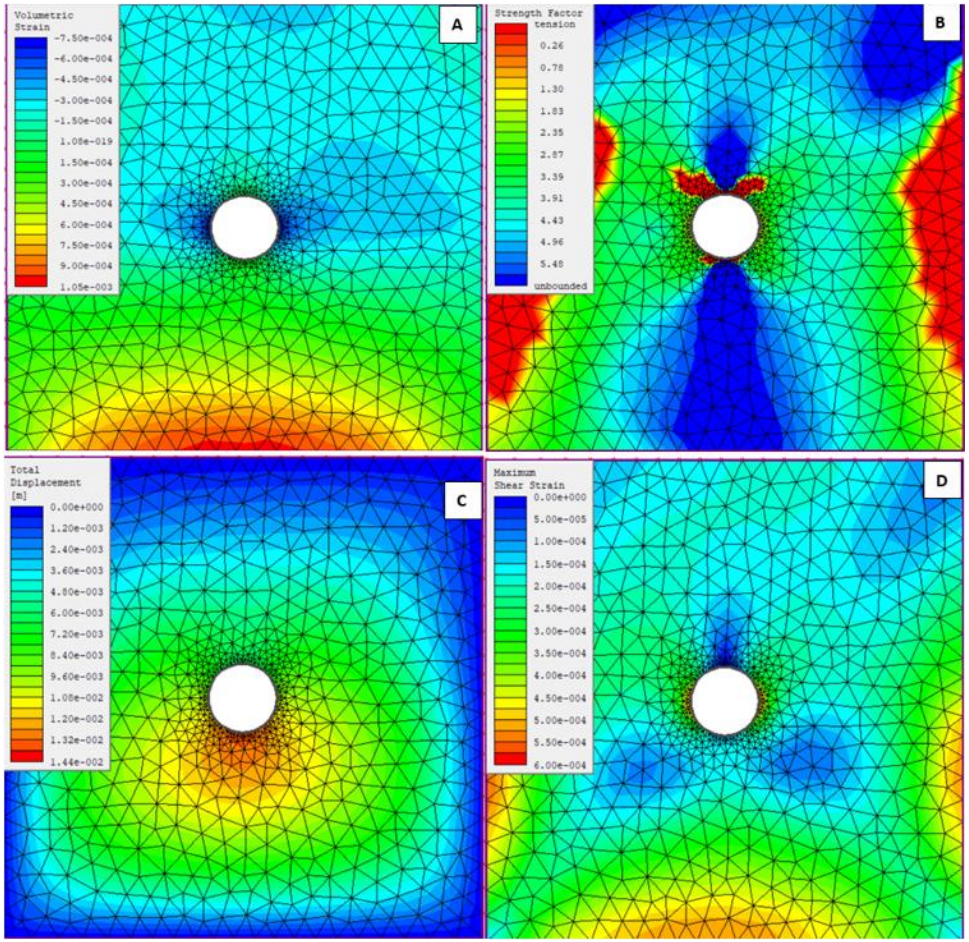


Figure 0-12: Key geomechanical properties of conventional shotcrete at 28 days – (A) Maximum shear strain, (B) Strength factor, (C) Total displacement, and (D) Volumetric strain

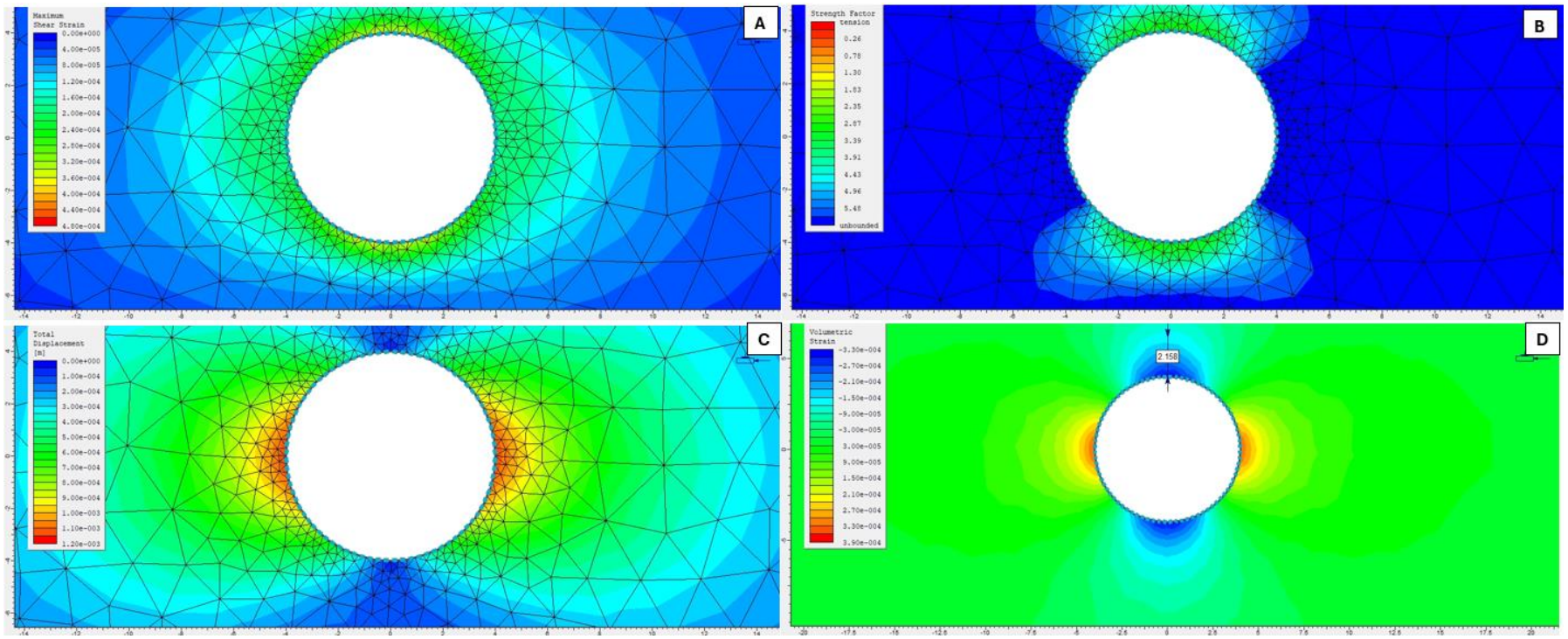


Figure 0-13: Key geomechanical properties of Dolerite–Xorex shotcrete at 4 days – (A) Maximum shear strain, (B) Strength factor, (C) Total displacement, and (D) Volumetric strain

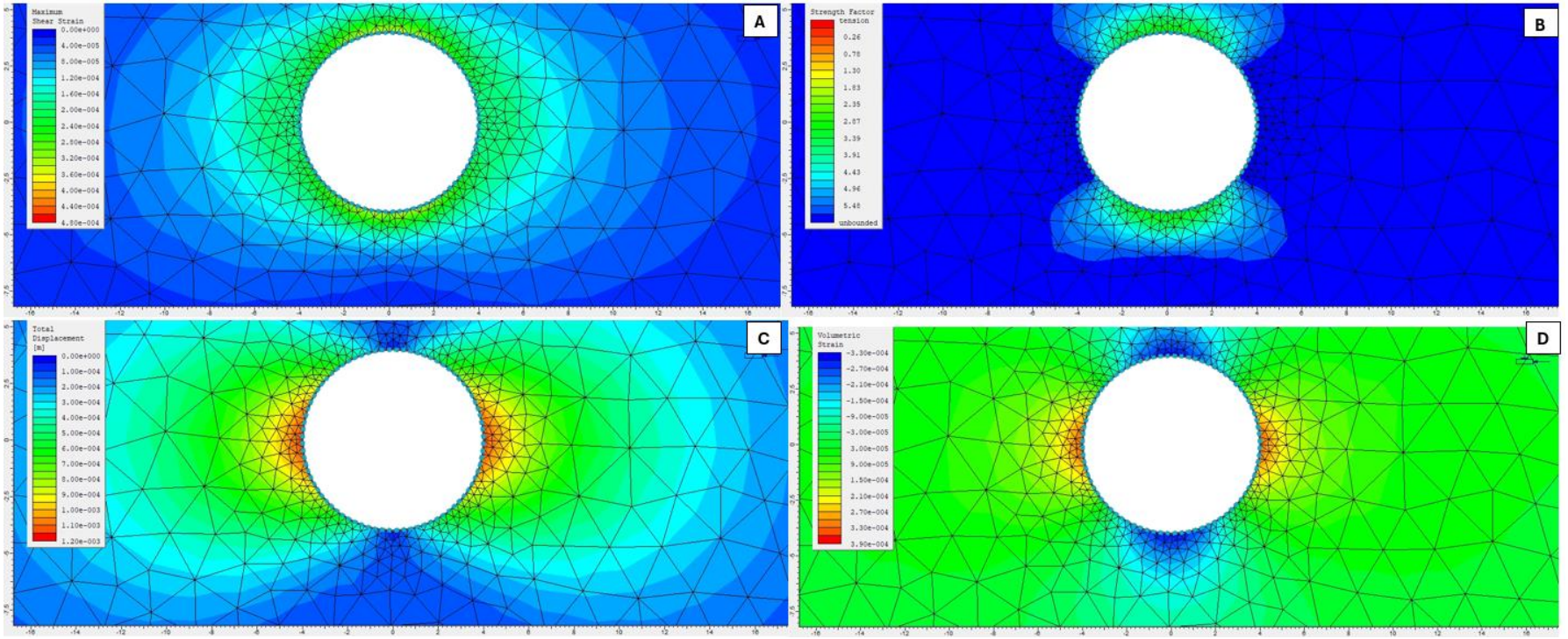


Figure 0-14: Key geomechanical properties of Dolerite–Xorex shotcrete at 7 days – (A) Maximum shear strain, (B) Strength factor, (C) Total displacement, and (D) Volumetric strain

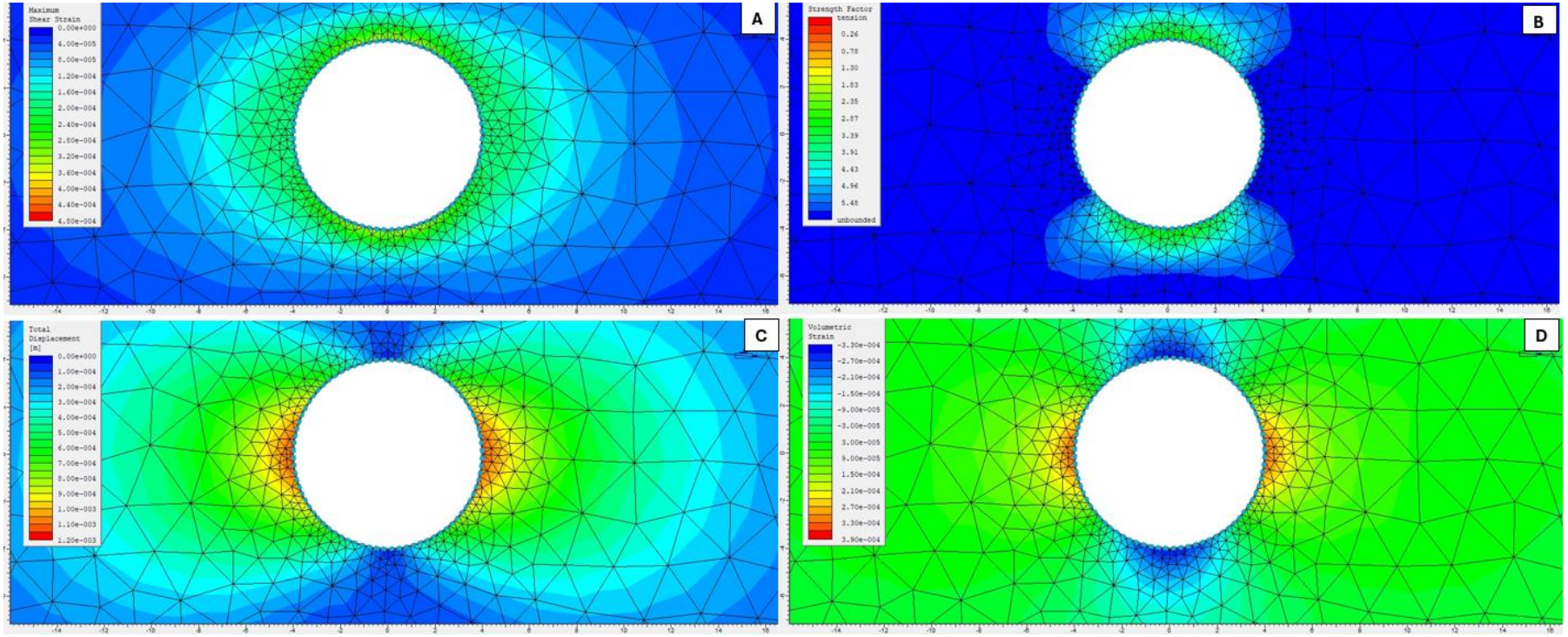


Figure 0-15: Key geomechanical properties of Dolerite-Xorex shotcrete at 28 days – (A) Maximum shear strain, (B) Strength factor, (C) Total displacement, and (D) Volumetric strain

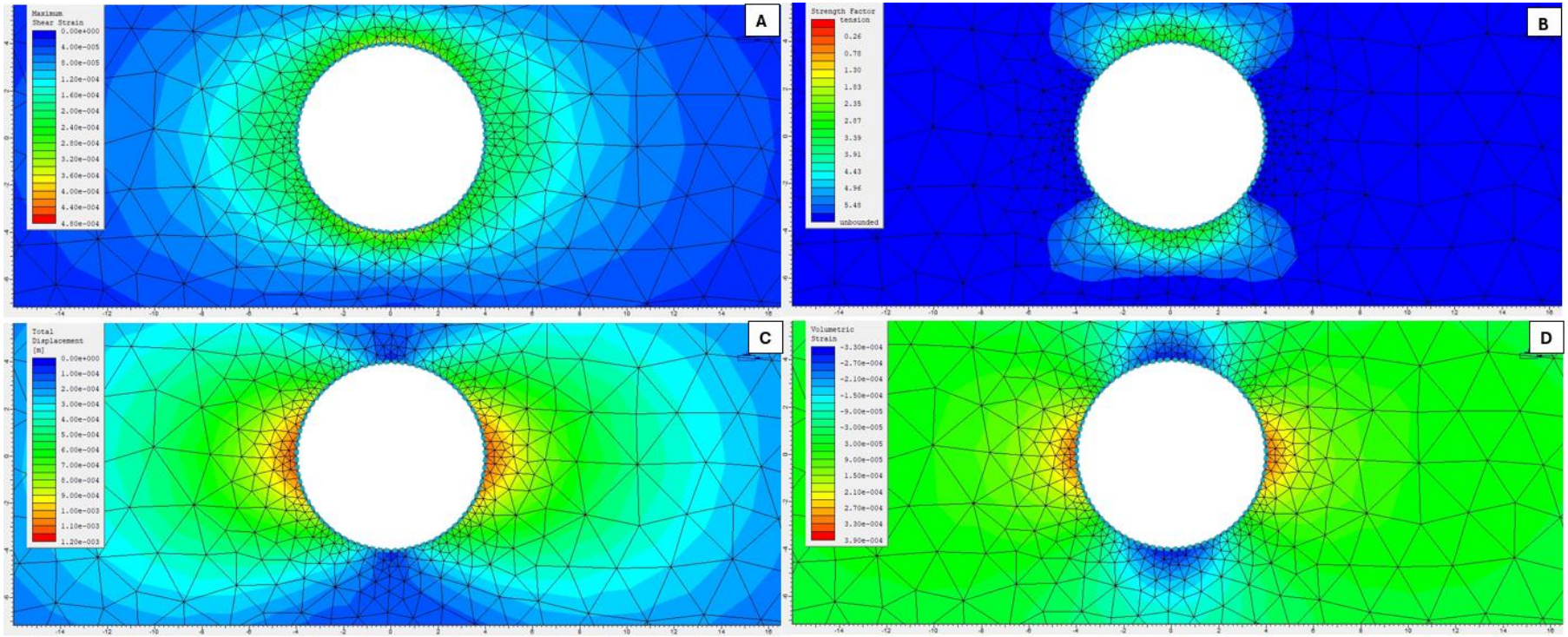


Figure 0-16: Key geomechanical properties of dolerite-Xorex shotcrete at 56 days – (A) Maximum shear strain, (B) Strength factor, (C) Total displacement, and (D) Volumetric strain

For conventional fibre-free shotcrete at 28 days (Figure 5-12), all deformation parameters show a clear dependence on depth. For volumetric strain, the value rises from 7.05×10^{-4} at 50 m to 9.0×10^{-4} at 200 m. This shows that the material experiences increased volumetric strain as in-situ stresses increase with depth. Similarly, maximum shear strain increases from 2.0×10^{-4} to 4.5×10^{-4} indicating enhanced deformation and shear localisation. Total displacement increases from 2.20×10^{-3} m to 4.80×10^{-3} m, the largest increase among the deformations. Overall, these tendencies are consistent with the notions of Win and Nur (2023). These authors noted that as depth increases and in-situ stress rises, volumetric strain, total displacement, and shear strain increase, but shotcrete deformation resistance decreases. Although strength parameters remain moderate (2.34–4.39), the increased deformation highlights the lack of ductility in conventional shotcrete.

At 4 days (Figure 5-13), the early-stage properties of the dolerite-Xorex fibre-reinforced shotcrete improve. Volumetric strain is very low (between 5.0×10^{-6} and 8.0×10^{-6}), and the maximum shear strain is also extremely low. This indicates little to no distortion of the concrete due to early-age loads. Additionally, the total displacement is also very small (between 5.0×10^{-5} m and 7.0×10^{-5} m). This shows that confinement mobilisation occurs very fast after applying the shotcrete. The strength factors were reported at 5.54 at 50 m 5.54 and 200 m it was 2.39, meaning that the shotcrete provides good support at an early age and surface level. This corroborates Win and Nur (2023), who showed that longer curing time increased shotcrete stiffness and reduced deformation.

Total displacement increased steadily with excavation depth for all curing durations. For 4 days of curing duration, total displacement ranged from 5.0×10^{-5} m at 50 m to 7.0×10^{-5} m at 200 m. This suggests that as the excavation deepened, soil movement increased due to high in-situ stress. As the curing period increased, displacement decreased. For instance, at 56 days, displacement decreased from 4.0×10^{-5} m to 2.0×10^{-5} m. This shows that the mechanical characteristics of shotcrete improve with time;

thus, the lining was able to confine and restrain the structure better over time.

The decrease in displacement with increasing curing time emphasises the importance of shotcrete maturation for excavation stability. According to Win and Nur (2023), longer curing increases shotcrete stiffness, resulting in decreased deformation. Thomas and Soroushian (2019) found that longer curing increases the compressive and bending strength of shotcrete, providing greater structural stability. Similarly, Naseri (2021) found that a shotcrete lining reduces the maximum radial displacement of the walls by about 2 mm compared with unsupported excavations. These results are consistent with the present study, where increased curing time led to strength development that minimised displacement and enhanced excavation stability.

Maximum shear strain after 4 days of curing increased from 1.2×10^{-5} at 50 m depth to 1.5×10^{-5} at 200 m depth. The trend showed an increase in maximum shear strain with increasing depth. This is because significant shearing occurred within the material around the excavation area.

Even at 7 days (Figure 5-14), the deformation parameters remained well controlled. The volumetric strain and the maximum shear strain were relatively low in the analysis. This implies the material resisted deformation under stress. Total displacement remains low, with no increase, even though stress redistributes within the rock mass. Strength factors were 5.70 at 50 m 5.54 and at 200 m, the strength factor was noted to be 3.80.

At 28 days (Figure 5-15), there is evidence of the approach towards the long-term equilibrium response. The strength factors increased from 7.86 at 50 m and decreased to 4.01 due to gradual stress redistribution between the lining and the surrounding rock mass. Yet volumetric strains, shear strains, and displacements are still substantially smaller than in ordinary shotcrete (Fig. 5-12). Therefore, despite increased stress redistribution, the matrix can retain sufficient deformation resistance.

After 56 days (Figure 5-16), the strength parameter was noted at 9.10 at 50 m and as the tunnel deepened at 200 m it was reduced to 6.10, but deformation remains constant. Volumetric strains of low values (4.0×10^{-6} – 6.3×10^{-6}) were measured. This implies that longer curing periods enhanced the stiffness and confinement capabilities of the shotcrete support system. Bernard (2010) showed that longer curing periods make fibre-reinforced shotcrete more rigid and better able to confine excavations in stressed environments.

The maximum shear strain at 50 m depth decreased from 1.2×10^{-5} at 4 days to 1.02×10^{-5} at 56 days. This trend indicates that longer curing periods stiffen the shotcrete lining and therefore reduce shearing strains around the excavation zone.

In summary, the findings indicate that excavation depth plays a vital role in the extent of deformation and strain because of increasing overburden stresses. Additionally, as the duration of shotcrete curing increases, excavation stability improves due to reduced deformations. The minimum deformations were observed in curing after 56 days of curing, demonstrating better performance of the material.

5.5 Summary of the findings

Computational modelling showed that excavation stability depended on excavation depth and shotcrete strength development over curing time. An increase in depth raises in-situ stress, leading to greater deformation and strain.

Unwedge simulations showed marginal stability when the tunnels were unsupported. The low factors of safety observed in some wedge zones indicate a probability of instability. The conclusion is that the rock mass alone cannot ensure stability under these conditions and geological parameters.

Using 50 mm dolerite-Xorex fibre-reinforced shotcrete positively affects wedge stability regardless of curing time (4 days, 7 days, 28 days, and 56 days). Regardless of curing time, the factors of safety increased noticeably compared with the unsupported wedges. The shotcrete cured for 4 days performed well in providing confinement. Shotcrete cured for 7 days showed higher stiffness and better load distribution.

There was a change in the Ground Reaction Curve from the unstable unsupported stage to the stable reinforced stage. The excavation became more stable at 4, 7, 28, and 56 days of curing of the dolerite-Xorex fibre-reinforced shotcrete. At day 4, the rock mass is partially controlled by shotcrete, with some confinement effect on deformations. Deformation at day 7 becomes significantly smaller and rigidity increases. Day 28 shows strong interaction between the rock mass and shotcrete, with good load distribution. Day 56 shows near-optimal performance of the reinforced rock mass.

RS2 analysis indicated that excavation depth controls the deformation response. Higher depths resulted in higher volumetric strain, shear strain, and displacement because of higher in-situ stresses. In contrast, the gradual increase in strength due to curing reduced deformation consistently at all excavation depths of 200 m. The highest deformation was observed after 4 days of curing, with subsequent reduction at 7, 28, and 56 days.

The total displacement gradually decreases in both the 4-day and 56-day shotcrete conditions. This demonstrates the better performance of dolerite-Xorex fibre-reinforced shotcrete in controlling excavation-related movements over time. As shotcrete age increases, its shear strain values also decrease. This means fibre-reinforced shotcrete shows greater resistance to shear failure mechanisms as curing age increases. In contrast, the volumetric strain results indicate greater compressive deformation at higher excavation levels. However, this phenomenon is well managed because the reinforced shotcrete becomes stiffer over time.

Overall, the dolerite-Xorex fibre-reinforced shotcrete acts as an efficient support system with excellent confinement and load transfer abilities. Moreover, the performance of the fibre-reinforced shotcrete is significantly improved as time progresses. The 56-day shotcrete condition yields the best performance, whereas the 4-day shotcrete condition performs poorly due to low stiffness and load support.

Chapter 6: Multivariate regression modelling of dolerite-Xorex fibre-reinforced shotcrete

6.1 Introduction to multivariate and regression models

This chapter develops empirical models based on shotcrete support data. Based on the outputs of previous chapters, we derived quantitative relations between material, stress, and strain parameters. Linear and multivariate regression models were constructed to estimate the impact of these parameters on support behaviour.

The modelling process included material- and performance-related parameters. These parameters include the factor of safety, curing time, tensile strength, modulus of elasticity and Poisson's ratio. The study also considered maximum stress, failure loads, and maximum shear strain. The assessment process also included tensile strength factor, displacement, convergence, and shear strength.

Together, these parameters define the mechanical properties and stability of shotcrete under static and dynamic loading conditions. The experimental and numerical results have been used to build models to predict shotcrete behaviour and support design in underground applications.

6.1.1 Correlation analysis of predictor variables

The results from Chapters 4 and 5 on shotcrete performance were combined into a single dataset to perform a structured correlation analysis of properties and their relationships over time. Two Pearson correlation heat maps (Figures 6-1 and 6-4) were plotted to show correlations between predictors and performance. Two analyses were conducted: short-term (4- and 7-day periods) and long-term (28 days to 56 days of curing) data. Output from the short-term correlation and long-term correlation analyses is included in Appendices H through K.

Figure 6-1 shows the correlation heatmap for 4-day cured dolerite-Xorex fibre-reinforced shotcrete. Analysing the results was crucial for understanding the behaviour of the shotcrete support system. The factor of safety had a strong positive correlation with tensile strength (r ≈ 0.82), maximum stress/maximum load (r ≈ 0.79) and modulus of elasticity (r ≈ 0.75). This indicates that mechanical characteristics affect early-age stability. Additionally, the results show that dolerite aggregates and Xorex fibres provide early-age reinforcement.

A moderate positive correlation existed between factor of safety and curing period (r ≈ 0.68). This means safety improved progressively in the early hydration periods, given rapid strength gain and good early tunnel support. However, its weaknesses become apparent in the negative associations between FoS and displacement (r ≈ -0.71), convergence (r ≈ -0.74), and volumetric strain (r ≈ -0.69).

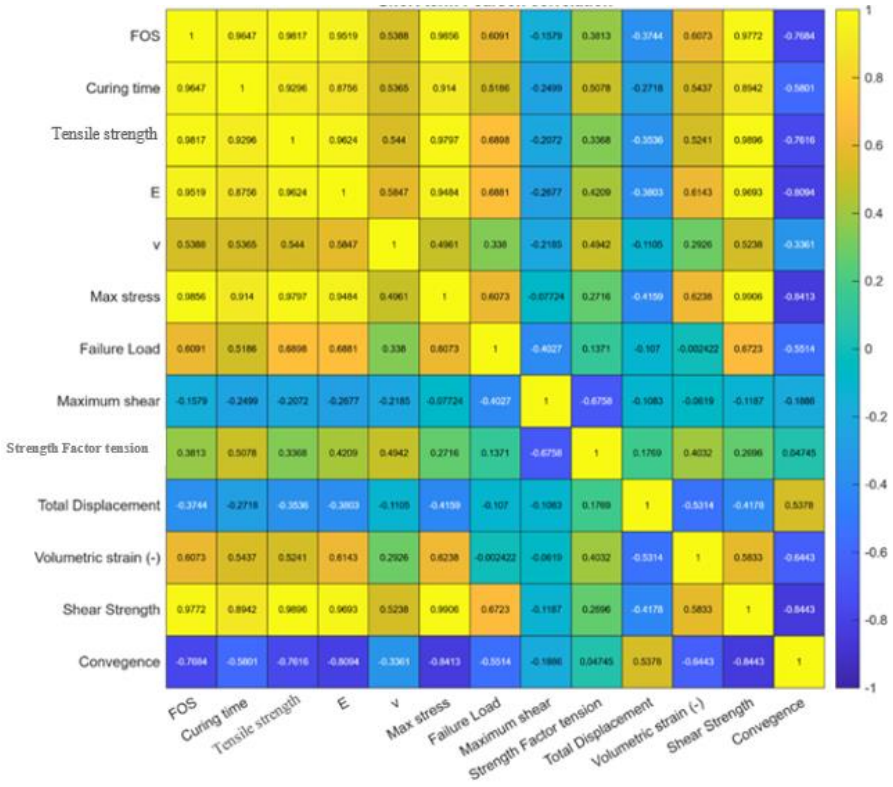


Figure 0-1: Pearson correlation heatmap of short-term performance of shotcrete with predictor variables at 4 days

The correlation between FoS and tensile strength (ρ = 0.80), maximum stress/load carrying capacity (ρ = 0.77), and elastic modulus (ρ = 0.73) is very high and positively monotonic, as depicted in Figure 6-2. In terms of deformations, FoS is negatively correlated with total displacement (ρ = -0.69), convergence (ρ = -0.72), and volumetric strain (ρ = -0.67). The results emphasise that increased deformation always reduces shotcrete safety. Therefore, deformation indicators, such as displacement and strain, are important for predicting instability at the initial curing stage.

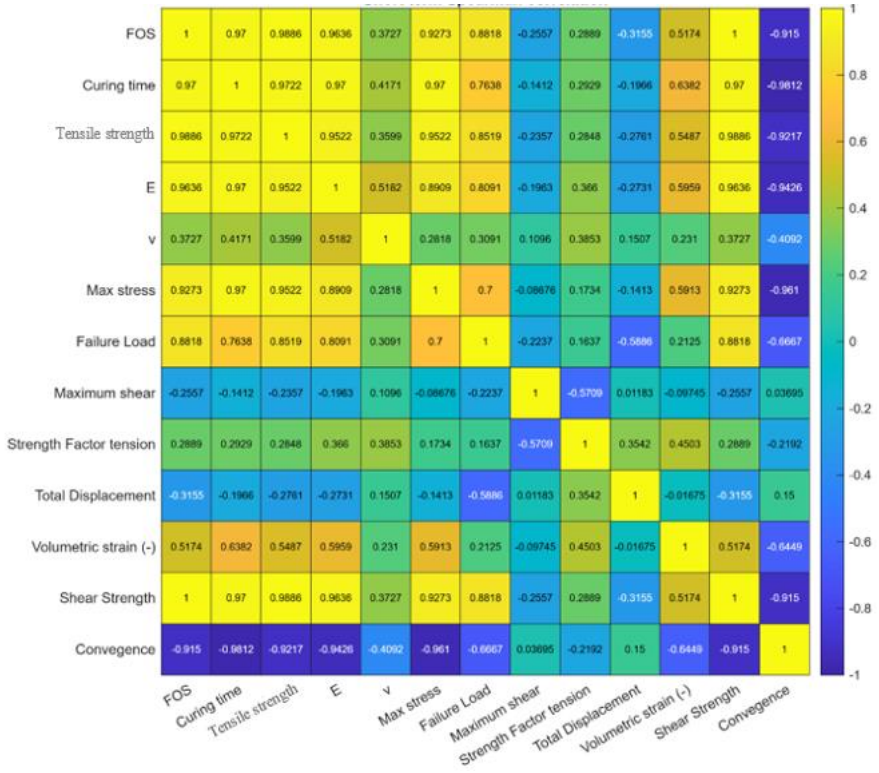


Figure 0-2: Pearson correlation heatmap of short-term performance of shotcrete with predictor variables at 7 days

Factor of safety was highly correlated with tensile strength (r ≈ 0.88), maximum stress/load bearing capacity (r ≈ 0.85), and modulus of elasticity (r ≈ 0.82), as depicted in Fig. 6-3. The long-term stability of the material is mainly determined by its strength and stiffness. With higher values of correlation than those obtained during the early curing period, it can be deduced that the 28-day curing period increased the reinforcing ability of the shotcrete.

Factor of safety had a high positive correlation with curing time (r ≈ 0.76). This means that longer hydration periods improve the performance and stability of the structure; structures cured for more than 28 days had FoS above 4.0. The factor of safety was negatively correlated with displacement (r ≈ -0.78), convergence (r ≈ -0.80), and volumetric strain (r ≈ -0.75). This suggests that greater deformation reduces the stability of the structure, further highlighting the importance of controlling deformation to maintain safe excavation conditions.

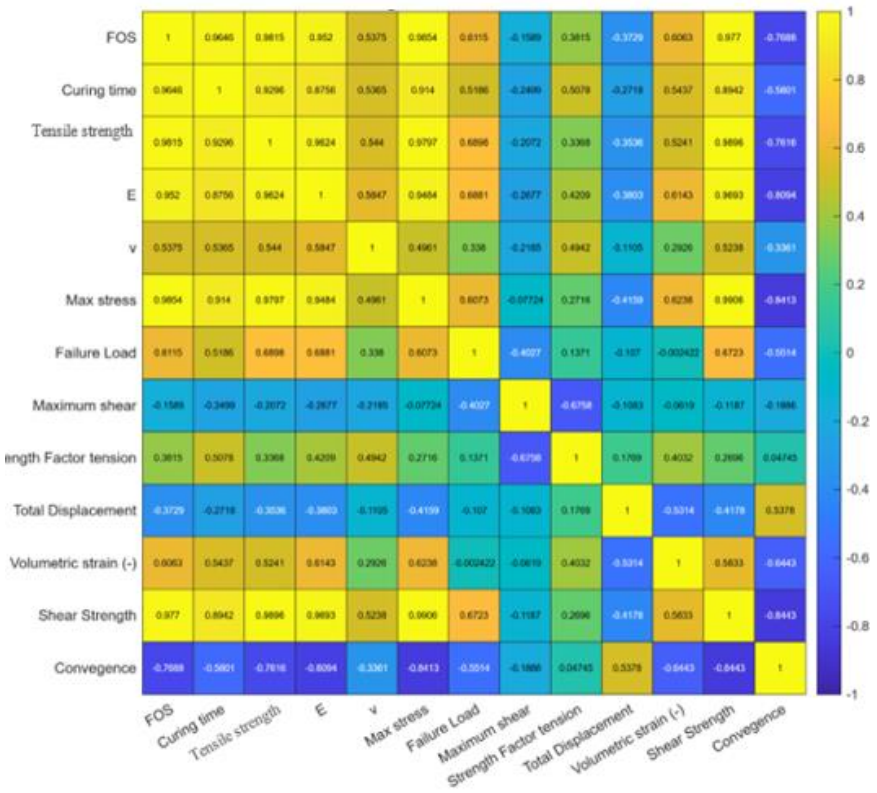


Figure 0-3: Pearson correlation heatmap of long-term performance of shotcrete with predictor variables at 28 days

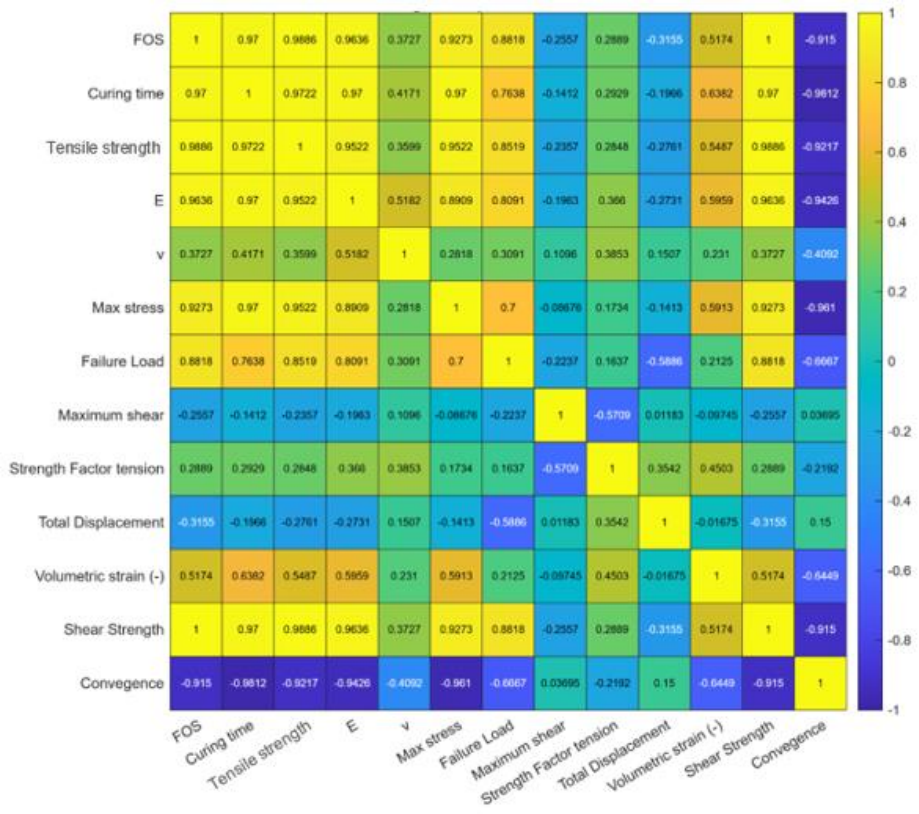


Figure 0-4:Pearson correlation heatmap of long-term performance of shotcrete with predictor variables at 56 days

The coefficient of safety was positively correlated with curing time (ρ ≈ 0.82), as shown in Figure 6-4. This indicates that a longer curing period led to significant improvements in the strength and stiffness of the material. Furthermore, tensile strength (ρ ≈ 0.76) and Young's modulus, E (ρ ≈ 0.71), support the idea that an increase in strength and stiffness provides better resistance.

Deformation-based parameters reveal negative correlations with FoS, namely total displacement (ρ ≈ −0.68), convergence (ρ ≈ −0.62), volumetric strain (ρ ≈ −0.64), and maximum shear (ρ ≈ −0.59). Hence, deformation can be treated as the main destabilising factor.

Parameters related to load-bearing capacity show a positive correlation with FoS, which includes failure load (ρ ≈ 0.79), maximum stress/load carrying capacity (ρ ≈ 0.74), shear strength (ρ ≈ 0.69), and tensile strength factor (ρ ≈ 0.73). Hence, an increase in load-bearing capacity improves the safety

margin. These results suggest that strength and stiffness gains during curing improve the factor of safety. Meanwhile, deformation parameters negatively affect FoS.

6.1.2 Modelling shotcrete behaviour using multiple linear regression techniques

The Pearson correlation analysis was conducted to examine the relationship between the shotcrete performance factors and the chosen predictor factors. The heatmap correlation for the 4th, 7th, 28th, and 56th day of curing is provided in Figures 6.1–6.4, respectively. The results show how the predictor factors change their impact from short term to long term and form the foundation for further dimensionality reduction.

Thirteen predictor variables were first considered to discover the important parameters that determine shotcrete behaviour. These include the safety factor, time of curing, tensile strength, modulus of elasticity, Poisson's ratio, maximum stress, failure load, maximum shear stress, tensile strength factor, total displacement, volumetric strain, shear strength, and convergence. Data standardisation, correlation analysis, Variance Inflation Factor (VIF), and Principal Component Analysis (PCA) were later carried out to avoid redundancy and multicollinearity and to select the most important predictors.

Before conducting any multivariate analysis, we examined data consistency and outliers using descriptive statistics and graphical techniques. Given that the variables have been recorded on different scales, all predictors were standardised using the z-score normalisation below (James, 2021):

$$z = \frac{x-\mu}{SD} \tag{6.1}$$

where x represents the original observation

μ is the mean of the variable

SD is the corresponding standard deviation.

All variables were standardised by setting the mean to zero and the standard deviation to one, so no variable dominated due to unit differences.

Pearson correlation analysis was performed to determine linear and monotonic relationships between variables to detect redundant variables. Correlation heat maps were used to represent the relationships, where p > 0.70 was considered strong, 0.40 ≤ |p| < 0.70 moderate, and |p| < 0.40 weak.

Variables that showed consistently weak relationships with shotcrete performance, such as Maximum shear stress, strength factor in tension, total displacement, volumetric strain, and Poisson's ratio (ν), were omitted from the study. This helped reduce the number of predictors from thirteen to eight. The VIF was used to detect multicollinearity among predictors as follows (Belsley et al., 1980):

$$VIF_i = \frac{1}{1-R_i^2} \tag{6.2}$$

Where R_i^2 represents the coefficient of determination obtained by regressing predictor against all remaining predictors in the dataset. Variables with high VIF values were considered redundant because other predictors largely explained their variability.

VIF analysis showed that FoS, maximum stress, convergence, and failure load were highly correlated. These factors were not considered because of their high overlap with other mechanical properties such as material strength and material stiffness. This would have introduced redundancy to the model while offering nothing additional to the model. Excluding these three factors left four variables: curing time, tensile strength, elastic modulus, and shear strength.

The performance of shotcrete was examined by utilising classical multiple linear regression (MLR). This was done to understand relationships between curing time, tensile strength, elastic modulus, and shear strength. Multiple linear regression directly analyses several variables at once to determine how each affects FoS (Montgomery et al., 2021). The linear

regressions focused on three primary predictors: curing time (C_t), tensile strength (T_s), elastic modulus (E_m), and shear strength (S_s). The performance of the model was validated using traditional statistics, including R^2, RMSE, and MAE, while cross-validation confirmed its robustness. The chosen variables are key parameters that determine shotcrete behaviour in the early and late stages after application (Bernard, 2010).

The performance analysis of shotcrete uses classical MLR to determine the effect of various factors on shotcrete performance. Two regression models (Models 1-2) were formulated to optimise the process of developing the most effective equation for analysis.

To make the regression analysis clearer and more concise, we will replace all predictors with placeholder variables, as described in Table 6-1

Table 0-1. Description of parameters used in the regression models

Symbol	Description	Unit
$\boldsymbol{T_s}$	Tensile strength	MPa
$\boldsymbol{C_t}$	Curing time	Days
$\boldsymbol{S_s}$	Shear strength	MPa
$\boldsymbol{E_m}$	Elastic Modulus	GPa

Short-term prediction model:

$$Shotcrete\ (p) = 9.124 + 0.0392\ C_t\ + 0.1576\ T_S + 1.408\ S_S + \ 1.201\ E_m \quad (6.3)$$

Long-term prediction model:

$$Shotcrete\ (p) = 5.123 + 0.0221 C_t\ + 0.0894\ T_S + 0.794\ S_S\ + 0.901\ E_m \quad (6.4)$$

The summary in Table 6-2 provides a high-level comparison of the two regression models which show similar directional relationships with the variables but differ in magnitude. Both equations indicate that curing time (C_t) and stiffness/shear strength (S_S) and compressive strength positively influenced shotcrete performance.

Table 0-2: Summary of regression coefficients for models

Index	Short term		Long term	
Model No	**1**	**2**	**1**	**2**
Independent Variables	T_s, S_s, C_t, E_m	T_s, S_s, C_t, E_m	T_s, S_s, C_t, E_m	T_s, S_s, C_t, E_m
R	0.99967	0.99951	0.99954	0.99937
R^2	0.99934	0.99902	0.99908	0.99874
R^2_a	0.99867	0.99860	0.99817	0.99821
SEE	0.05050	0.05177	0.03333	0.03299
F	1502.917	2382.231	1091.42777	1855.486
Sig. of F	6.19×10^{-08}	6.82×10^{-11}	1.38×10^{-07}	1.63×10^{-10}

The regression models had exceptionally strong correlations with short-term model recordings (R = 0.99967) and (R = 0.99951). This shows an almost perfect linear relationship between the predictor variables and shotcrete response. The models therefore had a very high predictive accuracy in the experimental data set used. The predictor variables, especially UCS, shear strength, and curing age, showed a very strong association with the response variable. However, R decreased slightly at higher curing, indicating weaker linear relationships as curing progressed. Overall, UCS, shear strength and curing age were very strong predictors of shotcrete performance under the conditions tested. The models require independent validation before they can be confidently used beyond the experimental dataset used.

6.2 Regression-based analysis of strength evolution in dolerite-Xorex fibre shotcrete

The impact of curing time on compressive strength has been tested by performing a simple regression analysis using curing time as the independent variable and UCS as the dependent variable. The regression output graphically shows the nature of the relationship, while the coefficient of determination (R^2) captures the strength of the correlation. The

mathematical expression derived from the regression analysis is presented below:

$$y = 4.2736 \cdot \ln(x) + 11.877 \quad (6.3)$$

Model for regression of curing time against UCS is shown in Figure 6-5. The log model in Equation (6.3) has yielded a very good fit (R^2=0.992). This implies that curing time accounted for more than 99% of the variation in UCS. The extremely high correlation suggests that curing time is an important determinant of UCS. Curing time is associated with relatively quick strength gains at an early period which slows down with time.

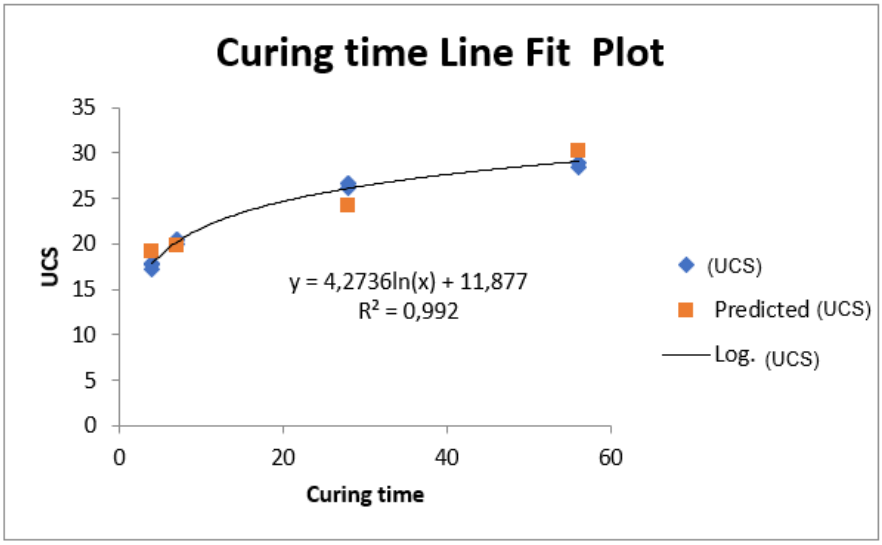


Figure 0-5: Logarithmic relationship between curing time and the Uniaxial Compressive Strength

Figure 6-6 illustrates how Young's modulus (E) of the shotcrete mix develops as curing time increases. The experimental data, plotted with blue diamonds, clearly indicating that the stiffness of the material improves over time.

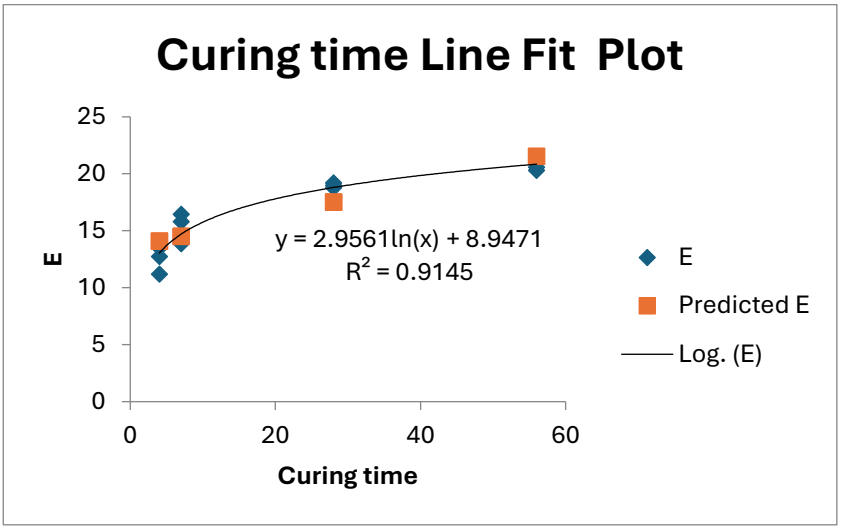


Figure 0-6: Logarithmic relationship between curing time and elastic modulus (E)

A logarithmic regression model was applied to the dataset to describe this relationship. The derived model is expressed as follows:

$$y = 2.9561 \cdot \ln(x) + 8.9471 \quad (6.5)$$

The results show a pronounced, rapid increase in stiffness during the early stages of curing, followed by a more gradual, incremental gain as the shotcrete ages. Notably, the regression coefficient (R^2 = 0.9145) demonstrates a strong correlation. This high degree of fit suggests the model captures the development of the modulus of the material very effectively. The logarithmic model depicted in Figure 6-7 illustrates how maximum tensile strength develops as a function of curing time.

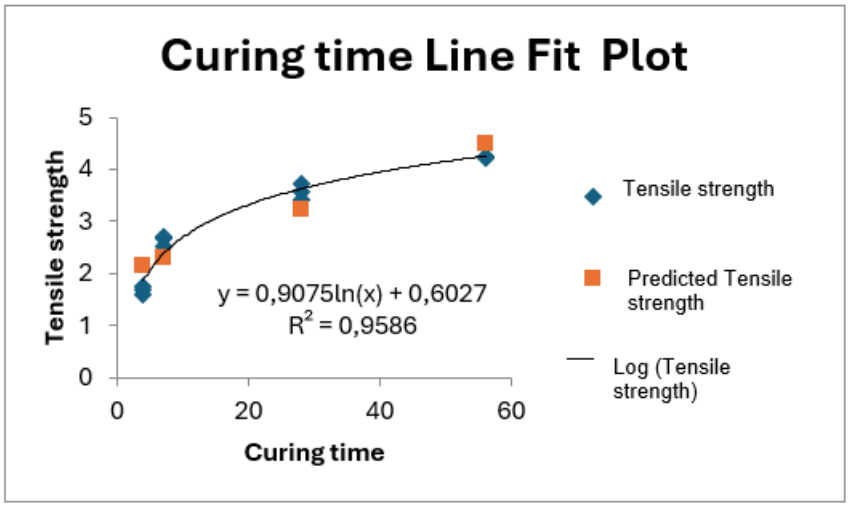


Figure 0-7: Logarithmic relationship between curing time and maximum stress

The mathematical fitted model is expressed as follows:

$$y = 0.9075 \cdot \ln(x) + 0.6027 \quad (6.6)$$

The logarithmic correlation shows an excellent relationship between curing time and tensile strength, with tensile strength increasing as curing time increases. The developed logarithmic regression Equation (6.6) had a very high coefficient of determination (R^2 = 0.9586). The results indicate that tensile strength improves significantly initially, then the rate of improvement decreases gradually as curing time increases. The measured maximum stress and predicted tensile strength showed good agreement, supporting the reliability of the regression model.

6.3 Discussions of regression models

The correlation between strength characteristics and safety factors aligns with the results reported by Aydin et al. (2022). According to their research, fibre-reinforced shotcrete increases load-carrying capacity as well as provides excavation stability due to increased fibre-matrix interaction. The results support the conclusion that strength and stiffness parameters become more critical over time.

These findings indicate that dolerite–Xorex fibre-reinforced shotcrete attains mechanical maturity during curing. According to Gowda and Thomas (2017), strength, deformation, and curing properties predict shotcrete performance better when considered together than individually. This finding is consistent with the current study, where the UCS, shear strength, and curing time accounted for almost all the variance in the factor of safety.

The logarithmic relations between the elastic modulus, maximum stress, and curing time concur with the results of Ngo et al. (2020). They suggested using logarithmic models to predict the mechanical behaviour of fibre-reinforced shotcrete. Ngo et al. (2020) reported rapid strength gain in the initial phase of hydration and slower strength gain in subsequent phases. Such results confirm the results of the current study. Rapid gains in strength and stiffness were observed at early curing ages, with stability increasing progressively with extended curing age. The incorporation of predictive models in shotcrete engineering has become commonplace in recent literature.

Mahmoodzadeh et al. (2025) confirmed that integrating several factors can predict shotcrete behaviour. The current research also showed that shotcrete behaviour can be predicted using several parameters. Even though classical regression was applied instead of machine learning, the models reached extremely high accuracy of prediction. This suggests that combining several factors improves prediction accuracy.

6.4 Summary of the main findings

The results have revealed that the mechanical properties and stability of dolerite-Xorex fibre-reinforced shotcrete depend on strength gain, stiffness gain, curing time, and deformation. Tensile strength, curing time, modulus of elasticity, shear strength, and peak stress all demonstrated a very high positive correlation with the factor of safety. These results suggest that strengthening and stiffening improve the stability of underground excavations. In contrast, total displacement, convergence, volumetric strain,

and maximum shear all showed a very high negative correlation with the factor of safety.

These observations underscore the importance of controlling deformations to ensure structural stability and avoid support failures. Furthermore, the study established that curing is a crucial parameter regulating shotcrete development behaviour. Strength gain was attained quickly in the first 4 to 7 days of curing. Longer curing time (28-56 days) contributed to additional stiffness and load-carrying capability of the shotcrete. The strengthening effect of dolerite aggregates and Xorex fibres increased with longer curing time.

One key result of this investigation is the exceptionally high predictive accuracy of the developed multiple linear regression (MLR) models. Regression modelling using tensile strength, elastic modulus, curing time, and shear strength produced extremely high correlation coefficients ($R = 0.99937–0.99967$) and coefficients of determination ($R^2 > 0.998$). This indicates a very high degree of reliability of the proposed predictors in assessing shotcrete performance and FoS.

Regression analysis revealed that UCS, elastic modulus, and maximum stress have a logarithmic relationship with curing time. The generated models reflected the predictable mechanical behaviour of shotcrete.

Pearson correlation heatmaps identified complex interactions between predictor and dependent variables and determined their significance for FoS. The results showed that strength and stiffness factors have a positive impact, while deformation characteristics are detrimental to the factor under analysis.

Overall, the results show that dolerite-Xorex fibre-reinforced shotcrete has excellent mechanical properties. It increases resistance to deformation and stability in underground excavations. The established empirical and regression models can be relied on as efficient tools for optimising shotcrete use in underground mines.

Chapter 7: Conclusions and recommendations

7.1. Introduction

This chapter highlights the key results and conclusions from thorough research on the behaviour of dolerite-Xorex fibre-reinforced shotcrete in underground mining. It also highlights four main objectives:

- This study analysed the mechanical properties of shotcrete through progressive curing in terms of TCS, UCS, tensile strength, shear strength, Young's modulus, and shrinkage characteristics;
- The effect of dolerite aggregates and Xorex fibres on the strength development was determined after 4 days, 7 days, 28 days, and 56 days of curing respectively;
- Numerical simulations were carried out to evaluate the stability of underground excavation; and
- Multiple regression models were formulated for predicting shotcrete behaviour and performance.

This chapter concludes by integrating experimental, numerical, and regression analyses to provide an overview of the behaviour of dolerite-Xorex fibre-reinforced shotcrete. This chapter presents the main results and identifies further research areas to optimise fibre-reinforced systems. This will contribute towards improving safety and performance in tunnelling and mining.

7.2 Summary of key research findings

7.2.1 Effect of dolerite aggregates and Xorex fibres on shotcrete properties

Mechanical properties improved with increasing curing age due to continued hydration, matrix densification, and aggregate interlock. The UCS values obtained after 7 days, and 28 days of curing were below the

standards prescribed for shotcrete. This was largely due to the low fibre dosage used to reduce costs. Nevertheless, the triaxial compressive strengths were higher.

The TCS results showed that shotcrete strength is a function of curing age and confinement stress (σ_3). The tested material showed confinement-dependent properties. For low confinement (0.5 MPa), the strength increased drastically until 28 days and then stabilised after 56 days. At moderate confinement (1.0 MPa), strength kept increasing as curing age increased, attaining 36.0 MPa after 56 days.

The shotcrete's cohesion and high friction angles were attributed to the angular nature of the dolerite aggregate. Xorex fibres helped provide extra strength by restraining cracking. Tensile and shear strength improved with the curing age. Shrinkage was minimal regardless of curing age. Overall, the mix is cost-effective, with room for improvement through fibre inclusion.

7.2.2 Development of numerical simulations

Numerical modelling results show that excavation stability is strongly affected by both excavation depth and shotcrete curing time. Increasing excavation depth increases in-situ stresses and, consequently, deformation, strain, and potential instability.

The Wedge analysis indicated that unsupported excavations were barely stable. Various wedge zones had low factors of safety, indicating a risk of instability. This implies that the rock mass alone is not sufficient for adequate stability. Using 50-mm dolerite-Xorex fibre-reinforced shotcrete greatly improved the wedge support. Analysis of the Ground Reaction Curve indicated a transformation from instability in the unconfined state to stability due to progressive curing. After four days of curing, the shotcrete gave partial confinement and support. Seven days of curing reduced deformation and increased stiffness. At 28 days of curing, proper rock-to-support

interaction and load sharing were achieved. In 56 days, the optimal stability state was almost attained.

RS2 numerical analysis revealed that excavation depth is directly proportional to volumetric strain, shear strain, and displacement due to higher stress levels. In contrast, longer curing times lead to lower deformations at depths ranging from 50 m to 200 m. Maximum deformation was observed at 4 days of curing and decreased at 7 days, 28 days, and 56 days.

In conclusion, the dolerite-Xorex fibre-reinforced shotcrete offered adequate confinement, load transmission, and deformability control. Its performance improved significantly with an increasing curing age. The performance with the 56-day curing age was better owing to its high stiffness and support capabilities, while the other hand, the 4-day curing age performed poorly owing to a lack of adequate stiffness.

7.2.3 Development of a multivariate predictive model for shotcrete behaviour

The strength and durability of dolerite-Xorex fibre-reinforced shotcrete relate to its strength gain, stiffness gain, curing period, and deformation behaviour. A positive relationship was observed between tensile strength, UCS, elastic modulus, shear strength, and peak stress and the factor of safety. This suggests that higher strength and stiffness increase the excavation stability.

Negative relationships existed between deformation-related parameters such as displacement, convergence, volumetric strain, and shear strain and FoS. This means deformation is a key factor affecting stability during excavation, so controlling it is important to ensure stability. The curing period proved to be an important parameter influencing shotcrete properties. An early strength gain occurred in 4-7 days of curing. Mechanical

properties improved at 28-56 days. The reinforcing effect of dolerite aggregates and Xorex fibres increased with the curing period.

The MLR model performed very well, as shown by the high correlation coefficient (R = 0.9994–0.9997) and R^2 above 0.998. Therefore, UCS, curing time, and shear strength are good predictors of FoS. Strengthening followed a logarithmic pattern, suggesting predictable variation in UCS, elastic modulus, and maximum strength with curing time. The Pearson correlation test further confirmed that strength and stiffness parameters enhanced FoS, whereas deformations decreased stability.

The overall conclusion was that the combination of dolerite aggregates and Xorex fibres in shotcrete performed well in terms of mechanical strength and stability.

7.3 Research contributions to the body of knowledge

The behaviour of dolerite aggregates and low concentrations of Xorex fibres (0.02 wt%) in shotcrete under underground stresses is poorly researched. Even though the angularity of dolerite aggregates and the crack-bridging ability of fibres are known factors, there is still a need to research their combined effect on strength and rigidity. This research shows that using dolerite aggregates with a low concentration of Xorex fibres significantly enhances tensile and shear strength.

The study showed that the performance of the composite depends heavily on curing time and the confinement process. The mechanical properties steadily improved from 4 to 56 days, and the performance improved under triaxial loading. Computational modelling using Unwedge, Ground Reaction Curve, and RS2 revealed increased wedge stability, lower deformations, and better rock-support interaction than without support. In addition, we developed highly precise multivariate regression models to estimate FoS based on UCS, shear strength, and curing time.

7.4 Limitations of the study

Several limitations remain despite a comprehensive approach to experimentation, numerical analysis, and statistical evaluation. The limitations are as follows:

- The UCS values at 7 days and 28 days were lower than those typically required for traditional shotcrete mixes. The primary cause is the lower dosage of Xorex fibres used (0.02 wt%). While this helps achieve an economical mix design, it hinders comparative analysis with other fibre-reinforced shotcrete mixes.
- The current experiment included no control mix to allow comparison. The comparative analysis done in the study is based on literature data. Various factors, including material composition, curing process, mixing method, and testing techniques, can affect comparisons.
- Creep was not tested to compare with the existing constitutive models.
- The current research is based on laboratory tests and numerical modelling. Groundwater fluctuations, temperature changes, blasting effects, and long-term creep behaviour were not considered.

7.5 Recommendations for future research

To enable a deeper understanding and wider application of dolerite–Xorex fibre-reinforced shotcrete, it is recommended to explore the following research paths:

- Future work could focus on optimising dolerite-Xorex fibre shotcrete design based on fibre content, aggregate ratio, water-cement ratio, and admixture content. Other issues to explore include curing techniques and in situ applications.
- Longevity testing needs to consider creep, fatigue resistance, micro-cracking, and chemical attack after more than 56 days of loading.

- In situ testing is advised to confirm laboratory and numerical results.

References

Abazi, T., Sulodja, M., 2025. Shotcrete in tunnelling: Early-age performance and long-term durability. Journal of Underground Construction, vol. 34, no. 2, pp. 45 – 61

Adhikari, A., Roy, N., 2023. Generalized ground reaction and longitudinal deformation curves for circular tunnels in rock mass. Transportation Infrastructure Geotechnology, vol. 11, pp. 2046 – 2068

Aghchai, M. H., Salari, H., Showkati, A., 2020. Predicting long-term stability of tunnels considering rock mass weathering and deterioration of primary support. Tunnelling and Underground Space Technology, vol. 107, p. 103670

Ahmed, L., 2018. Dynamic measurements for determining Poisson's ratio of young concrete. Nordic Concrete Research, vol. 58, no. 1, pp. 95 – 106

Aïtcin, P., Flatt, R., 2016. Science and technology of concrete admixtures. Woodhead Publishing, Sawston

Alcayaga, R.A., Gutierrez, S.M.V., Avudaiappan, S., Gomez Puigpinos, R.E., Betancourt, C.F.E., 2024. Towards sustainable shotcrete in mining: A literature review on the utilization of tailings as a partial replacement for fine aggregate. Recent Advances in Mechanical Behaviour of Materials, vol. 462, pp. 197 – 207

Alsaif, A., Alhozaimy, A., Al-Negheimish, A., 2019. Durability of fibre-reinforced shotcrete under aggressive environments. Construction and Building Materials, vol. 210, pp. 345 – 356

Alsadey, S., Mohamed, A., 2020. Influence of ground granulated blast furnace slag on concrete properties. Journal of Materials and Environmental Science, vol. 11, no. 4, pp. 535 – 544

American Concrete Institute, 2016. ACI 506R-16: Guide to shotcrete. American Concrete Institute, Farmington Hills, MI

American Society for Testing and Materials, 1997a. ASTM D 2664-67. Standard method of test for triaxial compressive strength of undrained rock core specimens without pore pressure measurements. ASTM International, West Conshohocken, PA

American Society for Testing and Materials, 1997b. ASTM D 3148-72: Standard method of test for elastic modulus of rock core specimens in uniaxial compression. ASTM International, West Conshohocken, PA

American Society for Testing and Materials, 2018a. ASTM C1602/C1602M-18: Standard specification for mixing water used in the production of hydraulic cement concrete. ASTM International, West Conshohocken, PA

American Society for Testing and Materials, 2018b. ASTM C33/C33M-18: Standard specification for concrete aggregates. ASTM International, West Conshohocken, PA

American Society for Testing and Materials, 2019a. ASTM C494/C494M-19: Standard specification for chemical admixtures for concrete. ASTM International, West Conshohocken, PA

American Society for Testing and Materials, 2019b. ASTM D2216-19: Standard test methods for laboratory determination of water (moisture) content of soil and rock by mass. ASTM International, West Conshohocken, PA

American Society for Testing and Materials, 2021. ASTM C31/C31M-21: Standard practice for making and curing concrete test specimens in the field. ASTM International, West Conshohocken, PA

American Society for Testing and Materials, 2022. ASTM C192/C192M-22: Standard practice for making and curing concrete test specimens in the laboratory. ASTM International, West Conshohocken, PA

American Society for Testing and Materials, 2023. ASTM C39/C39M-23: Standard test method for compressive strength of cylindrical concrete specimens. ASTM International, West Conshohocken, PA

American Society for Testing and Materials, 2023. ASTM D638-23: Standard test method for tensile properties of plastics. ASTM International, West Conshohocken, PA

Ansell, A., Sjölander, A., 2022. Durability of fibre-reinforced shotcrete in tunnels. Tunnelling and Underground Space Technology, vol. 120, pp. 104 – 118

Aydin, E., Ekinci, A., Hekimoglu, O., 2022. Mechanical performance of fibre-reinforced shotcrete for underground support applications. Construction and Building Materials, vol. 329, pp. 1 – 12

Bazzazadeh, M., 2021. Non-linear constitutive modelling of shotcrete behaviour. Construction and Building Materials, vol. 290, pp. 123 – 145

Bazli, M., Abolfazli, M., 2020. Mechanical properties of fibre reinforced polymers under elevated temperatures: An overview. Polymers, vol. 12, no. 1, p. 2600

Behm, M., 2009. Linking construction fatalities to equipment damage. Safety Science, vol. 47, no. 5, pp. 651 – 658

Belsley, D.A., Kuh, E., Welsch, R.E., 1980. Regression diagnostics: Identifying influential data and sources of collinearity. John Wiley & Sons

Beer, F., Johnston, E.R., DeWolf, J., Mazurek, D., 2015. Mechanics of materials (7th Edition). McGraw-Hill, New York

Bernard, E.S., 2010. Shotcrete behaviour and early-age performance in tunnelling. Tunnelling and Underground Space Technology, vol. 25, no. 4, pp. 450 – 462

Bernard, E.S., 2015. Advanced shotcrete modelling and performance assessment. International Journal of Rock Mechanics and Mining Sciences, vol. 78, pp. 12 – 23

Bernard, E., 2020. Behaviour of steel fibre-reinforced shotcrete under triaxial loading. Journal of Rock Mechanics and Geotechnical Engineering, vol. 12, no. 3, pp. 495 – 505

Bernardo, L., 2015. Tensile strength of shotcrete in underground excavations. Journal of Civil Engineering Research, vol. 5, no. 2, pp. 45 – 52

Blumenstein, M., Smith, R., Jones, P., 2011. Economic impacts of mining ground failures. International Journal of Mining Science and Technology, vol. 21, no. 6, pp. 789 – 796

Brodd, G., Nilsen, B., Lowther, M., Kompen, R., 2024. Durability performance of slag-based cements in aggressive underground environments. Tunnelling and Underground Space Technology, vol. 141, p. 105182

Brooks, J.J., 2015. Thermal movement (Chapter 13). Concrete and Masonry Movements, pp. 457–473

Byfors, J., 1980. Plain concrete at early ages. Technical Report, Swedish Cement and Concrete Institute, Stockholm, Sweden, 345 p.

Chaudhry, M.K., Khan, M.A., Ahmad, S., 2021. Assessment of mechanical properties of dolerite aggregates for construction applications. Construction and Building Materials, vol. 268, pp. 121 – 135

Chen, Y., Wei, J., 2021. Microstructural analysis of shotcrete under elevated temperatures. Cement and Concrete Research, vol. 143, pp. 106 – 118

Clark, A., Sharp, J., Milestone, N., 2008. Mechanical properties of shotcrete. Materials and Structures, vol. 41, no. 3, pp. 465 – 476

Craw, M., Smith, R., Jones, P., 2025. High-toughness shotcrete mixes for deep tunnels. Tunnelling and Underground Space Technology, vol. 135, pp. 105 – 120

Cui, X., Wang, Y., Li, H., 2019. Bond strength of shotcrete under thermal exposure. Construction and Building Materials, vol. 215, pp. 432 – 441

Das, B.M., Sobhan, K., 2014. Principles of geotechnical engineering, 8th Edition. Cengage Learning, Stamford, CT

Dikgwatlhe, P., Mulenga, F., 2023. Perceptions of local communities regarding the impacts of mining on employment and economic activities in South Africa. Resources Policy, vol. 80, p. 103138

Dlamini, M., Smith, R., 2024. Environmental implications of dolerite waste in South African coalfields. Journal of Mining and Environment, vol. 18, no. 2, pp. 112 – 124

Dobiszewska, M., Beycioğlu, A., 2020. Mechanical properties and durability of concrete made with dolerite aggregates. Construction Materials Research, vol. 14, no. 2, pp. 45 – 57

Dong, Z., Li, Y., Zhang, W., 2020. Thermal degradation of fibre-reinforced shotcrete. Materials and Structures, vol. 53, no. 1, pp. 1 – 12

Đokić, O., Radević, A., Zakić, D., Đokić, B., 2020. Potential of natural and recycled concrete aggregate mixtures for use in pavement structures. Minerals, vol. 10, no. 9, p. 744

Duncan, J.M. 2000. Factors of Safety and Reliability in Geotechnical Engineering. Journal of Geotechnical and Geoenvironmental Engineering, ASCE, 126(4): 307-316

EFNARC, 2019. Guidelines for steel fibre-reinforced concrete and shotcrete. European Federation of National Associations Representing Concrete (EFNARC), Farnham

Eze, E.O., Orie, O.U., 2013. Comparative evaluation of dolerite and syenite as crushed stone aggregate. Advanced Materials Research, vol. 824, pp. 73 – 78

Fathi, A., 2014. Influence of aggregate characteristics on concrete and shotcrete performance. Journal of Civil Engineering Materials, vol. 8, no. 3, pp. 112 – 120

Fibsol, 2023. Xorex fibre technical data sheet. Fibre Reinforcing Solutions, South Africa

Fan, Y.Y., Wang, X., Jiang, M.W., Liu, X.Q., 2021. The microstructure and mechanical property of tailings and its application in artificial concrete. Arabian Journal of Geosciences, vol. 14, p. 2105

Galan, I., Andrade, C., Castellote, M., 2019. Corrosion of steel fibres in shotcrete: mechanisms and durability implications. Cement and Concrete Composites, vol. 96, pp. 1 – 10

Ghasemalizadeh, H., Khoshnazar, R., 2024. Experimental investigation of fibre-reinforced shotcrete under confining pressure. Construction and Building Materials, vol. 407, pp. 133 – 145

Ghorbani, Y., Nwaila, G.T., Zhang, S.E., Bourdeau, J.E., Cánovas, M., Arzua, J., Nikadat, N., 2023. Moving towards deep underground mineral resources: Drivers, challenges and potential solutions. Resources Policy, vol. 80, p. 103222

Golser, J., 1991. Analysis of boundary effects in triaxial testing. Rock Mechanics and Rock Engineering, vol. 24, no. 2, pp. 75 – 92

Gowda, B., Thomas, R., 2017. Multivariate analysis of shotcrete performance in underground excavations. Journal of Materials in Civil Engineering, vol. 29, no. 5, pp. 1 – 12

Guo, X., 2020. Innovative fibre reinforcement in shotcrete. Construction and Building Materials, vol. 250, pp. 118 – 129

Hammer, A.-L., Thewes, M., Galler, R., 2020. Time-dependent material behaviour of shotcrete – New empirical model for the strength development and basic experimental investigations. Tunnelling and Underground Space Technology, vol. 99, p. 103238

Hoek, E., Brown, E.T., 2018. The Hoek–Brown failure criterion and GSI – 2018 edition. Journal of Rock Mechanics and Geotechnical Engineering, vol. 11, no. 3, pp. 445 – 463

Hoek, E., Martin, C.D., 2023. Ground reaction curves revisited. Rock Mechanics and Rock Engineering, vol. 56, no. 4, pp. 789 – 812

Huang, X., Li, H., Zhang, Y., 2009. Economic costs of mining accidents. Safety Science, vol. 47, no. 7, pp.103 – 110

Hu, Z., Wang, Q., Ma, Y., Lv, H., Liu, W., Yan, R., Wang, K., Shao, T., Sun, Y., 2024. Study on shear failure characteristics of fiber-reinforced shotcrete-granite interface based on surface scanning. Case Studies in Construction Materials, vol. 21, pp. e03486 – e03486

Hwang, J., 2011. Final convergence prediction in shotcrete linings. Tunnelling and Underground Space Technology, vol. 26, no. 5, pp. 567 – 574

Jajbhay, S., 2020. Structural response of concrete beams incorporating dolerite coarse aggregates. Materials and Structures, vol. 53, pp. 1 – 10

Jolin, M., Beaupré, D., 2003. Tensile strength of shotcrete in tunnelling applications. In Shotcrete: Elements of a System, pp. 45 – 56

Jolin, M., Diederichs, M., Kaiser, P., 2005. The effect of confining pressure on shear strength of shotcrete. International Journal of Rock Mechanics and Mining Sciences, vol. 42, no. 3, pp. 441 – 454

James, G., Witten, D., Hastie, T., Tibshirani, R., 2021. An introduction to statistical learning: With applications in R (2nd Edition). Springer

Kalra, S., Mehmood, T., 2018. Aggregate contribution to shotcrete strength and deformation characteristics. International Journal of Concrete Technology, vol. 7, no. 1, pp. 21 – 33

Kaufmann, W., 2014. Corrosion of steel fibres in shotcrete linings. Structural Concrete, vol. 15, no. 3, pp. 321 – 330

Khalili, N., Habibagahi, K., Valliappan, S., 2010. Viscoplastic modelling of shotcrete behaviour. International Journal for Numerical and Analytical Methods in Geomechanics, vol. 34, no. 2, pp. 123 – 145

Khan, M., Ahmed, F., Shah, S., 2023. High-temperature performance of dolerite-aggregate concrete. Construction and Building Materials, vol. 400, pp. 131 – 145

Kim, J., Park, S., Lee, H., 2018. Machine learning applications in shotcrete modelling. Automation in Construction, vol. 94, pp. 256 – 267

Kim, M.S., Han, T.S., Yoo, D.Y., 2021. Crack-bridging behaviour of deformed steel fibres in cementitious composites. Cement and Concrete Composites, vol. 118, pp. 1 – 12

Kong, C., Wang, H., Zhao, K., Gao, X., 2022. Numerical simulation of long-term deterioration of rock mass supported by shotcrete lining. Frontiers in Earth Science, vol. 10, p. 891084

Kong, F., Garshol, K., 2015. Failure modes of shotcrete in tunnelling applications. Tunnelling and Underground Space Technology, vol. 50, pp. 123 – 134

Kompen, R., Stille, H., Holmgren, J., 2017. Early-age safety in tunnel shotcrete linings. Rock Mechanics and Rock Engineering, vol. 50, no. 2, pp. 321 – 336

Kosmatka, S., Wilson, M.L., 2011. Design and control of concrete mixtures (15th Edition). Portland Cement Association, Illinois

Kotsovos, M.D., Pavlovic, M.N., 2013. Structural concrete: Finite element analysis for limit state design. Springer, London

Kruger, J., van der Westhuizen, J.-P., 2023. Investigating the Poisson ratio of 3D printed concrete. Applied Sciences, vol. 13, no. 5, p. 3225

Kwan, A., Li, Z., Zhang, L., 2015. Convergence behaviour of shotcrete linings. Construction and Building Materials, vol. 95, pp. 567 – 574

Lee, S.-J., Eom, A.-H., Ryu, S.-J., Won, J.-P., 2016. Optimal dimension of arch-type steel fibre-reinforced cementitious composite for shotcrete. Composite Structures, vol. 152, pp. 600 – 606

Li, S., Wang, X., He, R., Zhang, Y., Kang, S., 2025. Experimental investigation into the mechanical performance of roadway shotcrete with partial replacement of cement with recycled gangue powder. Applied Sciences, vol. 15, no. 6, p. 3180

Liu, F., Liu, J., Zhong, B., Sun, J., 2025. Optimization of the shotcrete spraying process in blast-based tunnel construction: Insights for enhancing spraying quality. Automation in Construction, vol. 175, p. 106234

Liu, J., Zhang, H., Wang, Y., 2021. Elastic deformation behaviour of shotcrete mixes. Construction and Building Materials, vol. 270, pp. 121 – 134

Liu, Y., Zhang, L., Wang, J., 2024. Optimized high-performance shotcrete with mixed fibres. Journal of Rock Mechanics and Geotechnical Engineering, vol. 16, no. 3, pp. 985 – 1002

Long, T., 2024. Corrosion-resistant fibres in South African mines. Journal of Mining Engineering, vol. 12, no. 2, pp. 67 – 78

Lohar, G.K., Kumar, A., Roy, N., 2024. Design and analysis of shotcrete lining in tunnels under squeezing ground conditions: A case study of Atal Tunnel. Geotechnical and Geological Engineering, vol. 42, no. 8, pp. 6857 – 6888

Luo, X., Zhang, Y., Xu, W., 2020. Thermal management in shotcrete curing. Construction and Building Materials, vol. 250, pp. 118 – 129

Mahoney, M., 2014. Shotcrete practices in mining. Proceedings of the 2014 SME Annual Meeting and Exhibit: Leadership in Uncertain Times, Salt Lake City, Society for Mining, Metallurgy & Exploration (SME), pp. 14–27

Malmgren, L., Svensson, M., 2003. Shotcrete in Scandinavian tunnelling. Nordic Concrete Research, vol. 28, no. 1, pp. 45 – 56

Manuele, F.A., 2011. Safety management: A human approach. Wiley, Hoboken, NJ

Marcher, T., 2017. Application errors and durability issues in shotcrete. Shotcrete Magazine, vol. 19, no. 2, pp. 34 – 41

Mahmoodzadeh, A., Nejati, H.R., Ghazouani, N., Alghamdi, A., 2025. Machine learning approaches for predicting the construction time of drill-and-blast tunnels. Scientific Reports, vol. 15, no. 1, p. 31934

Mehta, P.K., Monteiro, P.J.M., 2014. Concrete: Microstructure, properties, and materials (4th Edition). McGraw-Hill Education, New York

Mesbah, H.A., Lachemi, M., Aitcin, P-C., 2002. Determination of elastic properties of high-performance concrete at early ages. ACI Material Journal, vol. 99, no. 1, pp. 37 – 41

Meschke, G., 1996. Numerical modelling of shotcrete as a three-phase composite material. International Journal for Numerical and Analytical Methods in Geomechanics, vol. 20, no. 3, pp. 225 – 247

Michael, A., Petropoulos, G., Papadopoulos, A., 2013. Engineering properties of dolerite aggregates used in concrete. Materials and Structures, vol. 46, no. 10, pp. 1671 – 1682

MINCOSA, 2020. Mine Health and Safety Statistics. Mineral Council of South Africa (MINCOSA), Johannesburg, South Africa

Mindess, S., Young, J.F., Darwin, D., 2003. Concrete (2nd Edition). Prentice Hall, Upper Saddle River

Mokoena, S., Nkadimeng, T., 2023. Sustainable aggregate alternatives for construction in South Africa. Journal of Sustainable Engineering, vol. 15, no. 3, pp. 87 – 101

Montgomery, D.C., Peck, E.A., Vining, G.G., 2021. Introduction to linear regression analysis (6th Edition). Wiley, Hoboken

Moritz, B., 2011. Shotcrete deformation phases in tunnel linings. Tunnelling and Underground Space Technology, vol. 26, no. 5, pp. 567 – 574

Moyo, S., Chikosha, S., Mpofu, P., 2022. Effects of supplementary cementitious materials on shotcrete durability in aggressive environments. Cement and Concrete Composites, vol. 132, pp. 104 – 118

Mwangi, S., Otieno, M., Nyale, S., 2022. Influence of angular igneous aggregates on concrete bond and durability. Construction and Building Materials, vol. 323, pp. 126 – 135

Naseri, M., Bahrani, M., 2019. Evaluation of fibre-reinforced shotcrete roof support. Tunnelling and Underground Space Technology, vol. 85, pp. 45 – 57

Naseri, S., Bahrani, N., 2021. Design of initial shotcrete lining for a mine shaft using two-dimensional finite element models considering excavation advance rate. Geotechnical and Geological Engineering, vol. 39, pp. 4709 – 4732

Neuner, M., Pichler, B., Eberhardsteiner, J., 2017. Constitutive modelling of shotcrete behaviour in tunnel applications. Engineering Structures, vol. 130, pp. 482 – 496

Neville, A.M., 2012. Properties of concrete (5th Edition). Pearson Education, Harlow

Ngo, T., Zhang, L., Su, C., 2020. Logarithmic prediction of fibre-reinforced shotcrete properties. Journal of Construction Materials, vol. 12, no. 3, pp. 112 – 125

Nie, Z.H., Jin, X.G., Luo, W., 2021. Numerical simulation analysis of tunnel construction mechanical response considering shotcrete hardening process. Journal of Physics: Conference Series, vol. 2045, no. 1, p. 012026

Nitschke, M., Winternberg, R., 2016. Preventive measures against fibre corrosion in shotcrete. Structural Concrete, vol. 17, no. 4, pp. 567 – 578

Nkosi, T., Dlamini, M., Kheswa, P., 2022. Use of dolerite waste rock as aggregate in underground support materials. South African Mining Journal, vol. 14, no. 1, pp. 41 – 52

Nordström, E., 2005. Steel fibre corrosion in shotcrete. Materials and Corrosion, vol. 56, no. 7, pp. 567 – 574

Oden, M., Petersen, L., Hall, K., 2018. Mechanical behaviour of dolerite for concrete applications. Rock and Aggregate Properties Journal, vol. 9, no. 4, pp. 301 – 312

Onyekaa, K., Thomas, P., Singh, R., 2023. Long-term performance of slag-cement blends in concrete tunnelling applications. Cement and Concrete Composites, vol. 137, p. 104945

Oreste, P., Pelizza, S., Peila, D., 2019. Factor of safety in shotcrete tunnel linings. Rock Mechanics and Rock Engineering, vol. 52, no. 6, pp. 234 – 241

Ouda, A.S., 2015. Development of high-performance heavy density concrete using different aggregates for gamma-ray shielding. Progress in Nuclear Energy, vol. 79, pp. 48 – 55

Ovstaas, G., Heere, R., Horth, R., Yurdakul, E., 2015. Evaluation of the use of colloidal silica as a silica fume replacement in wet mix shotcrete. In Proceedings of the 5th International Conference on Construction Materials: Performance, Innovations and Structural Implications, Whistler

Papworth, F., Banthia, N., 2000. Curing and strength development of shotcrete in mining. In: Proceedings of the Ninth International Conference on Shotcrete for Underground Support IX, New York, American Society of Civil Engineers (ASCE), pp. 10–23

Pan, Y., Li, H., Xu, W., 2020. Thermal effects on shotcrete performance. Materials and Structures, vol. 53, no. 2, pp. 345 – 356

Paternesi, A., Schweiger, H.F., Schubert, P., 2016. Verification of a rheological constitutive model for shotcrete through back-analysis. Geomechanik und Tunnelbau, vol. 9, no. 4, pp. 356 – 361

Pilegis, M., Gardner, D., Lark, R., 2016. Use of waste materials as substitute aggregates in concrete production. Construction and Building Materials, vol. 125, pp. 800 – 808

Polat, H., Ozel, C., 2024. Investigation of ferrochrome slag utilization in wet mix shotcrete: Mechanical strength and radiation shielding performance. Radiation Physics and Chemistry, vol. 223, p. 111963

Ponzi, H., Ramos, F., Li, S., 2021. Aggregate grading and packing density effects on shotcrete workability. Journal of Materials in Civil Engineering, vol. 33, no. 6, p. 04021088

Qu, Y., Liu, Z., Han, J., 2024. Performance improvements in shotcrete using optimised aggregate blends. Construction and Building Materials, vol. 420, pp. 132 – 148

Rameshwar, P., Shrikant, G., 2017. Common aggregate types in concrete and shotcrete. International Journal of Construction Materials, vol. 12, no. 1, pp. 55 – 62

Reddy, B., Reddy, N., 2007. Environmental benefits of crushed rock aggregates in concrete. Sustainable Construction Review, vol. 5, no. 2, pp. 18 – 26

Rouhani, A., Gusiatin, M.Z., Hejcman, M., 2023. An overview of the impacts of coal mining and processing on soil: Assessment, monitoring, and challenges in the Czech Republic. Environmental Geochemistry and Health, vol. 45, pp. 7459 – 7490

Saw, T., 2015. Early re-entry safety in tunnels supported by shotcrete. Tunnelling and Underground Space Technology, vol. 49, pp. 89 – 97

Schädlich, B., Schweiger, H., Marcher, T., Saurer, E., 2014. Application of a novel constitutive shotcrete model to tunnelling. In Rock Engineering and Rock Mechanics: Structures in and on Rock Masses, pp. 799 – 804

Schutz, R., 2010. Numerical modelling of shotcrete for tunneling. Doctoral dissertation, Imperial College London

Seńczuk, M., Kowalczyk, R., Wójcik, M., 2022. Influence of fine and coarse aggregates on deformation behaviour of sprayed concrete. Engineering Structures, vol. 256, p. 113758

Serati, M., Jakson, N., Asche, H., Basireddy, S., Malgotra, G., 2022. Sustainable shotcrete production with waste glass aggregates. SN Applied Sciences, vol. 4, p. 82

Serati, M., Kamel, A., Mousavi, S., 2022. Performance of crushed-rock aggregates in modern shotcrete systems. Materials Today: Proceedings, vol. 56, pp. 2450 – 2470

Shah, S.P., Ahmad, S.H., Yang, S., 2021. Thermal stability of dolerite aggregate shotcrete. Construction and Building Materials, vol. 290, pp. 123 – 145

Shotcrete Technology Committee, 2024. Guidelines for sustainable shotcrete practice. International Shotcrete Association

Sjölander, A., Bergström, A., Johansson, D., 2023a. Early-age strength development of OPC-based shotcrete in tunnelling operations. Tunnelling and Underground Space Technology, vol. 132, pp. 104 – 156

Sjölander, A., Khosravani, M., Johansson, F., 2023b. Shotcrete behaviour under dynamic loading. Journal of Rock Mechanics and Geotechnical Engineering, vol. 15, no. 5, pp. 1243 – 1257

Skarżyński, Ł., Suchorzewski, J., 2018. Corrosion effects on steel fibre reinforced shotcrete. Construction and Building Materials, vol. 170, pp. 637 – 648

Singh, R., Patel, D., Kumar, V., 2016. Mechanical characterisation of dolerite for civil engineering applications. International Journal of Rock Mechanics and Mining Sciences, vol. 86, pp. 157 – 165

Stacey, T.R., 2009. Excavation support in mines. University of the Witwatersrand Press, Johannesburg

Stille, H., Holmgren, J., 2015. Factor of safety in shotcrete tunnel linings. Rock Mechanics and Rock Engineering, vol. 48, no. 3, pp. 789 – 802

Tannant, D.D., Kaiser, P.K., McCreath, D.R., 1999. Evaluation of shotcrete and thin membrane support liners for underground rock support. CIM Bulletin, vol. 92, no. 1026, pp. 88 – 94

Thomas, A., 2018. The influence of fibre reinforcement on residual strength of sprayed concrete. Tunnelling and Underground Space Technology, vol. 18, no. 3, pp. 327 – 332

Toderaş, M., Danciu, I., 2020. Support performance in deep, seismically active underground excavations. Mining Technology, vol. 129, no. 2, pp. 89 – 101

Twort, A.C., Ratnayaka, D.D., Brandt, M.J., 2002. Water supply (5th Edition). Butterworth-Heinemann, Oxford

Ubi, E., Osei, Y., Alias, J., 2020. Aggregate morphology effects on shotcrete performance. Construction Science Journal, vol. 18, no. 2, pp. 100 – 114

Ulyeva, G.A., Yemelyanova, O.V., 2024. Production of special coke for electrothermal silicon production from Central Kazakhstan coal. Coke Chemistry, vol. 67, pp. 243 – 250

Uomoto, T., Sugiyama, R., 2006. Outlines of JSCE recommendations for shotcreting for tunnels by NATM method. Concrete Journal, vol. 44, no. 10, pp. 3 – 10

Uotinen, L., 2011. Failure modes of shotcrete in underground excavations. Tunnelling and Underground Space Technology, vol. 26, no. 5, pp. 567 – 574

Van Niekerk, L., Vermeulen, P., 2004. Utilisation of mining waste materials in civil applications. Journal of the Southern African Institute of Mining and Metallurgy, vol. 104, no. 5, pp. 275 – 282

Vandewalle, L., 1998. Early-age strength development in shotcrete. Materials and Structures, vol. 31, no. 2, pp. 123 – 129

Wang, J., Li, H., Cui, X., 2019. Bond strength of shotcrete under thermal exposure. Construction and Building Materials, vol. 215, pp. 410 – 423

Win, K., Nur, A., 2023. Shotcrete for slope stabilization under environmental loading. International Journal of Geotechnical Engineering, vol. 17, no. 4, pp. 567 – 578

Xie, J., 2024. Advancements in crushed-rock aggregate shotcrete for tunnel support. Journal of Underground Materials Engineering, vol. 12, no. 1, pp. 33 – 49

Yun, T., Kim, H., Lee, J., 2020a. Cement behaviour in early-age shotcrete. Cement and Concrete Research, vol. 138, pp. 106 – 118

Yun, H., Kim, Y., Park, J., 2020b. Early-age mechanical performance of fibre-reinforced shotcrete. Tunnelling and Underground Space Technology, vol. 98, pp. 1 – 12

Yurdakul, E., Rieder, K.A., 2015. Effect of pozzolanic based rheology control agent as a replacement for silica fume on wet-mix shotcrete performance. Shotcrete Magazine, pp. 26 – 31

Zhao, J., Meng, X., Chen, L., Liu, G., Zhang, Z., Xu, Q., 2021. Correlation between the mechanical properties and the fiber breaking morphology of fiber reinforced shotcrete (FRS). Composite Structures, vol. 277, p. 114641

Zhao, Y., Li, X., Wang, J., 2021. Mechanical strength of shotcrete in underground tunnels. Construction and Building Materials, vol. 302, pp. 124 – 567

Zhou, Q., Chen, Z., Hu, Y., 2022. Predictive constitutive models for shotcrete. Engineering Modelling, vol. 74, pp. 201 – 213

Zhou, F., Zhang, B., Pan, Y., Zhou, Y., 2025. Mechanical performance of fiber-reinforced shotcrete for underground mines. Buildings, vol. 15, p. 3689

Zhu, W., Zhang, L., Li, H., 2021. Plastic yielding behaviour of shotcrete in deep tunnels. Tunnelling and Underground Space Technology, vol. 108, pp. 103 – 118

Zhu, C., Zhou, N., Guo, Y., Li, M., Cheng, Q., 2021. Effect of doped glass fibers on tensile and shear strengths and microstructure of the modified shotcrete material: An experimental study and a simplified 2D model. Minerals, vol. 11, no. 10, p.1053

Appendices

The appendices include experimental, numerical, and statistical data for the performance assessment of dolerite–Xorex fibre reinforced shotcrete. Appendix A provides shrinkage test data for the purpose of deformation stability analysis during curing. Mechanical test data, including triaxial compressive strength, tensile strength, UCS, elastic modulus, and Poisson's ratio is provided in Appendices B–D to facilitate performance evaluation and strength development. The Unwedge simulation data for assessing wedge stability and support performance is included in Appendix E and the Ground Reaction Curve data for convergence and excavation stability assessment is given in Appendix F. The MATLAB codes utilized in correlation analysis and multivariate modelling are provided in Appendix G. Regression models for the short- and long-term curing periods and the accuracy of the models and the impact of predictors on factor of safety are provided in Appendices H–K.

Appendix A: Shrinkage data

Shrinkage Tests:- Shotcrete Cores																							
Δ % :	Shrinkage (%)																						
Specimen No:		**1**					**Specimen No:**		**2**						**Specimen No:**			**3**					
Mass (g)		**547,70**					**Mass (g)**		**470,70**						**Mass (g)**			**473,00**					
Diameter (mm)		**57,46**					**Diameter (mm)**		**58,11**						**Diameter (mm)**			**57,64**					
Height (mm)		**85,05**					**Height (mm)**		**72,35**						**Height (mm)**			**72,76**					
Day	**Date**	**Time**	**Total**	**in Water:-**			**Day**	**Date**	**Time**	**Total**	**in Water:-**				**Day**	**Date**		**Time**	**Total**	**in Water:-**			
	YYYYMMDD	**hh:mm**	**Hrs**	**Δ mm**	**Δ %**			**YYYYMMDD**	**hh:mm**	**hrs**	**Δ mm**	**Δ %**				**YYYYMMDD**		**hh:mm**	**hrs**	**Δ mm**	**Δ %**		
Fri	2025/05/23	15:51	0,0	9,000	0,000		Fri	2025/05/23	15:51	0,0	6,000	0,000			Fri	2025/05/23		15:51	0,0	6,000	0,000		
Mon	2025/05/26	08:00	64,2	8,987	0,015		Mon	2025/05/26	08:00	64,2	5,970	0,041			Mon	2025/05/26		08:00	64,2	5,995	0,007		
Thu	2025/05/29	14:00	142,2	8,960	0,047		Thu	2025/05/29	14:00	142,2	5,964	0,050			Thu	2025/05/29		14:00	142,2	5,954	0,063		
Thu	2025/06/19	14:08	646,3	8,950	0,059		Thu	2025/06/19	14:08	646,3	5,958	0,058			Thu	2025/06/19		14:08	646,3	5,945	0,076		
Thu	2025/07/17	14:10	1318,3	8,949	0,060		Thu	2025/07/17	14:10	1318,3	5,951	0,068			Thu	2025/07/17		14:10	1318,3	5,940	0,082		
				Max	0,060						Max	0,068								Max	0,082		
Stopped test on the:							Stopped test on the:								Stopped test on the:								
	2025/07/17	at	14:10					2025/07/17	at	14:10						2025/07/17		at	14:10				
	After	54,9	days					After	54,9	days						After		54,9	days				
			Remarks:-												▪ Reference for the Duncan Swelling Tests:								
			▪ All tests were based on the paper published by Duncan et.al. (1968).																				
			▪ Specimen is exposed to air throughout the test.												Duncan, N., Dunne, M.H. and Petty, S.W. (1968). Swelling Characteristics of Rocks. Water Power, May, pp. 185-192.								
Technical Signatory:			▪ Vertical shrinkage (deformation) is measured.																				
Halil YILMAZ – PhD			▪ Data is recorded over time (up to ~ 55 days).																				
16.07.2025																							

Appendix B: Triaxial compressive strength data

Specimen Number	Curing Days	Mass (g)	Diameter (mm)	Length (mm)	Failure Load (kN)	L/D	Density (kg/m^3)	Confinement (MPa)	TCS (MPa)
1;N109;RE311	4	892,0	58,5	135,7	50,1	2,3	2446	0,5	18,7
1;N109;RE310	4	902,5	57,7	135,4	70,9	2,3	2546	1,0	27,1
1;N109;RE311	4	900,3	57,6	135,6	76,0	2,4	2552	2,0	29,2
1;N109;RE312	7	877,0	57,3	136,2	59,5	2,4	2502	0,5	23,1
1;N109;RE314	7	888,3	57,8	136,7	76,2	2,4	2476	1,0	29,0
1;N109;RE315	7	894,2	57,8	136,7	90,8	2,4	2490	2,0	34,6
1;N109;RE316	28	876,6	57,2	135,7	79,4	2,4	2514	0,5	30,9
1;N109;RE317	28	872,2	58,5	136,0	92,0	2,3	2386	1,0	34,2
1;N109;RE318	28	873,0	58,0	135,1	113,7	2,3	2449	2,0	43,1
1;N109;RE319	56	905,7	57,2	137,3	84,0	2,4	2563	0,5	32,6
1;N109;RE320	56	889,7	57,2	135,7	92,3	2,4	2555	1,0	36,0
1;N109;RE321	56	903,8	57,5	137,2	112,7	2,4	2541	2,0	43,5
1;N109;RE322									

UCS (MPa)	β	C_o	ϕ	R^2
4	**Days**			
17,59	**6,32**	**3,5**	**46,6**	**0,75**
7	**Days**			
20,34	**7,34**	**3,8**	**49,5**	**0,96**
28	**Days**			
26,48	**8,23**	**4,6**	**51,6**	**1,00**
56	**Days**			
28,86	**7,29**	**5,3**	**49,3**	**1,00**

Appendix C: Tensile strength data

Specimen No	Curing Period (Days)	Liner Width (mm)	Liner Thickness (mm)	Maximum Load (kN)	Maximum Stress (MPa)
1	4	13,4	12,7	0,27	1,60
2	4	12,9	12,7	0,29	1,74
3	4	13,0	11,8	0,26	1,67
4	7	13,3	12,3	0,44	2,71
5	7	13,4	12,8	0,46	2,67
6	7	12,9	13,9	0,45	2,51
7	28	13,3	12,6	0,59	3,57
8	28	13,0	11,9	0,58	3,73
9	28	13,4	12,8	0,58	3,42
10	56	12,8	11,9	0,64	4,21
11	56	13,3	11,4	0,65	4,25
12	56	13,1	11,7	0,64	4,15

Appendix D: Uniaxial compressive strength data

Specimen	Curing time	Mass	Diameter	Length	Failure	L/D	Density	UCS	E	ν
No	Days	(g)	(mm)	(mm)	Load (kN)	(-)	(kg/m^3)	(MPa)	(GPa)	(-)
1	4	447,7	45,44	113,40	13,50	2,5	2434	11.04	13.50	0.21
2	4	407,8	45,48	100,05	18,14	2,2	2509	11.17	11.18	0.21
3	4	379,8	45,63	93,09	13,57	2,0	2495	10.35	12.74	0.21
4	7	441,9	45,27	110,67	19,90	2,4	2481	12.36	13.86	0.21
5	7	344,5	45,20	88,60	20,54	2,0	2423	12.80	15.80	0.21
6	7	440,1	45,45	111,07	19,22	2,4	2442	11.84	16.43	0.21
7	28	414,8	45,90	106,62	29,03	2,3	2351	19.48	18.78	0.26
8	28	411,5	44,95	106,95	32,90	2,4	2425	20.73	18.96	0.26
9	28	321,9	45,64	82,25	19,61	1,8	2392	19.53	19.21	0.26
10	56	419,7	45,82	104,61	26,55	2,3	2433	21.37	20.57	0.27
11	56	408,7	45,45	101,03	21,62	2,2	2493	21.33	20.29	0.27
12	56	294,9	44,58	77,18	21,58	1,7	2448	23.52	20.17	0.27

Appendix E: Information of tunnel Deformation

Wedge	FS (Case 1)	Weight (t)	FS (Case 2)	Weight (t)	FS (Case 3)	Weight (t)	FS (Case 4)	Weight (t)
Floor wedge [3]	stable	12.900	stable	12.900	stable	12.900	stable	12.900
Lower Right wedge [4]	39.589	0.787	43.188	0.787	47.586	0.787	48.986	0.787
Upper Left wedge [5]	11.572	0.985	12.746	0.985	14.181	0.985	14.638	0.985
Roof wedge [6]	2.827	3.104	3.118	3.104	3.474	3.104	3.587	3.104

Appendix F: Output parameters from Ground Reaction Curve (GRC)

Curing days	Condition	Convergence (%)	Factor of Safety
4	Final	1,35	0,57
	Long term	2,49	0,33
	Tunnel face	0,62	
	Support	0,88	
7	Final	0,94	1,56
	Long term	1,11	0,89
	Tunnel face	0,62	
	Support	0,88	
28	Final	0,91	2,92
	Long term	0,94	1,65
	Tunnel face	0,62	
	Support	0,88	
56	Final	0,9	4,25
	Long term	0,92	2,41
	Tunnel face	0,62	
	Support	0,88	

Appendix G: MATLAB code for the correlation multivariate modelling

The results from the simulations and experimental set up were used as input data from that was saved on a Microsoft Excel file which was later used in MATLAB

Contents

- Correlation analysis with Excel, heatmaps, LaTeX, and PNG tables
- 1. Import with original headers preserved
- 2. Correlations with p values
- 3. Write everything to Excel
- 4. Heatmaps for figures
- 5. LaTeX tables for marked matrices
- 6. Word ready PNG images for marked matrices
- ===== Helper functions. Keep everything below in the same file =====

Correlation analysis with Excel, heatmaps, LaTeX, and PNG tables

Input. Data.xlsx in Current Folder. Sheets: "short term stability (2)" and "Long term stability" Outputs created in Current Folder: correlation_outputs.xlsx Fig_short_term_Pearson.png Fig_long_term_Pearson.png Fig_short_term_Spearman.png Fig_long_term_Spearman.png Short_Pearson_marked.tex Short_Pearson_marked.png Long_Pearson_marked.tex Long_Pearson_marked.png Short_Spearman_marked.tex Short_Spearman_marked.png Long_Spearman_marked.tex Long_Spearman_marked.png

```
clear; clc;

fname = 'Data.xlsx';
```

1. Import with original headers preserved

```
short_opts = detectImportOptions(fname, 'Sheet','short term stability (2)', ...
    'VariableNamingRule','preserve');
short_opts.DataRange = '5:2000';
Tshort = readtable(fname, short_opts);

long_opts = detectImportOptions(fname, 'Sheet','Long term stability', ...
    'VariableNamingRule','preserve');
long_opts.DataRange = '5:2000';
Tlong  = readtable(fname, long_opts);

% Columns we use. Names must match the sheet headers exactly.
vars = {'FOS','Curing time','TCS','E','v','Max stress','Failure Load', ...
        'Maximum shear','Strength Factor tension','Total Displacement', ...
        'Volumetric strain (-)','Shear Strength','Convegence'};

Tshort = Tshort(:, intersect(vars, Tshort.Properties.VariableNames, 'stable'));
Tlong  = Tlong(:,  intersect(vars, Tlong.Properties.VariableNames,  'stable'));

% Coerce all columns to numeric
coerceToNumeric = @(x) double( str2double( strrep(string(x),',','.') ) );
for k = 1:width(Tshort)
    if ~isnumeric(Tshort.(k)), Tshort.(k) = coerceToNumeric(Tshort.(k)); end
end
for k = 1:width(Tlong)
    if ~isnumeric(Tlong.(k)),  Tlong.(k)  = coerceToNumeric(Tlong.(k));  end
end

% Remove any rows that still have NaN
Tshort = rmmissing(Tshort);
Tlong  = rmmissing(Tlong);

Xshort = table2array(Tshort);
Xlong  = table2array(Tlong);
labels = Tshort.Properties.VariableNames;
```

2. Correlations with p values

```
[rP_short, pP_short] = corr(Xshort, 'Type','Pearson',  'Rows','pairwise');
[rS_short, pS_short] = corr(Xshort, 'Type','Spearman', 'Rows','pairwise');

[rP_long,  pP_long ] = corr(Xlong,  'Type','Pearson',  'Rows','pairwise');
[rS_long,  pS_long ] = corr(Xlong,  'Type','Spearman', 'Rows','pairwise');

% Mark significance at alpha = 0.05
alpha = 0.05;
fmtMark = @(R,P) arrayfun(@(r,p) sprintf('%.2f%s', r, (p<alpha && r~=1)*'*'), R, P, 'UniformOutput', false);
markPshort = fmtMark(rP_short,pP_short);
markSshort = fmtMark(rS_short,pS_short);
markPlong  = fmtMark(rP_long,pP_long);
markSlong  = fmtMark(rS_long,pS_long);
```

3. Write everything to Excel

```
outFile = 'correlation_outputs.xlsx';

% Pearson
writetable(array2table(rP_short,'VariableNames',labels,'RowNames',labels), outFile, 'Sheet','Short Pearson r',   'WriteRowNames',true);
writetable(array2table(pP_short,'VariableNames',labels,'RowNames',labels), outFile, 'Sheet','Short Pearson p',   'WriteRowNames',true);
writetable(cell2table(markPshort,'VariableNames',labels,'RowNames',labels),outFile, 'Sheet','Short Pearson marked','WriteRowNames',true);

writetable(array2table(rP_long,'VariableNames',labels,'RowNames',labels),  outFile, 'Sheet','Long Pearson r',    'WriteRowNames',true);
writetable(array2table(pP_long,'VariableNames',labels,'RowNames',labels),  outFile, 'Sheet','Long Pearson p',    'WriteRowNames',true);
writetable(cell2table(markPlong,'VariableNames',labels,'RowNames',labels), outFile, 'Sheet','Long Pearson marked','WriteRowNames',true);

% Spearman
writetable(array2table(rS_short,'VariableNames',labels,'RowNames',labels), outFile, 'Sheet','Short Spearman r',  'WriteRowNames',true);
writetable(array2table(pS_short,'VariableNames',labels,'RowNames',labels), outFile, 'Sheet','Short Spearman p',  'WriteRowNames',true);
writetable(cell2table(markSshort,'VariableNames',labels,'RowNames',labels),outFile, 'Sheet','Short Spearman marked','WriteRowNames',true);

writetable(array2table(rS_long,'VariableNames',labels,'RowNames',labels),  outFile, 'Sheet','Long Spearman r',   'WriteRowNames',true);
writetable(array2table(pS_long,'VariableNames',labels,'RowNames',labels),  outFile, 'Sheet','Long Spearman p',   'WriteRowNames',true);
writetable(cell2table(markSlong,'VariableNames',labels,'RowNames',labels), outFile, 'Sheet','Long Spearman marked','WriteRowNames',true);
```

4. Heatmaps for figures

```
figure('Position',[100 100 900 800]);
heatmap(labels, labels, rP_short, 'Colormap', parula, 'ColorLimits', [-1 1]);
title('Short term Pearson correlation');
set(gca,'FontSize',10);
exportgraphics(gcf,'Fig_short_term_Pearson.png','Resolution',300);

figure('Position',[100 100 900 800]);
heatmap(labels, labels, rP_long, 'Colormap', parula, 'ColorLimits', [-1 1]);
title('Long term Pearson correlation');
set(gca,'FontSize',10);
exportgraphics(gcf,'Fig_long_term_Pearson.png','Resolution',300);

figure('Position',[100 100 900 800]);
heatmap(labels, labels, rS_short, 'Colormap', parula, 'ColorLimits', [-1 1]);
title('Short term Spearman correlation');
set(gca,'FontSize',10);
exportgraphics(gcf,'Fig_short_term_Spearman.png','Resolution',300);

figure('Position',[100 100 900 800]);
heatmap(labels, labels, rS_long, 'Colormap', parula, 'ColorLimits', [-1 1]);
title('Long term Spearman correlation');
set(gca,'FontSize',10);
exportgraphics(gcf,'Fig_long_term_Spearman.png','Resolution',300);
```

```
Error using exportgraphics
Input was not a valid graphics object.

Error in run_correlations (line 114)
exportgraphics(gcf,'Fig_long_term_Spearman.png','Resolution',300);
^^^^^^^^^^^^^^^^^^^^^^^^^^^^^^^^^^^^^^^^^^^^^^^^^^^^^^^^^^^^^^^^^^^^
```

5. LaTeX tables for marked matrices

```
writeLatexTable('Short_Pearson_marked.tex',  'Short term Pearson correlations. p < 0.05 marked.', 'tab:shortPearson',  labels, markPshort);
writeLatexTable('Long_Pearson_marked.tex',   'Long term Pearson correlations. p < 0.05 marked.',  'tab:longPearson',   labels, markPlong);
writeLatexTable('Short_Spearman_marked.tex', 'Short term Spearman correlations. p < 0.05 marked.','tab:shortSpearman', labels, markSshort);
writeLatexTable('Long_Spearman_marked.tex',  'Long term Spearman correlations. p < 0.05 marked.', 'tab:longSpearman',  labels, markSlong);
```

6. Word ready PNG images for marked matrices

```
renderTablePNG('Short_Pearson_marked.png',  labels, markPshort,  'Short term Pearson marked');
renderTablePNG('Long_Pearson_marked.png',   labels, markPlong,   'Long term Pearson marked');
renderTablePNG('Short_Spearman_marked.png', labels, markSshort,  'Short term Spearman marked');
renderTablePNG('Long_Spearman_marked.png',  labels, markSlong,   'Long term Spearman marked');

disp('All outputs created. You can download the Excel, PNGs, and TEX files.');
```

===== Helper functions. Keep everything below in the same file =====

```
function writeLatexTable(texFile, captionText, labelText, labels, markedCell)
    % Creates a LaTeX tabular using booktabs. Ready to \input{} in LaTeX.
```

```
    esc = @(s) strrep(strrep(strrep(strrep(strrep(s,'_','\_'),'&','\&'),'%','\%'),'#','\#'),'$','\$'),'^','\^{}');
    L = cellfun(@(c) esc(string(c)), labels, 'UniformOutput', false);

    fid = fopen(texFile,'w');
    assert(fid>0, 'Cannot open file for writing: %s', texFile);
    n = numel(labels);

    fprintf(fid, '%% Auto generated by MATLAB\n');
    fprintf(fid, '\\begin{table}[!ht]\n\\centering\n\\small\n');
    fprintf(fid, '\\caption{%s}\n', captionText);
    fprintf(fid, '\\label{%s}\n', labelText);
    fprintf(fid, '\\begin{tabular}{l%s}\n', repmat('c',1,n));
    fprintf(fid, '\\toprule\n');

    % Header
    fprintf(fid, ' & ');
    for j = 1:n
        fprintf(fid, '%s', L{j});
        if j < n, fprintf(fid, ' & '); else, fprintf(fid, ' \\\\\n'); end
    end
    fprintf(fid, '\\midrule\n');

    % Body
    for i = 1:n
        fprintf(fid, '%s & ', L{i});
        for j = 1:n
            val = string(markedCell{i,j});
            fprintf(fid, '%s', esc(val));
            if j < n, fprintf(fid, ' & '); else, fprintf(fid, ' \\\\\n'); end
        end
    end

    fprintf(fid, '\\bottomrule\n\\end{tabular}\n\\end{table}\n');
    fclose(fid);
end

function renderTablePNG(pngName, labels, markedCell, figTitle)
% Renders a matrix of strings as a table like PNG using plain graphics.
% Works in MATLAB Online. No uifigure. Exports with exportgraphics.

    cellW = 1;       % cell width units
    cellH = 0.6;     % cell height units
    fsHdr = 11;      % header font size
    fsCell = 10;     % cell font size
    hdrBG = [0.92 0.92 0.95];
    gridC = [0.8 0.8 0.85];
    titleFS = 14;

    n = numel(labels);
    W = (n+1) * cellW;   % plus one for row header
    H = (n+2) * cellH;   % plus one for column header and a title band

    fig = figure('Position',[100 100 1100 700], 'Color','w', 'Visible','off');
    ax = axes(fig, 'Position',[0 0 1 1], 'Units','normalized');
    axis(ax, [0 W 0 H]); axis(ax, 'ij'); axis(ax, 'off'); hold(ax, 'on');

    % Title
    text(ax, W/2, 0.6, figTitle, 'HorizontalAlignment','center', ...
         'VerticalAlignment','middle', 'FontSize', titleFS, 'FontWeight','bold');

    % Column headers
    for j = 1:n
        x0 = j*cellW; y0 = 1*cellH;
        rectangle(ax, 'Position',[x0, y0, cellW, cellH], 'FaceColor', hdrBG, 'EdgeColor', gridC);
        text(ax, x0+cellW/2, y0+cellH/2, labels{j}, 'HorizontalAlignment','center', ...
             'VerticalAlignment','middle', 'FontSize', fsHdr, 'Interpreter','none');
    end

    % Row headers
    for i = 1:n
        x0 = 0; y0 = (i+1)*cellH;
        rectangle(ax, 'Position',[x0, y0, cellW, cellH], 'FaceColor', hdrBG, 'EdgeColor', gridC);
        text(ax, x0+cellW/2, y0+cellH/2, labels{i}, 'HorizontalAlignment','center', ...
             'VerticalAlignment','middle', 'FontSize', fsHdr, 'Interpreter','none');
    end

    % Body cells
    for i = 1:n
        for j = 1:n
            x0 = j*cellW; y0 = (i+1)*cellH;
            rectangle(ax, 'Position',[x0, y0, cellW, cellH], 'FaceColor','w', 'EdgeColor', gridC);
            val = string(markedCell{i,j});
```


https://matlab.mathworks.com 3/4

```
            text(ax, x0+cellW/2, y0+cellH/2, val, 'HorizontalAlignment','center', ...
                'VerticalAlignment','middle', 'FontSize', fsCell, 'Interpreter','none');
        end
    end

    % Outer border
    rectangle(ax, 'Position',[cellW, cellH, n*cellW, n*cellH], 'EdgeColor', [0.5 0.5 0.5], 'LineWidth', 1);

    exportgraphics(fig, pngName, 'Resolution', 300);
    delete(fig);
end
```

Published with MATLAB® R2025a

Appendix H: Short-term statistical modelling of 4 days

SUMMARY OUTPUT

Regression Statistics	
Multiple R	0,999667
R Square	0,999335
Adjusted R Square	0,99867
Standard Error	0,050497
Observations	11

ANOVA

	Df	*SS*	*MS*	*F*	*Significance F*
Regression	5	19,16214095	3,832428	1502,917	6,19E-08
Residual	5	0,012749962	0,00255		
Total	10	19,17489091			

	Coefficients	*Standard Error*	*t Stat*	*P-value*	*Lower 95%*	*Upper 95%*	*Lower 95,0%*	*Upper 95,0%*
Intercept	-6,60858	1,770216346	-3,7332	0,013526	-11,1591	-2,05809	-11,1591	-2,05809
Curing time	0,035453	0,003539378	10,01659	0,00017	0,026354	0,044551	0,026354	0,044551
UCS	-0,12362	0,041327073	-2,99122	0,030405	-0,22985	-0,01738	-0,22985	-0,01738
E	0,025508	0,022638886	1,126736	0,311006	-0,03269	0,083703	-0,03269	0,083703
Max stress	0,263952	0,180928509	1,458875	0,20441	-0,20114	0,729044	-0,20114	0,729044
Shear Strength	0,967041	0,317591945	3,044918	0,02859	0,150645	1,783438	0,150645	1,783438

Appendix I: Short term statistical modelling of 7 days

SUMMARY OUTPUT

Regression Statistics	
Multiple R	0,999510622
R Square	0,999021484
Adjusted R Square	0,998602121
Standard Error	0,051772759
Observations	11

ANOVA

	Df	*SS*	*MS*	*F*	*Significance F*
Regression	3	19,15612798	6,385376	2382,231	6,82093E-11
Residual	7	0,01876293	0,00268		
Total	10	19,17489091			

	Coefficients	*Standard Error*	*t Stat*	*P-value*	*Lower 95%*	*Upper 95%*	*Lower 95,0%*	*Upper 95,0%*
Intercept	-9,124215688	0,63925625	-14,2732	1,97E-06	-10,63581652	-7,61261	-10,6358165	-7,6126149
Curing time	0,039189281	0,002523825	15,52773	1,11E-06	0,033221383	0,045157	0,033221383	0,04515718
UCS	-0,157628554	0,034546183	-4,56284	0,002596	-0,239317297	-0,07594	-0,2393173	-0,0759398
Shear Strength	1,407938637	0,134475896	10,46982	1,58E-05	1,089953672	1,725924	1,089953672	1,7259236

Appendix J: Long-term statistical modelling of 28 days

SUMMARY OUTPUT

Regression Statistics	
Multiple R	0,999542199
R Square	0,999084608
Adjusted R Square	0,998169215
Standard Error	0,033327173
Observations	11

ANOVA

	df	*SS*	*MS*	*F*	*Significance F*
Regression	5	6,061246498	1,2122493	1091,428	1,37591E-07
Residual	5	0,005553502	0,0011107		
Total	10	6,0668			

	Coefficients	*Standard Error*	*t Stat*	*P-value*	*Lower 95%*	*Upper 95%*	*Lower 95,0%*	*Upper 95,0%*
Intercept	-3,66562311	1,168302684	-3,137562857	0,025737	-6,668840764	-0,6624054	-6,668840764	-0,66240545
Curing time	0,019958773	0,002335909	8,544326224	0,000362	0,013954126	0,02596342	0,013954126	0,02596342
UCS	-0,07002913	0,027274932	-2,567527232	0,050186	-0,140141577	8,3314E-05	-0,140141577	8,3314E-05
E	0,015750257	0,014941152	1,054152799	0,340065	-0,022657196	0,05415771	-0,022657196	0,05415771
Max stress	0,151422582	0,119408717	1,26810325	0,2606	-0,155527297	0,45837246	-0,155527297	0,45837246
Shear Strength	0,538149509	0,209603489	2,567464468	0,05019	-0,000653411	1,07695243	-0,000653411	1,07695243

Appendix K: Long-term statistical modelling of 56 days

SUMMARY OUTPUT

Regression Statistics	
Multiple R	0,999371826
R Square	0,998744047
Adjusted R Square	0,998205782
Standard Error	0,032992672
Observations	11

ANOVA

	Df	*SS*	*MS*	*F*	*Significance F*
Regression	3	6,059180385	2,019727	1855,486	1,634E-10
Residual	7	0,007619615	0,001089		
Total	10	6,0668			

	Coefficients	*Standard Error*	*t Stat*	*P-value*	*Lower 95%*	*Upper 95%*	*Lower 95,0%*	*Upper 95,0%*
Intercept	-5,124375582	0,407371981	-12,5791	4,63E-06	-6,087657	-4,161094	-6,08765725	-4,16109392
Curing time	0,022105722	0,001608331	13,74451	2,55E-06	0,0183026	0,025909	0,018302624	0,025908821
UCS	-0,089444479	0,022014876	-4,06291	0,004792	-0,141501	-0,037388	-0,14150139	-0,03738757
Shear Strength	0,794262226	0,085696014	9,268368	3,52E-05	0,5916234	0,996901	0,591623354	0,996901098

Appendix L: Input parameters for conventional shotcrete

Parameter	Symbol	28-Day Value
Uniaxial Compressive Strength	UCS	31.91 MPa
Modulus of Elasticity	E	25 GPa
Poisson's Ratio	v	0.22
Tensile Strength	σ_t	3.02 MPa
Shear Strength	τ	3.5 MPa

Sourced from Hammer et al., (2020)